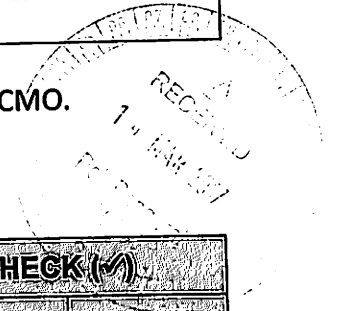


Please use this checklist to self-assess your report before submitting to RCMO.
Checklist should accompany the report.

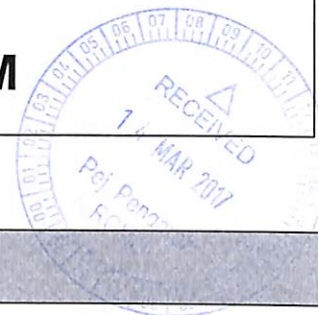


NO.	ITEM	PLEASE CHECK (✓)		
		PI	JKPTJ	RCMO
1	Completed Final Report Form	✓		✓
2	Project Financial Account Statement (e-Statement)	✓		✓
3	Asset/Inventory Return Form (Borang Penyerahan Aset/Inventori)	✓		✓
4	A copy of the publications/proceedings listed in Section D(ii) (Research Output)	✓		✓
5	Comprehensive Technical Report	✓		✓
6	Other supporting documents, if any			
7	Project Leader's Signature	✓		✓
8	Endorsement of PTJ's Evaluation Committee	✓		✓
9	Endorsement of Dean/ Director of PTJ's	✓		✓

Project Code :
(for RCMO use only)



RU GRANT FINAL REPORT FORM



Please email a softcopy of this report to rcmo@usm.my

A	PROJECT DETAILS
i	Title of Research: Development of low-cost rubber tensile property tester using digital image correction (DIC) and flatbed scanner
ii	Account Number: 1001/PMEKANIK/814182
iii	Name of Research Leader: Prof. Mani Maran a/l Ratnam
iv	Name of Co-Researcher: 1. Prof. Hanafi Ismail 2. Dr. Yen Kin Sam 3.
v	Duration of this research: a) Start Date : 15 Disember 2012 b) Completion Date : 14 Disember 2015 c) Duration : 3.5 Years (after extension) d) Revised Date (if any) : 14 June 2016
B	ABSTRACT OF RESEARCH
	<p><i>(An abstract of between 100 and 200 words must be prepared in Bahasa Malaysia and in English. This abstract will be included in the Report of the Research and Innovation Section at a later date as a means of presenting the project findings of the researcher/s to the University and the community at large)</i></p> <p>In this research, a novel 2-D scanner-based digital image correlation (2-D SB-DIC) method has been developed. This method enables acquisition of a large field-of-view of a natural rubber specimen at large deformation. A motorized loading rig was designed to act as the tensile load applicator. The images were scanned and processed using MATLAB to obtain the displacements, strains, load applied and the stress data. The Young's moduli and Poisson's ratios of the rubber specimens were determined up to 350% axial strain using the same set of images. The images were processed using the incremental image correlation algorithm. A new algorithm for mapping large</p>

deformation in the rubber specimens in a single-step is also proposed. Non-homogeneous strain distribution tests were also conducted by analysing the deformation of two rectangular rubber specimens containing circular and square holes. The Young's moduli obtained by using the incremental 2-D SB-DIC algorithm showed maximum errors of 9.5% at 250% axial strain and 4.2% at 50% axial strain in tangent modulus and secant modulus, respectively. The strain dependent Poisson's ratios obtained from the SB-DIC method in terms of engineering strain and true strain were validated with the Poisson function associated with incompressibility assumption of polymeric materials. The result shows that the experimental data fitted well with the theoretical result up to a stretch ratio of 2.0. A maximum absolute deviation of 10.7% at axial strains of 320% was found by using the proposed single-step 2-D SB-DIC algorithm. For the non-homogeneous strain distribution tests, the comparison of the resultant strain maps showed that the proposed SB-DIC method can be used to map strain accurately in large strain materials.

Dalam kajian ini, kaedah novel korelasi imej dua dimension (2-D SB-DIC) berasaskan pengimbas telah dibangunkan. Kaedah ini membolehkan perolehan imej medan luas spesimen getah pada anjakan besar. Suatu kelengkapan bermotor telah direkabentuk untuk bertindak sebagai pembeban beban regangan. Imej-imej diimbas dan diproses menggunakan MATLAB untuk mendapatkan data anjakan, terikan, dan tegasan. Modulus Young dan nisbah Poisson bagi spesimen getah ditentukan sehingga terikan paksi 350% dengan menggunakan set imej yang sama. Imej-imej tersebut diproses dengan menggunakan algoritma korelasi imej penokokan. Suatu algoritma baharu untuk memetakan ubah bentuk besar di dalam spesimen getah dalam satu langkah juga dicadangkan. Ujian taburan terikan takhomogen juga dijalankan dengan menganalisa ubahbentuk dua spesimen getah segi empat yang mengandungi lubang-lubang bulat dan empat segi sama. Modulus Young yang didapati dengan menggunakan algoritma penokokan 2-D SB-DIC menunjukkan ralat maksimum 9.5% pada terikan paksi 250% dan 4.2% pada terikan paksi 50% masing-masing. Nisbah-nisbah Poisson yang bergantung kepada terikan daripada kaedah SB-DIC dalam sebutan terikan kejuruteraan dan terikan asal disahkan dengan fungsi Poisson berkaitan dengan andaian ketakmampatan bagi bahan-bahan polimer. Keputusan menunjukkan bahawa data daripada eksperimen setuju dengan keputusan teori sehingga nisbah regangan 2.0. Sisihan mutlak maksimum sebanyak 10.7% pada terikan paksi 320% didapati dengan menggunakan algoritma langkah tunggal 2-D SB-DIC. Bagi ujian taburan terikan tak-homogen, perbandingan peta-peta terikan yang terhasil menunjukkan bahawa kaedah yang dicadangkan boleh digunakan untuk memeta terikan dengan tepat di dalam bahan terikan besar.

C BUDGET & EXPENDITURE

i

Total Approved Budget : RM 134,000.00

Yearly Budget Distributed

Year 1 : RM 58,300.00

Year 2 : RM 47,600.00

Year 3 : RM 28,100.00

Total Expenditure : RM 121,483.17

Balance : RM 12,516.83

Percentage of Amount Spent (%) : 90.7%

Please attach final account statement (eStatement) to indicate the project expenditure

ii Equipment Purchased Under Vot 35000

No.	Name of Equipment	Amount (RM)	Location	Status
1.	Personal Computer (DELL OPTIPLEX 3010DT)	3,229.00	Metrology Laboratory (SM057)	In proper working order
2.	CCD Flatbed scanner (CANON CANOSCAN 5600F SCANNER)	780.00	Metrology Laboratory (SM057)	In proper working order

Please attach the Asset/Inventory Return Form (Borang Penyerahan Aset/Inventori) – Appendix 1

D RESEARCH/ACHIEVEMENTS

i Project Objectives (as stated/approved in the project proposal)

No.	Project Objectives	Achievement
1	To design and develop a loading rig with motorized load applicator to test rubber specimens according to ASTM412 standard	Achieved
2	To develop DIC algorithms to determine the in-plane displacement and strain undergone by rubber and rubber-like specimens	Achieved
3	To develop user interface software that gives graphic view of the load-extension and stress-strain characteristics of the rubber specimen	Achieved
4	To verify the strain-stress relationship measured using the developed system with those obtained from a standard tensile test machine.	Achieved

ii Research Output

a) Publications in ISI Web of Science/Scopus

No.	Publication (authors,title,journal,year,volume,pages,etc.)	Status of Publication (published/accepted/ under review)
1.	C.P. Goh, M.M Ratnam, H. Ismail, Large in-plane deformation mapping and determination of Young's modulus of rubber using scanner-based digital image correlation, <i>Experimental Techniques</i> 40(3) (2016) 1117-1127 (Q3)	Published
2.	C.P. Goh, K.S. Yen,H.Ismail, M.M. Ratnam. Single-step scanner-based digital image correlation (SB-DIC) method for large deformation mapping in rubber, <i>Optics and Lasers in Engineering</i> 88 (2017) 167-177 (Q2).	Published

b) Publications in Other Journals

No.	Publication (authors, title, journal, year, volume, pages, etc.)	Status of Publication (published/accepted/ under review)

c) Other Publications
(book, chapters in book, monograph, magazine, etc.)

No.	Publication (authors, title, journal, year, volume, pages, etc.)	Status of Publication (published/accepted/ under review)

d) Conference Proceeding

No.	Conference (conference name, date, place)	Title of Abstract/Article	Level (International/National)

Please attach a full copy of the publication/proceeding listed above

iii Other Research Output/Impact From This Project
(patent, products, awards, copyright, external grant, networking, etc.)

Nil

E HUMAN CAPITAL DEVELOPMENT

a) Graduated Human Capital

Student	Nationality (No.)		Name
	National	International	
PhD	1		1. Goh Ching Pang (graduating in Nov. 2017) 2.
MSc			1. 2.
Undergraduate			1. Neoh Boon Ping 2.

b) On-going Human Capital

Student	Nationality (No.)		Name
	National	International	
PhD			1. 2.
MSc			1. 2.
Undergraduate			1. 2.

c) Others Human Capital

Student	Nationality (No.)		Name
	National	International	
Post Doctoral Fellow			1. 2.
Research Officer			1. 2.
Research Assistant	1		1. Goh Ching Pang 2.
Others (.....)			1. 2.

F COMPREHENSIVE TECHNICAL REPORT

Applicants are required to prepare a comprehensive technical report explaining the project. The following format should be used (this report must be attached separately):

- Introduction
- Objectives
- Methods
- Results
- Discussion
- Conclusion and Suggestion
- Acknowledgements
- References

G PROBLEMS/CONSTRAINTS/CHALLENGES IF ANY

(Please provide issues arising from the project and how they were resolved)

The completion of the project was delayed by six months due to the difficulty in getting a PhD student.

H**RECOMMENDATION**

(Please provide recommendations that can be used to improve the delivery of information, grant management, guidelines and policy, etc.)

1. The high tuition fee for PhD students has made finding postgraduate students very difficult. Many undergraduate students in USM are from average families and they cannot afford to stay on to complete postgraduate study.
2. The need to provide three quotations for purchases below RM20,000 is not practical in all cases. For services, such a fabrication, printing, repairs, calibration etc. it is very difficult to find three different companies that can offer such services. It is proposed that three quotations be required only for purchase of assets above RM1000.

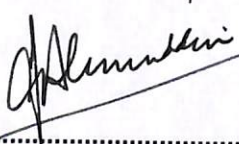
Project Leader's Signature:

Name : Prof. Mani Maran a/l Ratnam

Date : 4/08/17

I COMMENTS, IF ANY/ENDORSEMENT BY PTJ'S RESEARCH COMMITTEE

The project is interdisciplinary project involving Sch. of Mat & Mech Engrg. This sort of project is very much favorable.



Signature and Stamp of Chairperson of PTJ's Evaluation Committee

PROF ZAINAL ALIMUDDIN B. ZAINAL ALAUDDIN
Dekan

Name : Pusat Pengajian Kejuruteraan Mekanik
Kampus Kejuruteraan

Date : Universiti Sains Malaysia
14300 Nibong Tebal, Pulau Pinang.



Signature and Stamp of Dean/ Director of PTJ

Name : PROF ZAINAL ALIMUDDIN B. ZAINAL ALAUDDIN
Dekan

Date : Pusat Pengajian Kejuruteraan Mekanik
Kampus Kejuruteraan

Universiti Sains Malaysia
14300 Nibong Tebal, Pulau Pinang.



Single-step scanner-based digital image correlation (SB-DIC) method for large deformation mapping in rubber



C.P. Goh^a, H. Ismail^b, K.S. Yen^a, M.M. Ratnam^{a,*}

^a School of Mechanical Engineering, Engineering Campus, Universiti Sains Malaysia, Nibong Tebal, Penang 14300, Malaysia

^b School of Materials and Mineral Resources Engineering, Engineering Campus, Universiti Sains Malaysia, Nibong Tebal, Penang 14300, Malaysia

ARTICLE INFO

Article history:

Received 27 May 2016

Received in revised form

27 July 2016

Accepted 19 August 2016

Keywords:

Single-step digital image correlation

Incremental digital image correlation

Natural rubber

ABSTRACT

The incremental digital image correlation (DIC) method has been applied in the past to determine strain in large deformation materials like rubber. This method is, however, prone to cumulative errors since the total displacement is determined by combining the displacements in numerous stages of the deformation. In this work, a method of mapping large strains in rubber using DIC in a single-step without the need for a series of deformation images is proposed. The reference subsets were deformed using deformation factors obtained from the fitted mean stress-axial stretch ratio curve obtained experimentally and the theoretical Poisson function. The deformed reference subsets were then correlated with the deformed image after loading. The recently developed scanner-based digital image correlation (SB-DIC) method was applied on dumbbell rubber specimens to obtain the in-plane displacement fields up to 350% axial strain. Comparison of the mean axial strains determined from the single-step SB-DIC method with those from the incremental SB-DIC method showed an average difference of 4.7%. Two rectangular rubber specimens containing circular and square holes were deformed and analysed using the proposed method. The resultant strain maps from the single-step SB-DIC method were compared with the results of finite element modeling (FEM). The comparison shows that the proposed single-step SB-DIC method can be used to map the strain distribution accurately in large deformation materials like rubber at much shorter time compared to the incremental DIC method.

© 2016 Elsevier Ltd. All rights reserved.

1. Introduction

The digital image correlation (DIC) method is widely used to obtain displacement and strain fields in various materials by comparing the digital images acquired before and after the deformation. The advantages of the DIC method are: (i) it is contactless and is, therefore, suitable for strain measurement in soft materials like rubber and biological tissues, (ii) the specimen surface preparation is simple, either it is unnecessary if the material is naturally textured or the speckle pattern can be created artificially, (iii) it provides full-field displacement and strain thus enabling the mapping of non-uniform deformation.

In the DIC method the random speckle pattern on the specimen surface is used to perform the tracking between the reference (undeformed) image and the deformed image. A predefined subset that has a unique speckle pattern is selected from the reference image as the reference subset. The reference subset is used to track the area of the highest similarity of speckle patterns in the

deformed image. A correlation criterion is predefined to evaluate the degree of similarity between the reference subset and the subset on the deformed image. The tracking process is completed once the position of a subset with the highest correlation coefficient is detected in the deformed image. Errors in the displacement can occur if there is de-correlation or a mismatch between the speckle patterns from the reference and the target subsets. This usually occurs in cases where the deformation is large since the speckle patterns in the target subset are significantly distorted compared to the speckle patterns in the reference subset. The problem due to de-correlation can be overcome by acquiring and analysing a series of deformed images at different stages of loading to track large deformations. This approach, known as the incremental DIC method, has been used by several researchers for large deformation measurement. Fang et al. [1] used the incremental DIC method to obtain the stress-strain curve for polycarbonate-acrylonitrile butadiene styrene (PC/ABS) alloy up to 70% true strain. The authors investigated the non-homogeneity of the polymer at large deformations. De Almeida et al. [2] developed a 3-D incremental DIC method using a mirror placed at 45° to the side of the specimen relative to the camera. The mechanical

* Corresponding author.

E-mail address: mmaran@usm.my (M.M. Ratnam).

properties of impact-modified polypropylenes were studied up to 70% true strain. Han et al [3] compared the matching accuracy between the direct DIC method and the incremental DIC method. The results showed that the incremental DIC method yielded much better results compared to the direct DIC method. Hysteresis analysis and cyclic tensile tests were performed using the incremental DIC method up to 80% true strain.

Although the incremental DIC method is able to provide accurate displacement and strain measurement at large deformations, the limited field-of-view of the camera, which is fixed relative to the specimen, limits the range of strain that can be measured. Laraba-Abbes et al. [4,5] improved the conventional incremental DIC method by mounting the camera onto a motor driven micro-displacement stage so that the camera followed the study area of the specimen during loading. The mechanical characteristics of the carbon-black (CB) filled natural rubber (NR) up to 400% strain were studied using this new technique coupled with the incremental DIC method. Similar techniques were used by other researchers to study the various mechanical behaviours of soft materials [6,7]. Goh et al. [8] proposed a new incremental DIC technique by replacing the camera with a flatbed scanner as the image acquisition device so that the images of the specimens can be captured directly without the aid of a camera translation stage. This method, known as the scanner-based DIC (SB-DIC) method, was used to measure the Young's modulus of natural rubber (NR) up to 350% strain.

Although the incremental DIC method has been successfully applied in large deformation problems in the past, this approach has two main limitations: (a) cumulative errors in the displacement can arise from the error at each loading and deformation stage because the reference subset used for the tracking process in the current image is dependent upon the tracking accuracy in the previous stage, and (b) a large number of digital images must be recorded and analysed at each deformation stage, thus increasing the total computation time needed to complete the strain mapping. Tang et al. [9] proposed a large deformation measurement scheme by combining an improved coarse search method and updating the reference image to study the large tensile deformation of polymeric material up to 450% strain. This method, however, requires information from a series of deformation images to 're-shape' the reference subset for the tracking process, thus slowing down the tracking process.

The objective of this work is to develop a single-step SB-DIC

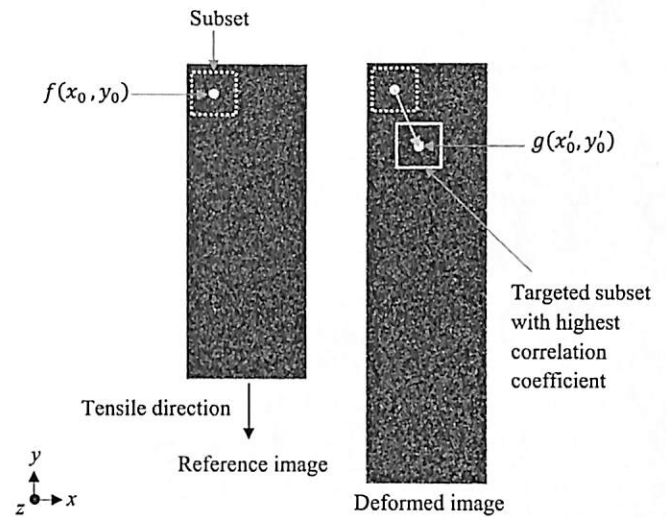


Fig. 1. Conventional DIC principle.

deformed in tension and compared with the resultant strain maps obtained from FEM.

2. Methodology

2.1. The DIC principle

In the DIC method the random speckle pattern in a predefined reference subset is correlated with the deformed image. Fig. 1 shows simulated speckle images before and after deformation. A square reference subset with a predefined size centred at point f is first selected. The tracking process is carried out to find the location of a subset centred at point g that gives the highest correlation coefficient. The displacement and direction from the point f to g gives the in-plane displacement vector. The correlation coefficient is computed by using either the cross-correlation (CC) criterion or the sum-squared difference (SSD) correlation criterion [10]. In this work, the following normalized cross-correlation criterion (NCC) was adopted since the NCC is more stable than CC criterion [10]:

$$C_{NCC} = \sum_{i=-M}^M \sum_{j=-M}^M \left[\frac{f(x_i, y_j)g(x'_i, y'_j)}{\left(\sqrt{\sum_{i=-M}^M \sum_{j=-M}^M [f(x_i, y_j)]^2} \right) \left(\sqrt{\sum_{i=-M}^M \sum_{j=-M}^M [g(x'_i, y'_j)]^2} \right)} \right] \quad (1)$$

method for large deformation mapping without the need for a series of deformation images. The reference subset from the undeformed image is reshaped using deformation factors before correlating with the deformed images. The deformation factors were extracted from the mean stress-axial stretch ratio curve obtained from the standard tensile test and the theoretical Poisson function. The single-step SB-DIC method was applied on natural rubber specimens and the axial strains obtained were compared with those from the incremental SB-DIC method up to 350%. In addition, the resultant strain maps of two rectangular rubber specimens containing a circular hole and a square hole were

where $f(x_i, y_j)$ is the pixel value in the reference image while $g(x'_i, y'_j)$ is the pixel value in the deformed image. For the tensile tests of the dumbbell-shaped rubber specimens the correlation was performed by matching 66 subsets (six in the x -direction and 11 in the y -direction). Each reference subset was stepped in the horizontal and vertical directions by 20 pixels and 50 pixels, respectively. Whereas, for the tensile tests on the rectangular rubber specimens containing holes the correlation was performed by matching 1830 subsets (30 in the x -direction and 61 in the y -direction). Each reference subset was stepped in the horizontal and vertical directions by 42 pixels and 26 pixels, respectively. The size

of the reference subsets used in the SB-DIC method was chosen carefully as it influences the accuracy of the displacement measurement. The size of the reference subset is dependent upon the average size of the speckle patterns generated on the specimen [11]. Since the average size of the speckles produced on the rubber specimen was 10 pixels the reference subset size of 31×31 pixels was chosen for correlation process in the SB-DIC method.

2.2. Constitutive hyperelastic models for finite element modeling of rubber

Engineering materials such as metals are classified as linear elastic material where the strain can be obtained at a particular stress value provided the stiffness of the material is known. However, rubber-like materials are non-linear elastic materials which undergo strains that are several orders of magnitude higher than those of the linear elastic materials. Thus, the strain energy density function, i.e. the constitutive hyperelastic model, must be defined in order to obtain the desired stress-strain relationship. Before describing the constitutive hyperelastic models used in this study some terms need to be defined first. The stretch ratio is defined as:

$$\lambda = \frac{l_f}{l_0} = \frac{l_0 + \Delta l}{l_0} = 1 + \epsilon \tag{2}$$

where l_f is the final length of a specimen, l_0 is the initial length of the specimen, Δl is the elongation and ϵ is the engineering strain. Three principal stretch ratios, namely λ_1 , λ_2 and λ_3 , are used in defining the constitutive hyperelastic models, where λ_1 is the axial stretch ratio, λ_2 is the lateral stretch ratio and λ_3 is the stretch ratio used to define the thickness variation. The three strain invariants in terms of stretch ratios used to define the constitutive hyperelastic models are [12]:

$$\left. \begin{aligned} I_1 &= \lambda_1^2 + \lambda_2^2 + \lambda_3^2 \\ I_2 &= (\lambda_1\lambda_2)^2 + (\lambda_2\lambda_3)^2 + (\lambda_3\lambda_1)^2 \\ I_3 &= \lambda_1^2\lambda_2^2 \end{aligned} \right\} \tag{3}$$

The third invariant I_3 is equal to 1 if the material is incompressible [4,5].

The constitutive hyperelastic model is denoted as W which can be either a direct function of the principal stretch ratios or a function of the strain invariants, i.e. $W=W(\lambda_1, \lambda_2, \lambda_3)$ or $W=W(I_1, I_2, I_3)$. The engineering strain ϵ can be determined based on W [12]:

$$\epsilon = \frac{dW}{d\sigma} \tag{4}$$

where σ is engineering stress.

In this work, three different constitutive hyperelastic models, which are the Mooney-Rivlin two-parameter, Mooney-Rivlin five-parameter and Ogden three-parameter models, were used to predict the stress-strain behavior of a single-ended dumbbell-shaped structure with gage dimensions 33×6×2 mm in FEM using SolidWorks 2013 (Cosmos non-linear simulation) (Fig. 2(a)). The Mooney-Rivlin two-parameter and Mooney-Rivlin five-parameter models are defined, respectively, as [4,5]:

$$W_{(MR2)} = C_1(I_1 - 3) + C_2(I_2 - 3) \tag{5}$$

$$W_{(MR5)} = C_1(I_1 - 3) + C_2(I_2 - 3) + C_3(I_1 - 3)(I_2 - 3) + C_4(I_1 - 3)^2 + C_5(I_1 - 3)^3 \tag{6}$$

where C_1, C_2, C_3, C_4 and C_5 are the material constants generated in

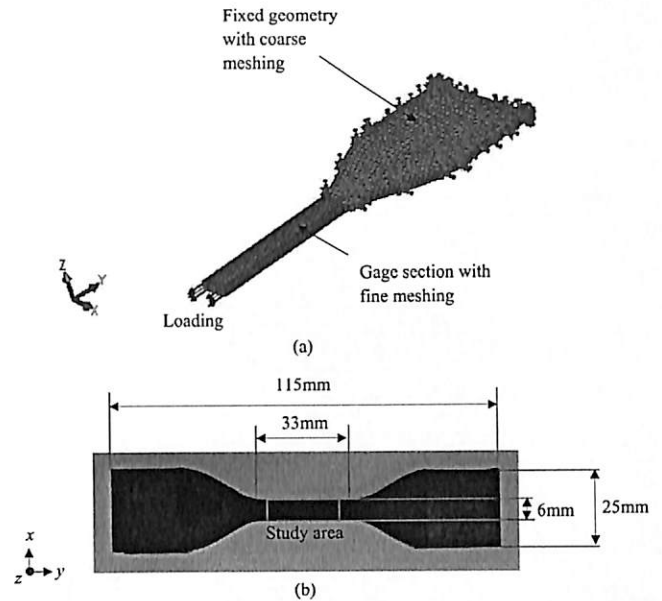


Fig. 2. (a) Single-ended dumbbell-shaped model used in finite element modeling and (b) dumbbell-shaped rubber specimen used in tensile tests.

the Cosmos non-linear simulation software using the experimental stress-strain data, obtained from the standard tensile tests on the dumbbell rubber specimens (Fig. 2(b)), and a predefined Poisson's ratio of 0.49. The Ogden three-parameter model is the only constitutive hyperelastic model which is expressed directly in terms of the principal stretch ratios and is defined as [12]:

$$W(\text{Ogden}) = \sum_{i=1}^n \frac{\mu_i}{\alpha_i} (\lambda_1^{\alpha_i} + \lambda_2^{\alpha_i} + \lambda_3^{\alpha_i} - 3) \tag{7}$$

where μ_i and α_i are the material constants also generated in the Cosmos non-linear simulation software using the experimental stress-strain data and Poisson's ratio of 0.49. The constitutive hyperelastic model which has the predicted stress-strain curve closest to the stress-strain curve obtained from the experimental standard tensile test was used to characterize the two rectangular models containing circular (Fig. 3(a)) and square (Fig. 3(c)) holes. The dimensions of the models were the same as the dimensions of the actual rubber specimens used in the SB-DIC experiments (Figs. 3(b) and (d)). The resultant strain maps obtained from the FEM were compared with the strains determined using the proposed single-step SB-DIC method for both rubber specimens.

2.3. Rubber specimen preparation

The composition of the specimen used to verify the proposed single-step SB-DIC method is listed in Table 1. The rubber was first masticated to reduce its high molecular weight and the other ingredients were added slowly into the rubber. The rubber was then vulcanized at 150 °C for six minutes. The vulcanizates were cut into the dumbbell-shaped specimens according to ISO37:2005 standard [13] with gage section dimensions of 33×6×2 mm (Fig. 2(b)). The stress-strain curves for five dumbbell-shaped rubber specimens were obtained using Instron 3366 (Instron Ltd., High Wycombe, UK) tensile test machine with crosshead speed of 500 mm min⁻¹ at room temperature. The mean stress-strain curve was obtained for two purposes: (i) determination of the deformation factor to reshape the reference subsets and (ii) determination of materials constants in the constitutive hyperelastic models. The specimen with the circular hole (Fig. 3(b)) was

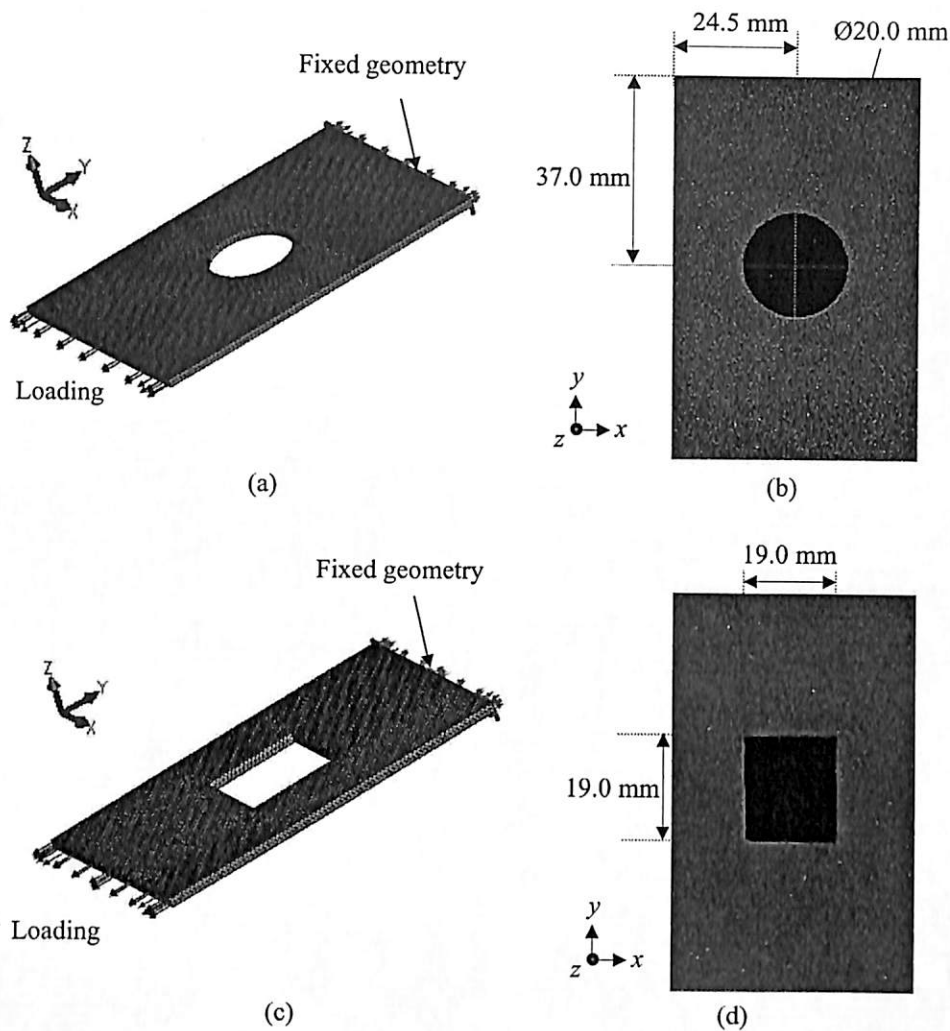


Fig. 3. (a) Circular-hole rubber model used in FEM, (b) circular-hole rubber specimen used in single-step DIC method (c) square-hole rubber model used in finite element modeling and (d) square-hole rubber specimen used in single-step DIC method.

Table 1
Composition of the natural rubber compounding.

Compositions	Parts per hundred rubber (phr)
Natural rubber (Standard Malaysia Rubber L-grade)	100.0
Zinc oxide (ZnO)	1.5
Stearic acid	1.5
N-cyclohexyl-benzothiazyl-sulphenamide (CBS)	1.9
N-isopropyl-N-phenyl-p-phenylenediamine (IPPD)	2.0
Sulfur	1.6
Total	108.5

prepared using a hole-punch with diameter of 20 mm while the specimen with the square hole (Fig. 3(d)) was prepared using a 19 mm chisel.

2.4. Experimental setup

The experimental setup of the single-step SB-DIC method and the customized loading rig used to load the specimen are shown in Fig. 4(a) and (b), respectively. The rubber specimen having a study area of 25×6 mm (Fig. 2(b)) was clamped onto the loading rig as

shown in Fig. 4(b). The clamping system was design and fabricated precisely to ensure that the surface of the specimen is parallel to the surface of the platen glass of the flatbed scanner, thus minimising any out-of-plane movement during loading. The rig was then placed onto a flatbed scanner (*Canoscan 5600F*). A stepper motor drive connected by a PR7 microcontroller was used to drive the gear train of ratio 2:1. The downward force F_d was exerted on the load applicator by rotating the lead screw attached to the gear train (Fig. 4(b)). The rotational motion of the lead screw was converted into linear motion of the load applicator. This was done by attaching two sliding rods on either side of the lead screw so that the rotational and linear motions in x - and z -directions are constrained. The restoring force F_s of the springs is of the same magnitude as the force applied onto the rubber specimen. The force applied onto the rubber specimen was determined from the two parallel springs mounted between the moveable clamp and the load applicator using the following equation,

$$F_s = (k_1 + k_2)x_{avg} \equiv k_{eq}x_{avg} \quad (8)$$

where k_1 and k_2 are the stiffness of the springs determined using the tensile testing machine, k_{eq} is the equivalent spring constant of the two parallel springs and x_{avg} is the average length of the springs obtained from the white indicators (Fig. 4(b)) by using image processing. The stress value σ used in the stress-strain curve

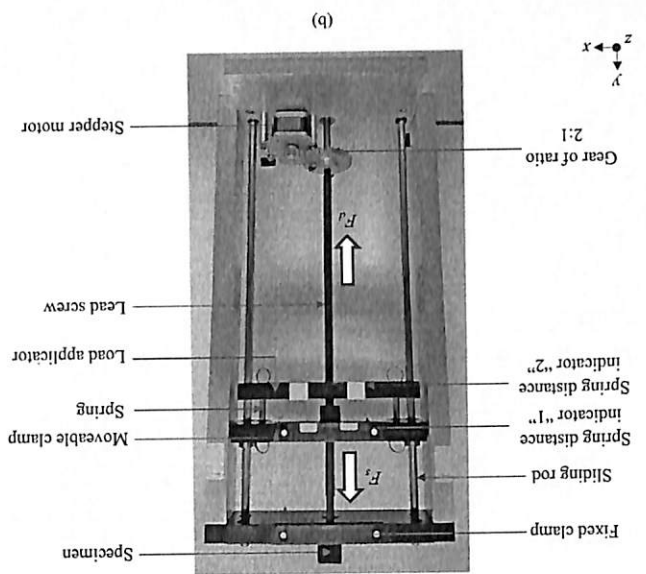
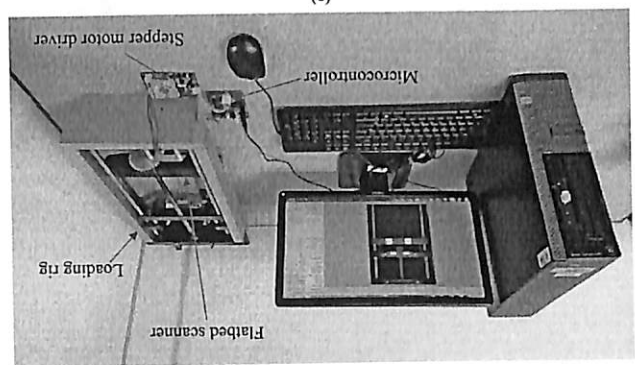


Fig. 4. (a) Experimental setup of single-step scanner-based DIC method and (b) motorized loading rig.

is the engineering stress which is defined as the force (Eq. (8)) divided by the original cross-sectional area of the rubber specimen. All the images of the specimens were captured using the scanner at a resolution of 600×600 dpi ($0.0423 \text{ mm pixel}^{-1}$). Calibration of the scanner was carried out since the rubber specimen was placed 5 mm above from the glass platen to prevent

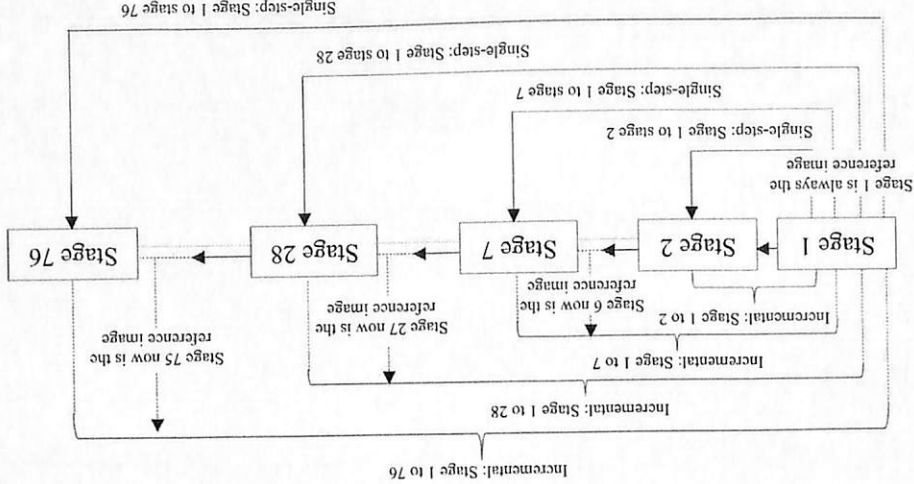


Fig. 5. Comparison of conventional incremental SB-DIC method and single-step SB-DIC method.

Fig. 7. Stress-axial stretch ratio curve obtained from standard tensile test.

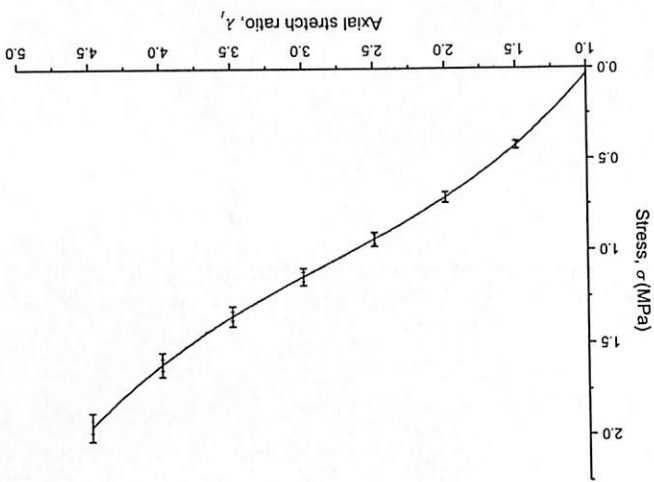
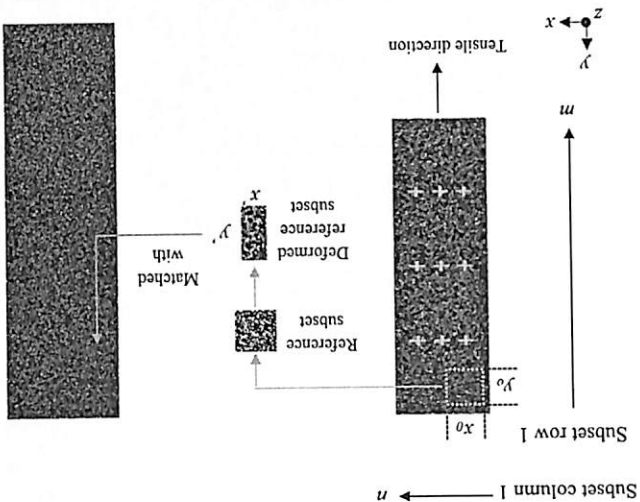


Fig. 6. Single-step correlation between shape-changed reference subset using mechanical properties of tested material.



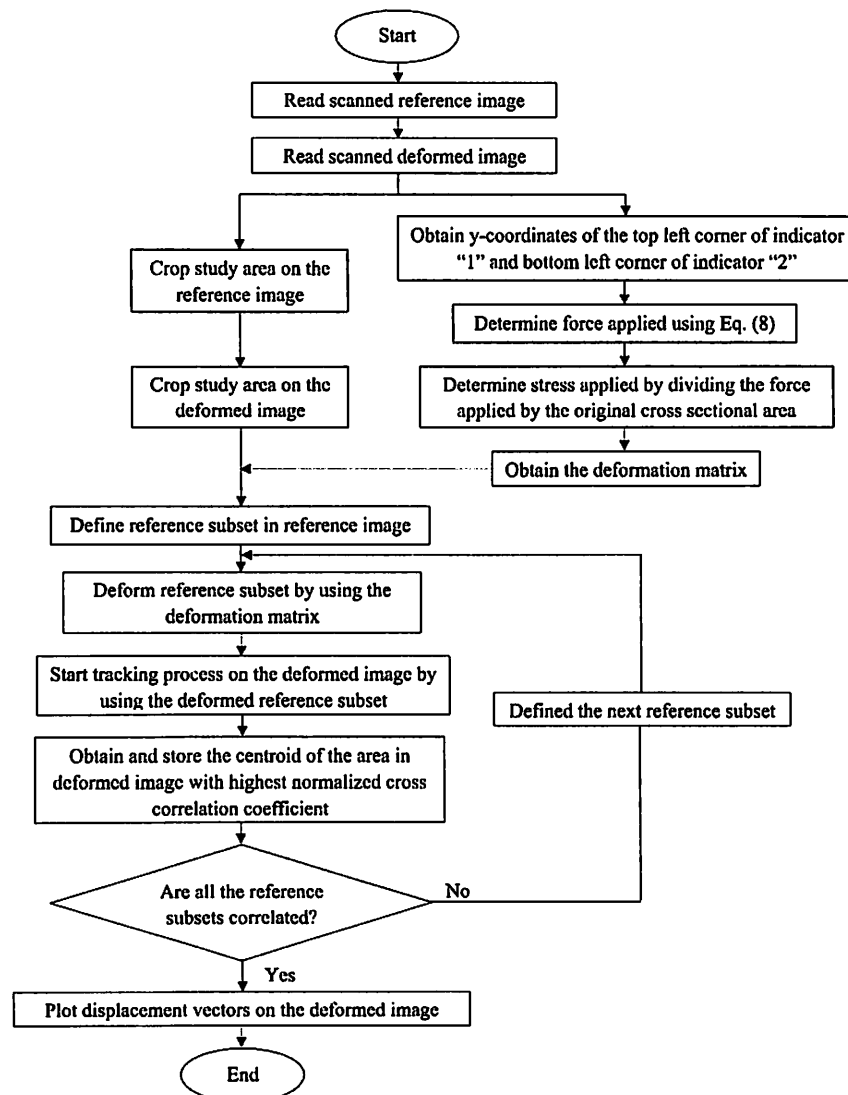


Fig. 8. Flowchart for the single-step SB-DIC algorithm.

results show that the actual scanning resolution of the flatbed scanner at 5 mm height is 588.19 dpi and 600.02 dpi in the horizontal (x) and vertical (y) directions, respectively, relative to the image plane. The in-plane displacement D_a in millimetres is given by:

$$D_a = \frac{d \times 25.4}{S} \quad (9)$$

where d is the displacement of the subset in pixels and S is the actual scanning resolution.

Although only two images, the un-deformed image (reference image) and deformed image at any loading stage, were needed to determine the displacement field using the proposed single-step SB-DIC method, the specimen was loaded incrementally up to 76 stages. Each load was applied to obtain 4–5% axial strain by controlling the stepper motor, with an image acquired at each loading stage. By doing so the axial strain (stretch ratio) values obtained using the single-step SB-DIC method can be compared with the results obtained from the conventional incremental SB-DIC method. The reference image in the incremental SB-DIC method was changed at each stage of tracking and the total displacement was determined by summing up the displacements at each stage

of loading. The difference between the incremental and the single-step method is illustrated in Fig. 5. For the rubber specimens containing circular and square holes the un-deformed specimen and the corresponding deformed specimen subjected to loads of 19.11 N and 10.18 N, respectively, were captured.

2.5. Single-step scanner-based digital image correlation method

2.5.1. Deformation factors from stress–strain curve and Poisson function

In the conventional DIC method the size of the target subset in the deformed image is approximately the same as that of the reference subset due to the small deformation at each stage. This method is accurate only when analysing rigid body translations and small deformations. At large deformations the reference subset size must be deformed or reshaped in order to track its corresponding location in the deformed image. Fig. 6 illustrates the image and its reference subset at the un-deformed and deformed states. The yellow dotted box is the reference subset of size $x_0 \times y_0$ which is deformed to $x' \times y'$. The deformed reference subset is then used to track the position on the deformed image having the highest correlation. In order to obtain the 2-D deformation

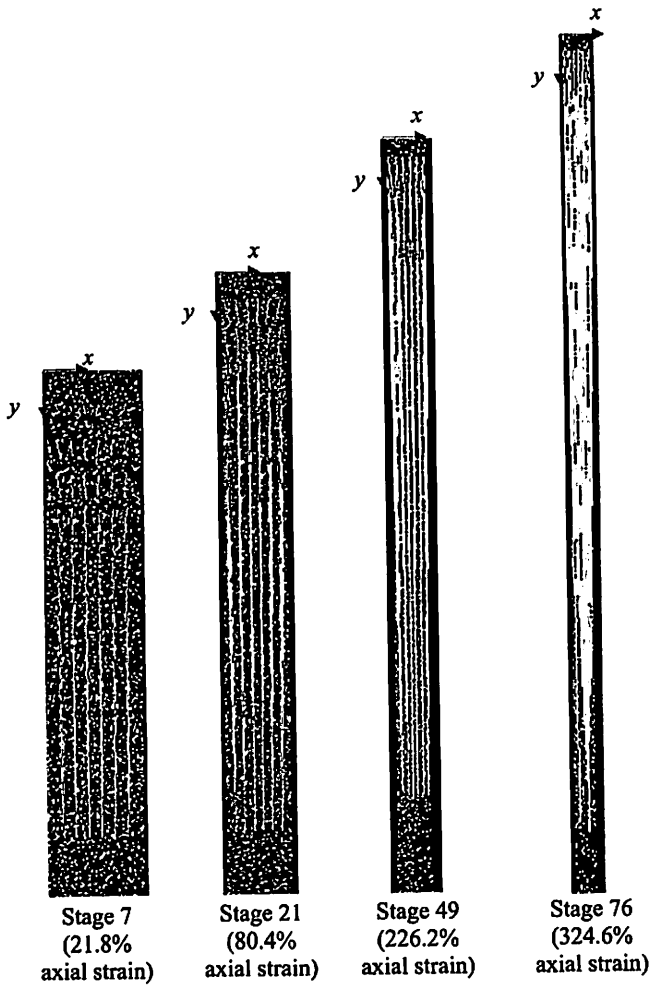


Fig. 9. 2-D displacement fields at Stages 7, 21, 49 and 76.

matrix F used to deform the reference subset the size of the reference subset was first represented by a vector \mathbf{a} which can be resolved into two components (i.e. i - and j -components). The reference subset is then assumed to be subjected to a uniform deformation such that F is uniform over the whole body. The size of the deformed reference subset is represented by vector \mathbf{b} . Vectors \mathbf{a} and \mathbf{b} are given by,

$$\mathbf{a} = x_0 \hat{i} + y_0 \hat{j} \quad (10)$$

$$\mathbf{b} = x' \hat{i} + y' \hat{j} \quad (11)$$

Thus, the mapping of the reference subset's vector to the deformed reference subset's vector is given by

$$\mathbf{b} = F \mathbf{a} \quad (12)$$

where F is the 2-D deformation factor which can be represented in matrix form as

$$F = \begin{bmatrix} \lambda_2 & 0 \\ 0 & \lambda_1 \end{bmatrix} \quad (13)$$

where λ_1 is the elongation deformation factor (equivalent to axial stretch ratio) and λ_2 is the lateral contraction deformation factor (equivalent to lateral contraction ratio). From Eqs. (13)–(13), the deformed reference subset can be represented in the matrix form as

$$\begin{bmatrix} x' \\ y' \end{bmatrix} = \begin{bmatrix} \lambda_2 & 0 \\ 0 & \lambda_1 \end{bmatrix} \begin{bmatrix} x_0 \\ y_0 \end{bmatrix} \quad (14)$$

A third order polynomial function given by the following equation was derived from the fitted mean stress–axial stretch ratio curve obtained from the standard tensile tests as shown in Fig. 7,

$$a\lambda_1^3 + b\lambda_1^2 + c\lambda_1 + d - \sigma = 0 \quad (15)$$

where a , b , c and d are constants and σ is the engineering stress. The polynomial function has one real root and two complex conjugate roots based on the cubic polynomial discriminant theorem at a particular of stress value [14]. The real root is the elongation deformation factor λ_1 which was used to obtain the Poisson's ratio ν from the theoretical Poisson function based on the engineering strain in terms of the axial stretch ratio for incompressible material given by [15]:

$$\nu = \frac{1}{(\lambda_1) + (\lambda_1)^{1/2}} \quad (16)$$

Also, the Poisson's ratio of any material can be defined as [15]

$$\nu = -\frac{(\lambda_2 - 1)}{(\lambda_1 - 1)} \quad (17)$$

Thus, at a particular point where $\lambda_1 = \lambda_1'$, the Poisson's ratio $\nu = \nu'$. By rearranging Eq. (17), the lateral contraction ratio λ_2' at a particular stress value σ' is reduced to

$$\lambda_2' = 1 - [\nu'(\lambda_1' - 1)] \quad (18)$$

Hence, the equation for the deformed reference subset in the matrix form is given by

$$\begin{bmatrix} x' \\ y' \end{bmatrix} = \begin{bmatrix} 1 - [\nu'(\lambda_1' - 1)] & 0 \\ 0 & \lambda_1' \end{bmatrix} \begin{bmatrix} x_0 \\ y_0 \end{bmatrix} \quad (19)$$

2.5.2. Tensile tests using single-step SB-DIC

A flow chart of the proposed single-step SB-DIC method is shown in Fig. 8. The study area in the reference image and deformed image were cropped after both images were read after scanning. The stress applied onto the rubber specimen was determined as explained in Section 2.4. The deformation matrix was then obtained from the third-order polynomial function derived from the fitted mean stress–axial stretch ratio curve and the Poisson function. The predefined reference subset was reshaped, i.e. deformed, using the deformation matrix with bi-cubic interpolation. The tracking process was started on the deformed image using the deformed reference subset. The centre coordinate of the area in the deformed image having the highest normalized cross-correlation coefficient was obtained and stored. The whole tracking and correlation process was completed once all the deformed reference subsets were correlated with the corresponding areas in the deformed image. Finally, the displacement vectors were drawn to obtain the full-field displacement.

3. Results and discussion

The 2-D displacement fields at loading stages 7, 21, 49 and 76 obtained from the SB-DIC on the dumbbell rubber specimens are shown in Fig. 9. The reference subsets were found to match accurately at deformations up to stage 28 (114% axial strain) but most of the vectors overlapped one another. The overlapping occurs because the displacement of the reference subset is higher

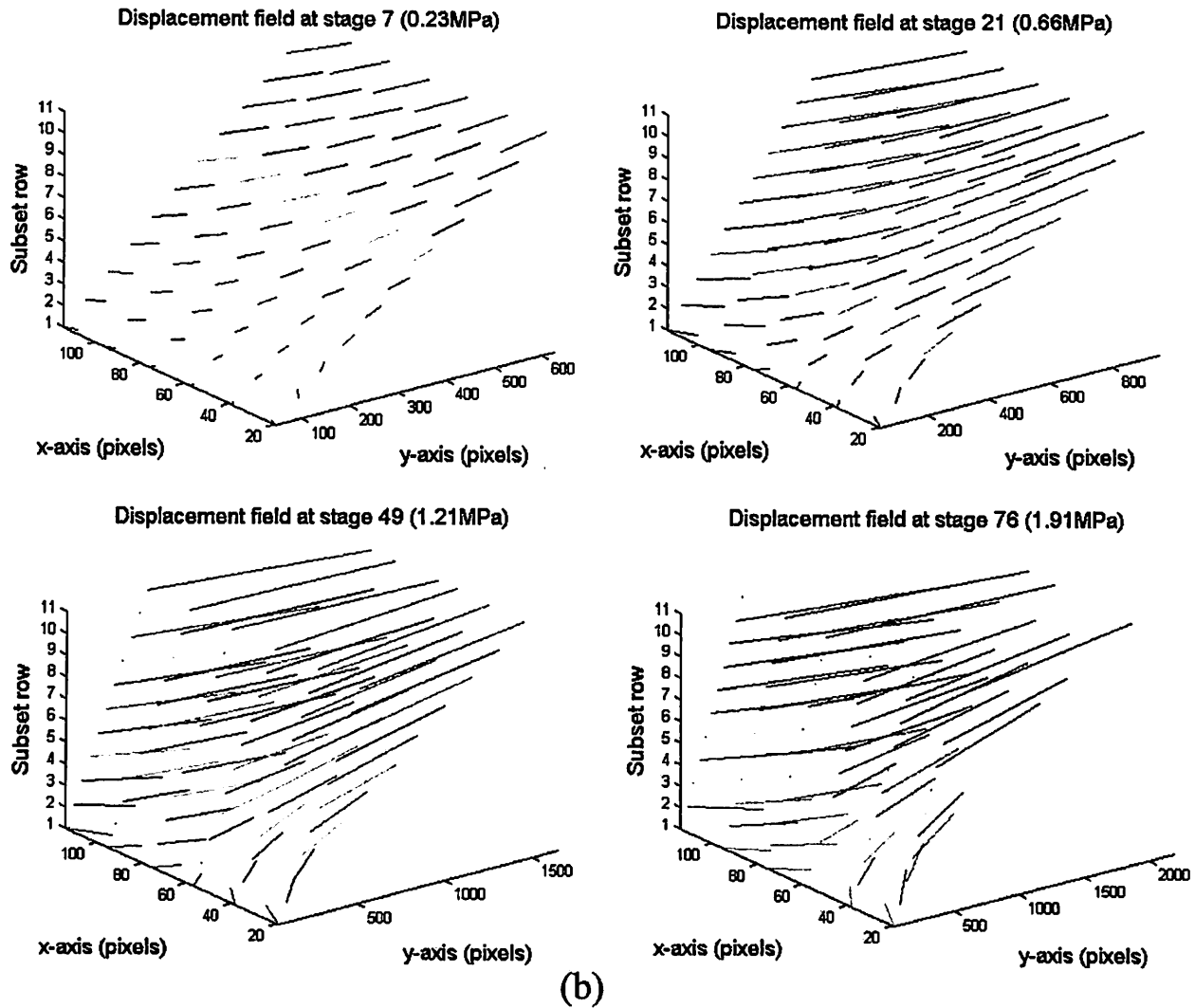


Fig. 10. 3-D representative of in-plane displacement field at Stages 7, 21, 49 and 76.

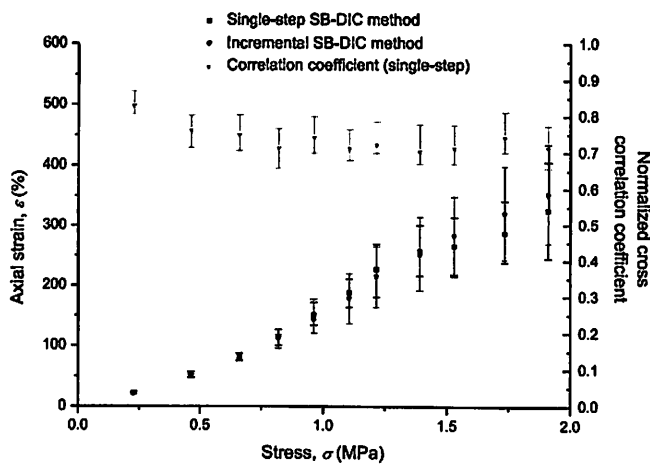


Fig. 11. Comparison of axial strain between incremental DIC and the single step SB-DIC and normalized cross correlation coefficient of single-step SB-DIC method.

Table 2
Comparison of mean axial strain between incremental DIC method and single-step DIC method.

Stage	Stress, σ (MPa)	Axial strain, ϵ (%)		
		Incremental DIC method	Single-step DIC method	Absolute deviation
7	0.23	21.1	21.8	3.3
14	0.46	50.3	51.1	1.6
21	0.66	82.6	80.4	2.7
28	0.82	112.1	114.3	2.0
35	0.96	143.2	150.5	5.1
42	1.10	178.4	187.5	5.1
49	1.21	214.3	226.2	5.6
56	1.39	251.2	256.4	2.1
63	1.53	282.5	264.7	6.3
70	1.73	320.6	286.3	10.7
76	1.91	351.4	324.6	7.6
Average				4.7

than the pre-defined centre location of the adjacent row of the reference subset. The 3-D representation of the 2-D displacement fields is shown in Fig. 10 to provide a better view of the deformation at the four stages. At deformations of more than 150%

axial strain (\geq stage 35) some of the deformed reference subsets failed to track the corresponding location on the deformed images. The mismatch displacement vectors were identified by using an outlier principle, whereby axial or lateral strains of more than 1.5 of the interquartile range below the first quartile or above the

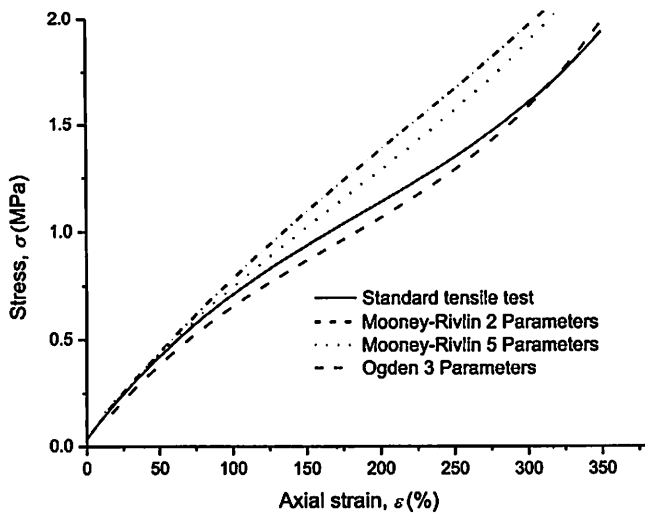


Fig. 12. Comparison of the fitted stress-strain curve between the three hyperelastic models and the standard tensile test.

third quartile were eliminated [16].

The comparison of the axial strain between the incremental SB-DIC method and the single-step SB-DIC method with normalized cross correlation coefficient is shown in Fig. 11. Since the accuracy of the incremental SB-DIC method was confirmed previously [8], this method was used as the reference to compare the results obtained from the newly developed single-step SB-DIC method. The range of the axial strains and normalized cross-correlation coefficients in Fig. 11 resulted from 66 reference subsets on a single rubber specimen image (6 subsets in the x -direction and 11 subsets in the y -direction). At deformations below 100% axial strain the range of the axial strain is small due to the homogeneous strain distribution. The reshaped (deformed) reference subsets were found to match accurately with their corresponding location on the deformed images. The mean normalized cross-correlation coefficient was between 0.75 (stage 21) and 0.83 (stage 7). The largest absolute deviation in the mean axial strain between the incremental SB-DIC method and the single-step SB-DIC method for deformations below 100% axial strain is 3.3% at stage 7 (Table 2). Above stage 28 the strain distribution has a larger range over the plane of the specimen. This is due to the non-uniform deformation in the specimen probably caused by the presence of voids in the rubber specimens as found in our previous study [8]. At regions where the voids are present the speckle patterns were slightly different compared to those on the deformed reference image. Nevertheless, due to the uniqueness of the speckle patterns in each subset the single-step SB-DIC method shows that deformed reference subsets were able to track the inhomogeneous strain distribution at stage 28 to stage 76. The maximum absolute deviation in the axial strain between the incremental SB-DIC method and the single-step SB-DIC method is 10.7% (at stage 70, $\sigma = 1.73$ MPa), while the average deviation for the entire loading range is 4.7%. The slightly larger deviation between the incremental SB-DIC method and single-step SB-DIC method observed at larger deformations (stages 63, 70 and 76) is suspected to be due to the accumulated errors introduced in the incremental SB-DIC method [9]. The normalized cross correlation coefficient in the single-step SB-DIC method has a decreasing trend with increase in stress (Fig. 11) probably due to the presence of voids in the rubber specimen, which causes unpredictable distortions in the speckle pattern a larger deformations. The displacement field and the axial strain data obtained from the single-step SB-DIC method, however, show that the proposed method is able to map the large

deformations in a single-step accurately.

3.1. Comparison with finite element modeling (FEM)

The comparison of the axial strain-stress graph between the fitted mean stress-strain data from the standard tensile test and the prediction of the three models (Mooney–Rivlin two-parameter, Mooney–Rivlin five-parameter and Ogden three-parameter models) is shown in Fig. 12. A third-order polynomial was used to fit the data from the standard tensile test and the FEM. At low deformations ($\leq 100\%$ axial strain) the stress-axial strain data predicted by FEM using the Mooney–Rivlin two-parameter, Mooney–Rivlin five-parameter and Ogden three-parameter models are close to the stress-strain curve data obtained from the standard tensile test. However, at deformations higher than 100% axial strain the stress-axial strain data from the Mooney–Rivlin two-parameter and five-parameter models deviate from the standard tensile data. This is because the two models do not take into account the stiffening effects of the rubber with increasing strain [17]. The Ogden three-parameter model, however, produced good stress-axial strain prediction from FEM for the whole range up to 350% axial strain when compared to the tensile test data. Thus, the Ogden three-parameter model was selected as the best hyperelastic model to predict the deformation of the rubber specimen and to analyze the hole-containing rubber specimens. Comparisons of the resultant strain maps on the rubber specimens containing circular and square holes between the single-step SB-DIC method and the FEM are shown in Fig. 13. The un-deformed image was subdivided into 1830 subsets (30 subsets in x -direction and 61 subsets in y -direction) with the reference subset size of 31×31 pixels. The technique used to obtain the deformed reference subsets and the procedures to obtain the displacement field were same as that used in the tensile tests for the dumbbell-shaped rubber specimen. The resultant strain maps in each case show significant inhomogeneity caused by the holes. The discontinuity in the geometry causes the localized stress to increase above the average stress close to the geometry changes. For the circular-hole rubber specimen the stress concentration is dependent upon the polar coordinate references from the centroid of the circular hole relative to the direction of loading [18]. The sideways exterior edges of the circular hole have the maximal strain values (53% and 63% strain for single-step SB-DIC method and FEM, respectively) since the stress concentration is the highest at these areas. The upper and lower exterior edges of the circular hole have the minimum strain distribution (4% and 2% strain for single-step SB-DIC method and FEM, respectively) due to the lower stress concentration in these areas. For the square-hole rubber specimen the stress concentrations focus on the sharp corners of the square due to the abrupt change in the surface area [18]. Thus, the four sharp corners of the specimen have the maximum resultant strains (18% and 17% strain for single-step SB-DIC method and FEM, respectively). The strain distribution for the circular-hole containing model predicted by FEM is slightly higher compared to those obtained from the single-step SB-DIC method. This is because the predicted stress-strain curve for the rubber model (Ogden three-parameter model) is offset to the right from the stress-strain curve obtained from the standard tensile test between 25% and 300% strain. Thus, at a particular stress value within 25% and 300% strain, the rubber model experiences larger deformation compared to the actual specimen in the single-step SB-DIC method. The strain distribution for the square-hole rubber specimen is similar to that of the FEM since the stress-strain curve predicted by FEM using the Ogden model is very close to that obtained from the tensile test for axial strains up to 25%.

3.2. Processing time comparison between single-step SB-DIC method

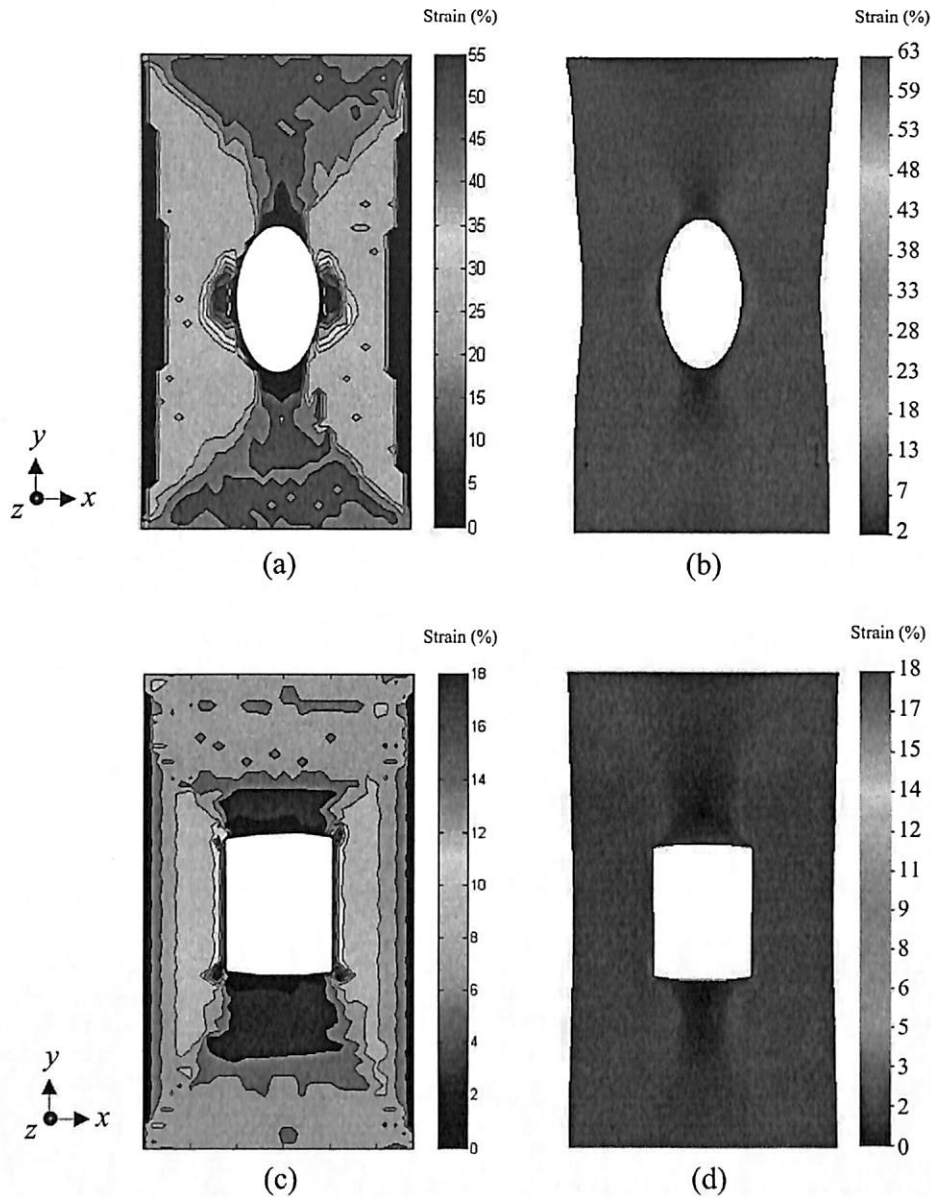


Fig. 13. Comparison of resultant strain maps of circular-hole rubber specimen and square-hole rubber specimen between single step DIC method and FEM.

and incremental SB-DIC method

The processing time of the SB-DIC method is the sum of the loading-image acquisition time and the DIC programme code running time. The loading time is the time taken to operate the microcontroller to turn the gear that moves the load applicator. The DIC programme code running time is the time taken to complete the tracking process and to obtain the results (i.e. displacement and strain field). The time taken was measured using a digital stopwatch. The total time taken of the incremental SB-DIC method for the loading-image acquisition process and the programme code running time for the 76 images are 33,684 s (9.36 h) and 3266 s (54.4 min) respectively. The time taken for the incremental SB-DIC method is cumulative since the particular image used for processing is dependent on the series of images before the current image. On the other hand, for the single-step SB-DIC method the time taken for the loading-image acquisition process and the programme code run are independent of the previous images. Thus, the processing time has been reduced significantly

compared to the incremental SB-DIC method. Although the acquired images are independent of one other the time taken for the loading-image acquisition process and programme code run increased with the number of images. This is because each of the loading stage is equivalent to 4–5% axial strain. In order to obtain large deformation image a higher load is required and thus the time taken for the loading-image acquisition process increases. In addition, as the deformed reference subset size increases as the loading increases, the time taken for the tracking process is longer at larger deformations. The maximum processing time for loading-image acquisition process and programme run are 233 s (3.88 min) and 309 s (5.15 min) respectively at image 76. The comparison of the total processing time taken between the single-step SB-DIC method and incremental SB-DIC method is shown in Fig. 14. The total processing time taken for the incremental SB-DIC method to obtain axial strains up to 350% is 36,950 s (10.3 h) which is 68 times higher than the time taken for the single-step SB-DIC method (0.15 h).

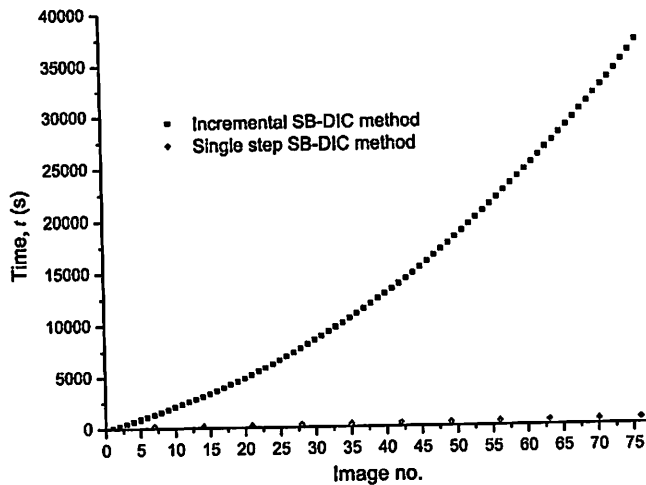


Fig. 14. Comparison of processing time between incremental DIC method and single-step DIC method.

4. Conclusion

A direct large deformation mapping method, namely the single-step SB-DIC method, is proposed to measure large deformations without the use of a series of incremental deformation images. The factors used to reshape (deform) the reference subsets were determined from the experimental tensile test data for the rubber material and the theoretical Poisson function. The single-step SB-DIC method enables the target subsets on the deformed image to be tracked directly using the deformed reference subsets without the use of the intermediate images. Dumbbell-shaped rubber specimens were tested to verify the proposed single-step SB-DIC method. Displacement and strain fields up to 350% axial strain have been successfully measured using the proposed single-step SB-DIC method. The mean deviation in the axial strain between the incremental SB-DIC and the proposed single-step SB-DIC method was found to be only 4.7%. The resultant strain maps on rubber specimens containing circular and square holes obtained from FEM using the Ogden three-parameter hyperelastic model show good agreement with those from the single-step SB-DIC method. The proposed method eliminates cumulative errors that can be introduced when using the incremental SB-DIC method and significantly reduces the processing time in image acquisitions and coding implementation.

Acknowledgement

The authors would like to thank Universiti Sains Malaysia for the offer of the Research University (RU) grant (1001/PMEKANIK/814182) that enabled this research to be carried out.

References

- [1] Fang QZ, Wang TJ, Li HM. Large tensile deformation behavior of PC/ABS alloy. *Polymer* 2006;47(14):5174–81.
- [2] De Almeida O, Lagattu F, Brillaud J. Analysis by a 3D DIC technique of volumetric deformation gradients: application to polypropylene/EPR/talc composites. *Compos Part A: Appl Sci Manuf* 2008;39(8):1210–7.
- [3] Han Y, Rogalasky AD, Zhao B, Hyock JK. The application of digital image correlation techniques to determine the large stress-strain behaviors of soft materials. *Polym Eng Sci* 2012;52(4):826–34.
- [4] Laraba-Abbes F, Jenny P, Piques R. A new 'Tailor-made' methodology for the mechanical behaviour analysis of rubber-like materials: I. Kinematics measurements using a digital speckle extensometry. *Polymer* 2003;44(3):807–20.
- [5] Laraba-Abbes F, Jenny P, Piques R. A new 'Tailor-made' methodology for the mechanical behaviour analysis of rubber-like materials: II. Application to the hyperelastic behaviour characterization of a carbon-black filled natural rubber vulcanizate. *Polymer* 2003;44(3):821–40.
- [6] de Crevoisier J, Besnard G, Merckel Y, Zhang H, Loisel FV, Caillard J, Bergehan D, Creton C, Diani J, Brieu M, Hild F, Roux S. Volume changes in a filled elastomer studied via digital image correlation. *Polym Test* 2012;31(5):663–70.
- [7] Jerabek M, Major Z, Lang RW. Strain determination of polymeric materials using digital image correlation. *Polym Test* 2010;29(3):407–16.
- [8] Goh CP, Ratnam MM, Ismail H. Large in-plane deformation mapping and determination of Young's modulus of rubber using scanner-based digital image correlation. *Exp Tech* 2015. <http://dx.doi.org/10.1111/ext.12170>.
- [9] Tang ZZ, Liang J, Xiao ZZ, Guo C. Large deformation measurement scheme for 3D digital image correlation method. *Opt Lasers Eng* 2012;50(2):122–30.
- [10] Pan B, Qian K, Xie H, Asundi A. Two-dimensional digital image correlation for in-plane displacement and strain measurement: a review. *Meas Sci Technol* 2009;20:062001.
- [11] Bornert M, Bremond F, Doumalin P. Assessment of digital image correlation measurement errors: methodology and results. *Exp Mech* 2009;49(3):353–70.
- [12] Ogden RW, Saccomandi G, Sgura I. Fitting hyperelastic models to experimental data. *Comput Mech* 2004;34(6):484–502.
- [13] ISO 37:2005 Standard: Rubber, vulcanized or thermoplastic – determination of tensile stress-strain properties.
- [14] Irving, Ronald S. *Integers, polynomials, and rings*. New York: Published Springer-Verlag, Inc.; 2004. p. 154–6.
- [15] Starkova O, Aniskevich A. Poisson's ratio and the incompressibility relation for various strain measures with the example of a silica-filled SBR rubber in uniaxial tension tests. *Polym Test* 2010;29(3):310–8.
- [16] Krzywinski M, Altman N. Points of significance: visualizing samples with boxplots. *Nat Methods* 2014;11:119–20.
- [17] Meunier L, Chagnon G, Favier D, Orgéas L, Vacher P. Mechanical experimental characterisation and numerical modeling of an unfilled silicone rubber. *Polym Test* 2008;27(6):765–77.
- [18] Pilkey WD, Pilkey DF. *Peterson's stress concentration factors*, 3rd ed.. Hoboken, New Jersey: Published John Wiley & Sons Inc; 2008. p. 180–4.

Large In-plane Deformation Mapping and Determination of Young's Modulus of Rubber Using Scanner-Based Digital Image Correlation

Experimental Techniques

June 2016, Volume 40, Issue 3, pp 1117–1127

- **Authors**
- **Authors and affiliations**
- C. P. Goh
- M. M. Ratnam
- H. Ismail

- C. P. Goh
 - 1
- M. M. Ratnam
 - 1
- H. Ismail
 - 2

1. 1.School of Mechanical Engineering University Sains Malaysia, Engineering Campus Penang Malaysia
2. 2.School of Materials and Mineral Resources Engineering University Sains Malaysia Penang Malaysia

Article

First Online:
26 April 2016

DOI (Digital Object Identifier): 10.1007/s40799-016-0113-x

Cite this article as:
Goh, C.P., Ratnam, M.M. & Ismail, H. Exp Tech (2016) 40: 1117. doi:10.1007/s40799-016-0113-x

- **Citations**

Abstract

We propose a novel scanner-based digital image correlation (DIC) method to determine the full-field in-plane displacement as well as the Young's modulus of elastomeric materials at strains up to 350%. A low-cost charged-couple device flatbed scanner was used as the image acquisition device instead of a digital camera in the conventional DIC method. A motorized loading fixture was designed to act as the specimen clamp as well as the tensile load applicator. The rubber specimens were made according to the ASTM:D412-06a standard and mounted into the fixture. Each specimen was scanned at increasing loads and the images were processed to obtain the full-field displacement maps using incremental cross-correlation algorithm. The Young's modulus of the rubber at strains of 50–350% obtained using the scanner-based DIC method was compared with those obtained from a universal tensile test machine. The comparison shows a maximum deviation in Young's modulus of 8.9 at 150% strain. The high-resolution flatbed scanner coupled with the built-in lighting was found to be an effective tool for low-cost DIC application for large deformation materials.

Keywords

Digital image correlation Large deformation Scanner Rubber

References

1. 1. Passieux, J.-C., Bugarin, F., David, C., Périé, J.-N., and Robert, L., "Multiscale Displacement Field Measurement Using Digital Image Correlation: Application to the Identification of Elastic Properties," *Experimental Mechanics* 55: 121–137 (2015). [CrossRef](http://dx.doi.org/10.1007/s11340-014-9872-4) (<http://dx.doi.org/10.1007/s11340-014-9872-4>) [Google Scholar](http://scholar.google.com/scholar_lookup?title=Multiscale%20Displacement%20Field%20Measurement%20Using%20Digital%20Image%20Correlation%20Application%20to%20the%20Identification%20of%20Elastic%20Properties&author=J.-C.%20Passieux&publication_year=2015) (http://scholar.google.com/scholar_lookup?title=Multiscale%20Displacement%20Field%20Measurement%20Using%20Digital%20Image%20Correlation%20Application%20to%20the%20Identification%20of%20Elastic%20Properties&author=J.-C.%20Passieux&publication_year=2015)
2. 2. Ahn, B., and Nutt, S.R., "Strain Mapping of Al–Mg Alloy with Multi-scale Grain Structure Using Digital Image Correlation Method," *Experimental Mechanics* 50: 117–123 (2010). [CrossRef](http://dx.doi.org/10.1007/s11340-008-9211-8) (<http://dx.doi.org/10.1007/s11340-008-9211-8>) [Google Scholar](http://scholar.google.com/scholar_lookup?title=Strain%20Mapping%20of%20Al%20Mg%20Alloy%20with%20Multi-scale%20Grain%20Structure%20Using%20Digital%20Image%20Correlation%20Method&author=B.%20Ahn&author=SR.%20Nutt&journal=Experimental%20Mechanics&volume=50&pages=117-123&publication_year=2010) (http://scholar.google.com/scholar_lookup?title=Strain%20Mapping%20of%20Al%20Mg%20Alloy%20with%20Multi-scale%20Grain%20Structure%20Using%20Digital%20Image%20Correlation%20Method&author=B.%20Ahn&author=SR.%20Nutt&journal=Experimental%20Mechanics&volume=50&pages=117-123&publication_year=2010)
3. 3. Chen, J.L., Zhan, N., Zhang, X.C., and Wang, J.X., "Improved Extended Digital Image Correlation for Crack Tip Deformation Measurement," *Optics and Lasers in Engineering* 65: 103–109 (2015). [CrossRef](http://dx.doi.org/10.1016/j.optlaseng.2014.06.010) (<http://dx.doi.org/10.1016/j.optlaseng.2014.06.010>) [Google Scholar](http://scholar.google.com/scholar_lookup?title=Improved%20Extended%20Digital%20Image%20Correlation%20for%20Crack%20Tip%20Deformation%20Measurement&author=J.L.%20Chen&author=N.%20Zhan&author=X.C.%20Zhang&author=J.X.%20Wang&publication_year=2015) (http://scholar.google.com/scholar_lookup?title=Improved%20Extended%20Digital%20Image%20Correlation%20for%20Crack%20Tip%20Deformation%20Measurement&author=J.L.%20Chen&author=N.%20Zhan&author=X.C.%20Zhang&author=J.X.%20Wang&publication_year=2015)
4. 4. Tang, Z.Z., Liang, J., Xiao, Z.Z., and Guo, C., "Large Deformation Measurement Scheme for 3D Digital Image Correlation Method," *Optics and Lasers in Engineering* 50: 122–130 (2012). [CrossRef](http://dx.doi.org/10.1016/j.optlaseng.2011.09.018) (<http://dx.doi.org/10.1016/j.optlaseng.2011.09.018>) [Google Scholar](http://scholar.google.com/scholar_lookup?title=Large%20Deformation%20Measurement%20Scheme%20for%203D%20Digital%20Image%20Correlation%20Method&author=ZZ.%20Tang&author=J.%20Liang&author=ZZ.%20Xiao&author=C.%20Guo&journal=Optics%20and%20Lasers%20in%20Engineering&volume=50&pages=122-130&publication_year=2012) (http://scholar.google.com/scholar_lookup?title=Large%20Deformation%20Measurement%20Scheme%20for%203D%20Digital%20Image%20Correlation%20Method&author=ZZ.%20Tang&author=J.%20Liang&author=ZZ.%20Xiao&author=C.%20Guo&journal=Optics%20and%20Lasers%20in%20Engineering&volume=50&pages=122-130&publication_year=2012)
5. 5. Laraba-Abbes, F., Jenny, P., and Piques, R., "A New 'tailor-made' Methodology for the Mechanical Behaviour Analysis of Rubber-like Materials: I. Kinematics Measurements Using a Digital Speckle Extensometry," *Polymer* 44: 807–820 (2003). [CrossRef](http://dx.doi.org/10.1016/S0032-3861(02)10071-8) ([http://dx.doi.org/10.1016/S0032-3861\(02\)10071-8](http://dx.doi.org/10.1016/S0032-3861(02)10071-8)) [Google Scholar](http://scholar.google.com/scholar_lookup?title=A%20New%20Tailor-made%20Methodology%20for%20the%20Mechanical%20Behaviour%20Analysis%20of%20Rubber-like%20Materials%20I.%20Kinematics%20Measurements%20Using%20a%20Digital%20Speckle%20Extensometry&author=F.%20Laraba-Abbes&author=P.%20Jenny&author=R.%20Piques&journal=Polymer&volume=44&pages=807-820&publication_year=2003) (http://scholar.google.com/scholar_lookup?title=A%20New%20Tailor-made%20Methodology%20for%20the%20Mechanical%20Behaviour%20Analysis%20of%20Rubber-like%20Materials%20I.%20Kinematics%20Measurements%20Using%20a%20Digital%20Speckle%20Extensometry&author=F.%20Laraba-Abbes&author=P.%20Jenny&author=R.%20Piques&journal=Polymer&volume=44&pages=807-820&publication_year=2003)
6. 6. Laraba-Abbes, F., Jenny, P., and Piques, R., "A New 'tailor-made' Methodology for the Mechanical Behaviour Analysis of Rubber-like Materials: II. Application to the Hyperelastic Behaviour Characterization of a Carbon-black Filled Natural Rubber Vulcanizate," *Polymer* 44: 821–840 (2003). [CrossRef](http://dx.doi.org/10.1016/S0032-3861(02)10071-8) ([http://dx.doi.org/10.1016/S0032-3861\(02\)10071-8](http://dx.doi.org/10.1016/S0032-3861(02)10071-8)) [Google Scholar](http://scholar.google.com/scholar_lookup?title=A%20New%20Tailor-made%20Methodology%20for%20the%20Mechanical%20Behaviour%20Analysis%20of%20Rubber-like%20Materials%20II.%20Application%20to%20the%20Hyperelastic%20Behaviour%20Characterization%20of%20a%20Carbon-black%20Filled%20Natural%20Rubber%20Vulcanizate&author=F.%20Laraba-Abbes&author=P.%20Jenny&author=R.%20Piques&journal=Polymer&volume=44&pages=821-840&publication_year=2003) (http://scholar.google.com/scholar_lookup?title=A%20New%20Tailor-made%20Methodology%20for%20the%20Mechanical%20Behaviour%20Analysis%20of%20Rubber-like%20Materials%20II.%20Application%20to%20the%20Hyperelastic%20Behaviour%20Characterization%20of%20a%20Carbon-black%20Filled%20Natural%20Rubber%20Vulcanizate&author=F.%20Laraba-Abbes&author=P.%20Jenny&author=R.%20Piques&journal=Polymer&volume=44&pages=821-840&publication_year=2003)
7. 7.



1 TECHNICAL ARTICLE

2
3 **Large In-plane Deformation Mapping and Determination**
4 **of Young's Modulus of Rubber Using Scanner-Based Digital**
5 **Image Correlation**
6

7 C. P. Goh¹, M. M. Ratnam¹, and H. Ismail²

8 AQI 9 1 School of Mechanical Engineering, Universiti Sains Malaysia, Penang, Malaysia

10 2 School of Materials and Mineral Resources Engineering, University Sains Malaysia, Penang, Malaysia

11

12

13

14 **Keywords**

15 Digital image correlation, Large deformation,
16 Scanner, Rubber

17 **Correspondence**

18 M. M. Ratnam,
19 School of Mechanical Engineering,
20 University Sains Malaysia,
21 Engineering Campus,
22 14300 Nibong Tebal,
23 Penang,
24 Malaysia
25 Email: mmaran@eng.usm.my

26 Received: January 23, 2015;
27 accepted: July 31, 2015

28 doi:10.1111/ext.12170

29

30

31

32

33

34

35

36

37

38

39

40

41

42

43

44

45

46

47

48

49

50

51

52

53

Abstract

We propose a novel scanner-based digital image correlation (DIC) method to determine the full-field in-plane displacement as well as the Young's modulus of elastomeric materials at strains up to 350%. A low-cost charged-couple device flatbed scanner was used as the image acquisition device instead of a digital camera in the conventional DIC method. A motorized loading fixture was designed to act as the specimen clamp as well as the tensile load applicator. The rubber specimens were made according to the ASTM:D412-06a standard and mounted into the fixture. Each specimen was scanned at increasing loads and the images were processed to obtain the full-field displacement maps using incremental cross-correlation algorithm. The Young's modulus of the rubber at strains of 50–350% obtained using the scanner-based DIC method was compared with those obtained from a universal tensile test machine. The comparison shows a maximum deviation in Young's modulus of 8.9 at 150% strain. The high-resolution flatbed scanner coupled with the built-in lighting was found to be an effective tool for low-cost DIC application for large deformation materials.

Introduction

The digital image correlation (DIC) method is an established noncontact optical tool for the mapping of in-plane displacements and strains in many different types of materials.^{1–3} The DIC setup is relatively simple, comprising one or more high-resolution digital cameras and a suitable lighting technique. A speckle pattern is created onto the specimen if it is not naturally textured. The images of the specimen before and after deformation are recorded and the speckle patterns are correlated with one another using predefined reference subsets to determine the displacement vectors. As the camera must remain fixed throughout the loading to avoid decorrelation in the speckle patterns, the maximum amount of deformation that can be mapped is usually limited to about 20%.⁴

The limitation of the conventional DIC method when applied to high-strain materials, such as polymer and rubber, is that large deformation can

cause the domain under study to go out of the field-of-view of the camera. Laraba-Abbes et al.^{5,6} solved this problem by mounting the camera onto a motor-driven micro-displacement stage so that the camera follows the same region under study as the lower clamp holding the specimen moved. Camera repositioning was done so that the previously recorded displacement data can be tracked and used as a reference for the next set of displacement data. Although this method enabled strains up to 500% to be measured, the limited field-of-view of the camera allowed only a small area of the specimen to be studied at any one time, thus requiring much time to analyze the whole specimen area. de Crevoisier et al.⁷ used a similar approach to solve the problem of specimens that are subjected to large deformation. The authors mounted the camera on an elevation stage so that the camera can be translated during the loading. This enabled the extent of strain measurement to be increased from 33 to 450%. The DIC analysis

1 provided the translation information to account for
 2 the change in the field-of-view, which was limited to
 3 about 15×5 mm at resolution of 4096×1400 pixels.
 4 Pan et al.⁸ used reliability-guided incremental DIC
 5 method to overcome the problem of decorrelation
 6 effects caused by large deformation in polymeric
 7 foam. The maximum strain was, however, limited
 8 to 36% while the field-of-view was approximately
 9 50×80 mm. A similar approach was used by Tang
 10 et al.⁴ for measurement of strains up to 450% in
 11 polymer material subjected to tensile load. The
 12 limited field-of-view allowed only the upper part
 13 of the specimen to be recorded for analysis at very
 14 high deformation. Jerabek et al.⁹ determined strain
 15 in polymeric material using the DIC method. Two
 16 high-speed cameras were mounted on a displaceable
 17 frame so that a fixed relative position of the cameras
 18 and the specimen can be maintained. The high focal
 19 length of the lens (105 mm), however, limits the area
 20 that can be observed.
 21 The problem caused by the limited field-of-view of
 22 the camera can be overcome by using a camera lens
 23 of a shorter focal length. This, however, reduces the
 24 image resolution as well as introduces optical distor-
 25 tions. An effective solution is to replace the camera
 26 with a standard flatbed scanner and use a special
 27 loading rig to deform the specimen. Flatbed scanners
 28 use a single array of photo sensors and are capable
 29 of acquiring images at high resolutions over a large
 30 area, thus enabling the measurement of deformation
 31 over a large area. The built-in lighting in the scanner
 32 offers a significant advantage over the conventional
 33 DIC setup as no external lighting is needed. Several
 34 researchers have used the common flatbed scanner
 35 for various metrological applications such as paper
 36 area measurement,¹⁰ measurement of fine wire
 37 diameter,¹¹ crack length measurement,¹² measure-
 38 ment of nose radii of cutting inserts,¹³ topography
 39 measurement using shadow moiré¹⁴, and determi-
 40 nation of size distribution of broken rice kernels.¹⁵ In
 41 spite of the increasing application of the scanner in
 42 metrology, the potential of the low-cost, commonly
 43 available flatbed scanner for full-field in-plane dis-
 44 placement mapping of elastomeric material based on
 45 the DIC principle has not been investigated in the past.
 46 The objective of this study is to determine the
 47 in-plane displacements and strains in rubber using
 48 a low-cost CCD (charged-couple device) flatbed
 49 scanner as the image input device. From the strain
 50 and load applied, the Young's modulus of the rubber
 51 at various strain values were computed and compared
 52 with those obtained from the standard tensile test
 53 machine.

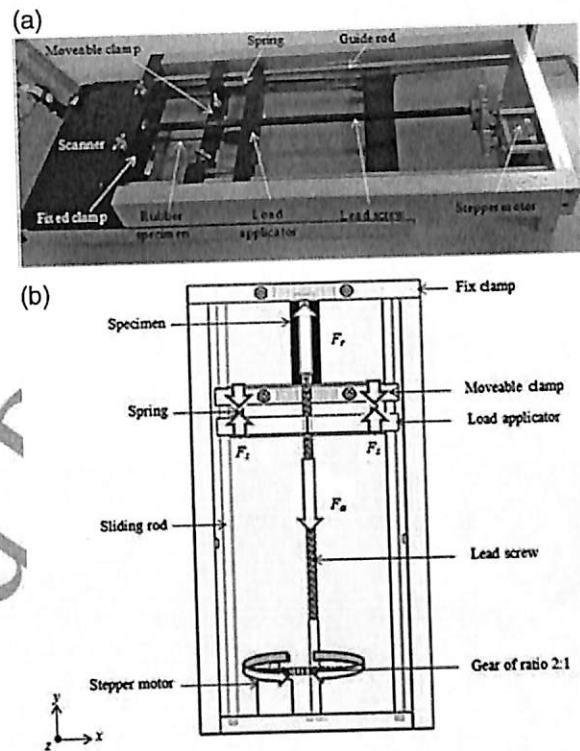


Figure 1 (a) Motorized loading rig on flatbed scanner and (b) schematic representation of working principle of loading fixture.

Methodology

Loading fixture design

The loading fixture shown in Fig. 1(a) was used to apply tensile load onto the rubber specimen. The fixture was placed horizontally on top of the scanner platen to obtain the reference and deformed images of the specimen. Figure 1(b) shows a schematic representation of the working principle of the motorized loading rig. The downward force (F_a) on the load applicator is exerted by rotating the lead screw which is attached on the gear train of ratio 2:1. A presetting stepper motor which was interfaced with a stepper motor driver and PR7 microcontroller was used to drive the gear train. Ball bearings were attached to both ends of the lead screw to constrain the translational motion and reduce frictional forces. The rotational motion of the lead screw was transformed into linear motion of the load applicator. Guide rods attached on both sides of the lead screw constrain the rotational motion of the load applicator as well as its linear motion in the x - and z -directions. The restoring forces (F_s) in the springs, which are attached between the load applicator and the

1 moveable clamp, are exerted in the direction opposite
 2 to the load applicator movement. The restoring force
 3 in the rubber specimen (F_r) and the downward
 4 force (F_a) exerted by the load applicator are of
 5 equal magnitudes and form an action–reaction pair.
 6 The force applied on the rubber specimen (F_r) was
 7 determined by calculating the total restoring forces in
 8 the two springs. The spring constants k_1 and k_2 were
 9 determined using a universal testing machine (Model:
 10 Instron 3367; Instron Ltd, High Wycombe, UK) as
 11 251.8 and 254.8 N/m, respectively. The average
 12 extension ($x_{avg.}$) of the two springs during the loading
 13 of the specimen in the scanner-based DIC setup was
 14 determined using the image processing steps outlined
 15 in section *Load application and image acquisition*.
 16 The load applied on the rubber specimen (F_r)
 17 is given by:

$$F_r = k_{eq} x_{avg.} \quad (1)$$

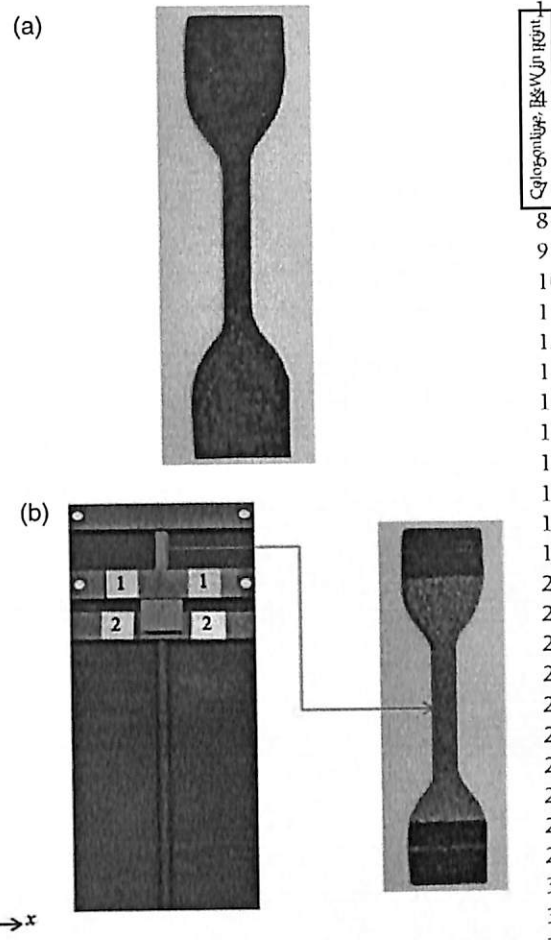
18 where the equivalent spring constant $k_{eq} = k_1 + k_2$.
 19
 20
 21

22 **Specimen preparation**

23 The rubber specimens were prepared according
 24 to the ASTM:D412-06a standard¹⁶ based on the
 25 compositions shown in Table 1. As natural rubber
 26 (NR) has very high molecular weight (MW), and
 27 therefore, high viscosity, it is difficult to mix any
 28 powder ingredients into it. In view of this, the NR
 29 material was softened by using a two-roll mill to
 30 reduce its MW. This process of softening by means
 31 of mechanical shearing is known as mastication.
 32 Mastication shortens rubber molecular chains which
 33 in turn results in a reduced MW and, hence, a
 34 reduced viscosity. These allow the compounding
 35 ingredients to be homogeneously distributed into
 36 the NR. A small piece of the masticated rubber was
 37 put into a rheometer (Model: MDR2000, Alpha
 38 Technologies, Heilbronn, Germany) to determine
 39 the vulcanization time for the subsequent process.
 40 After knowing the required vulcanization time the
 41
 42

43 **Table 1** Composition of rubber specimen

44 Compositions	45 Parts per hundred 46 rubber (phr)
47 Standard Malaysian Rubber L (SMR L)	100.0
48 Zinc oxide	1.5
49 Stearic acid	1.5
50 <i>N</i> -cyclohexyl-benzothiazyl-sulphenamide (CBS)	1.9
51 <i>N</i> -isopropyl- <i>N</i> -phenyl- <i>p</i> -phenylenediamine (IPPD)	2.0
52 Sulfur	1.6
53 Total	108.5



34 **Figure 2** (a) Rubber specimen before spraying and (b) scanned image
 35 showing part of the loading rig and rubber specimen.
 36

37 masticated rubber was put on the mold and placed
 38 in the vulcanization machine for 6 min at 150°C. The
 39 molded rubber was then cut into 10 dumbbell-shaped
 40 specimens according to the standard. A sample rubber
 41 specimen before spraying with white speckle pattern
 42 is shown in Fig. 2(a). Five of these specimens were
 43 used for the tensile test on Instron 3366 and another
 44 five were used in the DIC experiments. The speckle
 45 pattern on the rubber specimen was produced by
 46 using a matt-white aerosol spray. The average size
 47 of speckles was 10 pixels. Figure 2(b) shows a sample
 48 specimen with the speckle pattern and clamped onto
 49 the loading rig. The study area of the specimen in the
 50 DIC method is 25 × 6 mm. At the maximum strain of
 51 350% the maximum dimension obtained using the
 52 scanner is 112.5 mm. This value is 2.25 times longer
 53 than the maximum dimension used by Pan et al.⁸

1 Load application and image acquisition

2 The 2-D DIC analysis on the rubber specimens was
 3 carried out using a CCD flatbed scanner (CanoScan
 4 5600F), a personal computer (Intel Core i5, 3.20 GHz,
 5 8.00 GB RAM), and MATLAB 8.3 software for image
 6 processing. Each rubber specimen was clamped
 7 tightly onto the loading fixture. A pre-load was
 8 applied to ensure that the specimen surface is
 9 flat. The fixture was then placed on the scanner
 10 with the rubber specimen approximately 5 mm from
 11 the scanner platen surface. The fixture was covered
 12 using a black box to exclude ambient light. With the
 13 loading fixture placed on the scanner the available
 14 scanning area (field-of-view) is approximately
 15 120 × 215 mm when the specimen is stretched to
 16 the maximum. The scanned image showing part of
 17 the loading rig and the rubber specimen is shown in
 18 Fig. 2(b). The lengths of the springs before and after
 19 each loading were computed using image processing
 20 based on the white rectangular indicators shown
 21 in the figure. The "bounding box" command in
 22 MATLAB was used to identify the y -coordinates of
 23 the top left corner of indicator "1" (y_1) and bottom
 24 left corner of indicator "2" (y_2). The extension of each
 25 spring was determined by subtracting y_1 from y_2 . The
 26 average spring extension in pixels unit was converted
 27 into millimeters using a calibrated factor (see section
 28 *Calibration of flatbed scanner*) and the load applied to
 29 the specimen was determined using Eq. 1. One main
 30 problem in applying the DIC method on elastomeric
 31 materials is due to the inaccurate matching of subsets
 32 caused by the high elongation, thus leading to high
 33 distortions in the speckle pattern. Therefore, an incre-
 34 mental technique was used to analyze the images. In
 35 this method the displacement field is computed by
 36 considering two consecutive images obtained from a
 37 sequence of loading. The first image in the sequence
 38 was used as the reference image during the matching
 39 process. The specimen was stretched incrementally
 40 by applying small loads (equivalent to 4–5% strain of
 41 the original length) to the specimen by controlling the
 42 stepper motor. At each load the deformed image was
 43 scanned. The loading and scanning were continued in
 44 stages until the load applicator has reached the lower
 45 edge of the platen glass. Using this approach a total
 46 of 76 images including the undeformed specimen
 47 were scanned for a maximum strain of 350%. At the
 48 maximum strain the extended length of the specimen
 49 is 112.5 mm. A resolution of 600 dpi corresponding to
 50 an image resolution of 0.0423 mm/pixel was used to
 51 save computational time during the subset matching.
 52 The scanning was done manually.

1 The time taken for one loading cycle and the scan-
 2 ning of one image was 43 s. Thus, the total time taken
 3 to complete a single experiment is 55 min. The strain
 4 rate used was 0.045 per second which was obtained
 5 by controlling the rotational speed of the stepper
 6 motor using the microcontroller. The strain rate was
 7 determined by dividing the maximum global strain
 8 by the total time taken for the loading. Although
 9 the strain rate used in the tensile test experiments
 10 was 0.75 per second, which was 16.7 times higher
 11 than that used in the proposed method, the strain
 12 rate does not affect the stress–strain behavior of
 13 rubber provided these are not exceedingly high. Song
 14 et al.¹⁷ studied the effect of strain rate on elastomeric
 15 material and showed that the strain rate has no
 16 significant effect on stress–strain behavior at small
 17 strain rates. Large discrepancies were observed only
 18 at very high strain rates (3300 per second).

19 Five rubber specimens from the same batch were
 20 used in the scanner-based DIC experiment. The
 21 average stress–strain behavior and Young's modulus
 22 at various strains were compared with the average
 23 values from another five specimens using the Instron
 24 3366 universal tensile test machine.

25 Processing of the acquired images

26 The matching of the subset in the reference image
 27 to the deformed image was carried out using an
 28 algorithm coded in MATLAB. The degree of similarity
 29 between the reference and deformed subsets was
 30 evaluated using the simple cross-correlation (CC)
 31 criterion.¹⁸ A subset that has maximum correlation
 32 shows the new location of the object surface point
 33 after loading. The CC value for an $M \times M$ subset
 34 matching is given by:

$$C_{CC} = \sum_{i=-M}^M \sum_{j=-M}^M f(x_i, y_j) g(x'_i, y'_j) \quad (2)$$

35 where $f(x_i, y_j)$ is the subset in the un-deformed
 36 image, while $g(x'_i, y'_j)$ is the subset in the deformed
 37 image.

38 A flow chart of the algorithm used to process the
 39 images is shown in Fig. 3. The algorithm enables
 40 auto-cropping of the area of interest followed by
 41 subset matching before and after deformation.
 42 A virtual grid was superimposed onto the specimen
 43 image before loading and each subset within the
 44 grid was correlated with the image after loading.
 45 Figure 4 shows the region of interest (ROI) of the
 46 reference image with a superimposed virtual subset.
 47 The yellow dot is the center point of the subset that
 48 is used as the starting point to plot the displacement
 49
 50
 51
 52
 53

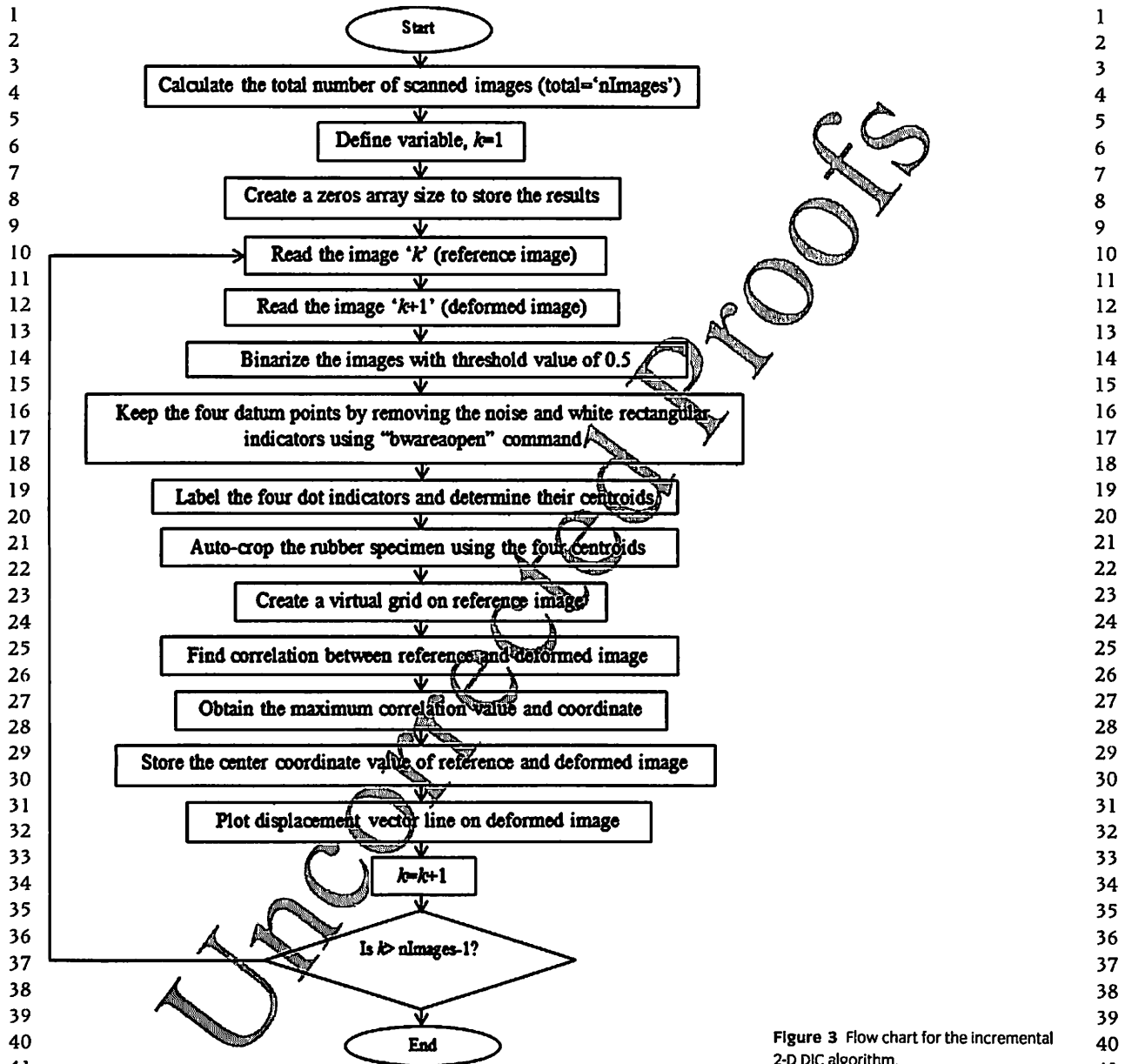


Figure 3 Flow chart for the incremental 2-D DIC algorithm.

vector. The scanning process was started from the left of the first row followed by the subsequent rows till the bottom right corner of the last row. The maximum correlation coefficient and the pixel coordinate of the subset center point having the highest correlation coefficient were determined. Finally, the displacement vector was drawn by using the stored center points having the highest correlation coefficient before and after deformation. A full-field displacement map was obtained by repeating the matching process of the other 23 subsets (three

subsets in each row with a total of eight rows). The second image which is used as the deformed image in the first incremental matching process is used as a new reference image when correlating with the third image (second deformed image). The process was completed once the last scanned image is correlated. The strain experienced by the specimen during each loading was computed using the following equation:

$$\epsilon = \frac{l_f - l_i}{l_i} = \frac{\Delta l}{l_i} \quad (3)$$

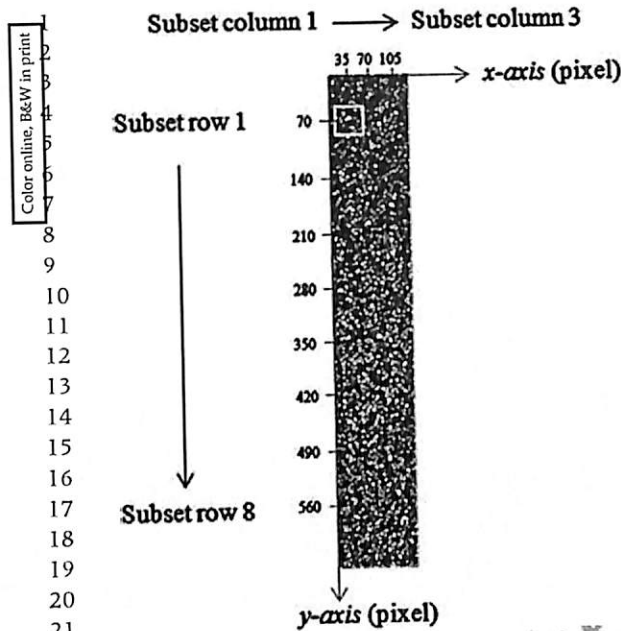


Figure 4 Subset superimposed on ROI used in matching process to obtain displacement vector.

where l_i is the initial length given by the distance of the centroid of each subset from the reference end, l_f is the corresponding final length, and Δl is the elongation. The global strain of the specimen was obtained from the average value of total local strains in the specimen at each applied load.

Scanner calibration and reliability test on motorized load applicator

Calibration of flatbed scanner

To avoid friction between the rubber specimen and the glass platen, during loading a 5-mm gap was introduced between the surface of the rubber specimen and glass platen. As the scanned object was lifted 5 mm above the glass platen, calibration of flatbed scanner was carried out to obtain the resolution at this height. A standard fixed frequency target was placed on nine sets of 5 mm gage blocks and scanned using a nominal resolution of 600 dpi. The mean resolutions in the horizontal and vertical directions (relative to the image) for three different sizes of dots are shown in Table 2. The in-plane displacement, D_a in millimeters, is given by:

$$D_a = \frac{d}{S/25.4} \quad (4)$$

where d is the displacement of the subset in pixels and S is the scanning resolution at a height of 5 mm.

Table 2 Scanning resolution when specimen is lifted 5 mm from measuring plane (nominal scanning resolution of 600 dpi)

Dot sizes on calibration target	Orientation	
	Horizontal (DPI)	Vertical (DPI)
Large	588.05	599.99
Medium	588.34	600.04
Small	588.18	600.04
Mean	588.19	600.02

Reliability of motorized load applicator

The reliability of the motorized load applicator was assessed in terms of the effectiveness of the clamping system and the force transmission efficiency. Ensuring good clamping is crucial because a small slippage in the rubber specimen will cause large errors in the displacement and strain values. A standard procedure was adopted to tighten the wing nuts when mounting the rubber specimens. The DIC method was used to investigate the existence of slippage in the rubber specimen. The wing nuts were at first rotated through two rotations by hand and then tightened by another two rotations using a tool. The loading fixture was then placed on the scanner and the rubber specimen having a speckle pattern was stretched to the maximum length of the platen glass of flatbed scanner. The stretched specimen was scanned as the reference image. Another nine images were scanned every ten minutes without disturbing the experiment setup. The experiment was repeated for another two different rubber specimens. The slipping displacements were then computed using the DIC method. The ROI studied is shown at Fig. 4. The three subsets used to compute the slipping displacements were the top (i.e. from pixel 133 to 183), center (i.e. pixel 290–340), and bottom (i.e. 450–500) regions. The displacement results show that there was zero displacement for the first 80 min. A small displacement (e.g. 0.0282 mm) occurred after 80 min due to the creep effect of rubber itself. Therefore, the clamping system is concluded to be firm enough to clamp the specimen and slippage effect can be neglected as the experiment for tensile test on the rubber was done within 60 m.

The force applied on the rubber specimen was determined by the restoring force induced by the springs attached to the load applicator. However, it is not possible to transmit the restoring force of springs fully to the rubber specimen as some of the forces will be lost due to friction in the moving parts of the loading rig. Therefore, the force transmission ratio was determined and used as a scaling factor to obtain

Table 3 Percentage of successfully matched subsets

Subset size	Number of successfully matched subsets out of 24 subsets	Percentage of successfully matched subsets (%)
11 × 11	8	33.33
31 × 31	14	58.33
51 × 51	24	100.00
71 × 71	24	100.00

the net force applied to the rubber. A calibrated spring ($k = 282.2 \text{ N/m}$) was clamped as a specimen to determine the output force. The loading fixture was placed on the flatbed scanner without applying any load. Next, 10 rotations were applied to the motor to stretch the spring and image of the loading rig with stretched springs was scanned. The stretching and scanning processes were repeated until a total six of images were scanned. This experiment was repeated for another two sets of readings using the same springs. The result showed that 97% of restoring forces from springs were transmitted to the specimens.

Subset size determination

Determination of the reference subset size is an important step in the DIC method because the size of the subset influences the accuracy of the displacement values. Smaller subsets lead to shorter computation time while larger subsets produce more accurate results.¹⁸ However, the size of the subset chosen depends largely on the mean size of the speckle pattern generated on specimen. Thus, the subset sizes used for the matching process must not be less than 10 pixels as the mean speckle size was 10 pixels. A test was conducted to determine the suitable subset size for matching process at the load of 0.0489 MPa. The four subset sizes tested were 11×11 , 31×31 , 51×51 , and 71×71 pixels. The results (Table 3) show that the higher the subset size used for matching, the higher the percentage of successfully matched subsets; but the use of large subsets size slows down the matching process. As a compromise between the computation time and accuracy the subset size 51×51 pixels was used in subsequent experiments.

Results and Discussion

Displacement vector field

The 2-D displacement field superimposed onto the specimen and plotted separately is shown in Fig. 5. At lower loads (0.0515 N) (Fig. 5(a)), the displacement field can be seen clearly but most of the vector

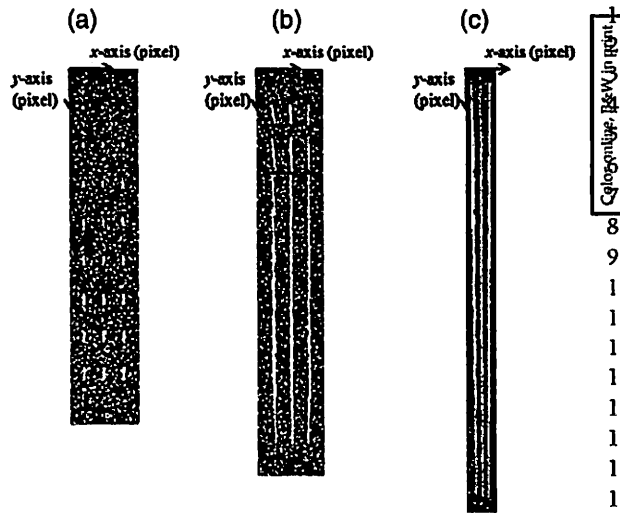


Figure 5 2-D displacement field at loads of (a) 0.0515 MPa (b) 0.3175 MPa and (c) 1.4869 MPa.

overlapped at higher loads (0.3175 MPa) as seen in Fig. 5(b). All displacement fields overlapped each other at the highest load of 1.4869 MPa (Fig. 5(c)). This is because the displacements of local subsets were higher than the pre-defined center position of local subset in the subsequent rows. The asymmetry of displacement field between the left and right sides of the specimens observed in Fig. 5(b) and (c) is caused by the slight offset of the specimen axis compared to that of the clamp axes. This offset will not affect the strain–stress data as the magnitude of the vector component in the tensile direction was used in the strain computation. The 3-D displacement field in Fig. 6(a) and (b) provides a better visualization of the deformation of the elastomeric material.

Comparison of stress–strain results from DIC method with that of tensile test machine

The mean stress–strain behavior of the DIC method from five rubber specimens was compared with those obtained from the tensile test machine (Instron). The mean stress–strain curves from both methods were plotted by best fitting the mean results obtained from the five rubber specimens using polynomial degree of three (Fig. 7). Table 4 shows the comparison of Young's modulus at strain value of 50–350% using the best-fit curve between the two methods. The Young's modulus at different strain levels were obtained from the first derivative of the cubic equation in the mean stress–strain curves (Fig. 7). For an elastomer-like rubber, whereby the stress–strain

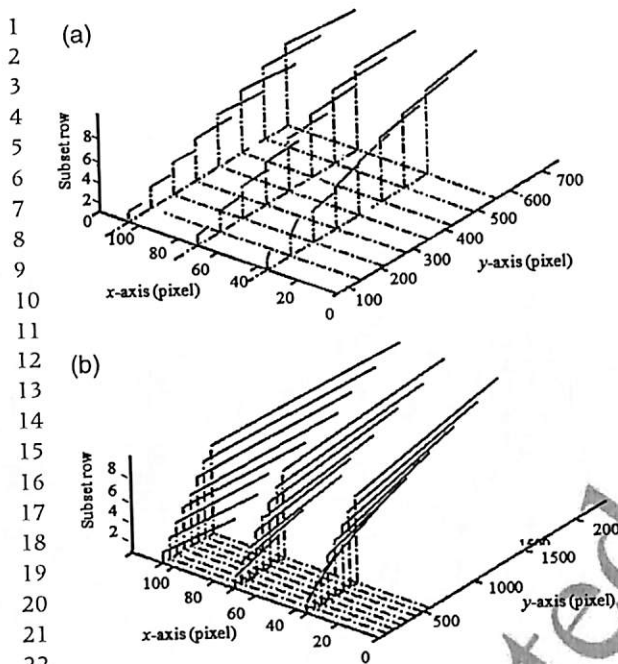


Figure 6 3-D view of displacement fields at (a) 0.3175 MPa and (b) 1.4869 MPa.

relationship is nonlinear, it is necessary to determine the tangent modulus given by the gradient (first derivative). The highest and lowest absolute percentage errors in the Young's modulus value are 8.9 and 4.4% at 150 and 350% strains, respectively, while the mean error is 7.1%. The deviation between the two methods is mainly due to the approach used in the computation of the strain data. In the proposed scanner-based DIC method, the overall strain is determined by using the individual strain values at various grid points on the specimen, whereas in the tensile test method the strain data are determined using the overall extension of the specimen. As the scanner-based method is sensitive to local variations in strains caused by material nonhomogeneity the two methods will not yield the same results.

Although the rubber specimens were stretched uniformly in the axial direction, the strain values are nonuniform along this direction as shown in Fig. 8. At lower stress values (0.05 and 0.31 MPa) the rubber specimen behaves as a linear elastic material. Therefore, the local strain values are uniform throughout the rows. However, at a higher strain the rubber specimen no longer obeys the linear stress-strain relationship, thus leading to lower strain values farther from the fixed end. The nonuniformity of strain distribution is caused by the voids present

in rubber specimen. The microstructure of rubber specimen was observed using a scanning electron microscope (SEM). The SEM micrograph (Fig. 9) was obtained at a section across the central part of rubber specimen without stretching. A significant number of voids can be seen in the figure. This is suspected to give rise to the nonuniform deformation of the specimen. The small gap between the two curves as seen in Fig. 7 could be attributed to the material nonhomogeneity and the manner in which strain data in the scanner-based DIC method are computed. The different number and locations of voids in different specimens could explain the higher error in Young's modulus at lower strains (150%) compared to that at higher strains (350%) (Table 4).

Comparison of proposed method with conventional DIC method and tensile test machine

The proposed scanner-based DIC method has the following advantages compared to the conventional DIC method for strain mapping in rubber. Unlike the conventional DIC method, whereby the area of study is limited by the camera field-of-view, the scanner-based DIC method enables a large area of the specimen to be studied. The area is limited only by the size of the scanner platen which is typically 215×298 mm. The image of the specimen can be acquired at a maximum optical resolution of 4800×9600 pixels. In the scanner-based DIC method uniform lighting is provided by the built-in LED source that moves with the photosensor array. External lighting used in the conventional DIC method could cause nonuniform illumination, thus requiring additional image processing stages. As a camera is not needed in the scanner-based DIC method, this results in an overall reduction in costs. Unlike the conventional DIC method which is used for studying various types of materials, however, the scanner-based DIC method is limited only to high-strain material like rubber and elastomers.

The proposed scanner-based DIC method is shown to be capable of providing accurate Young's modulus data up to 350% strain. Unlike the tensile test machine the distribution of the strain in the specimen can be mapped using the proposed DIC method. Images scanned at various loadings provide a permanent record of the deformation undergone by the specimen. The main limitation of the proposed method compared to the tensile test machine, however, is the upper limit (350%) on the amount of strain that can be applied. This limit can be overcome by modifying the loading rig and scanner to enable a longer travel.

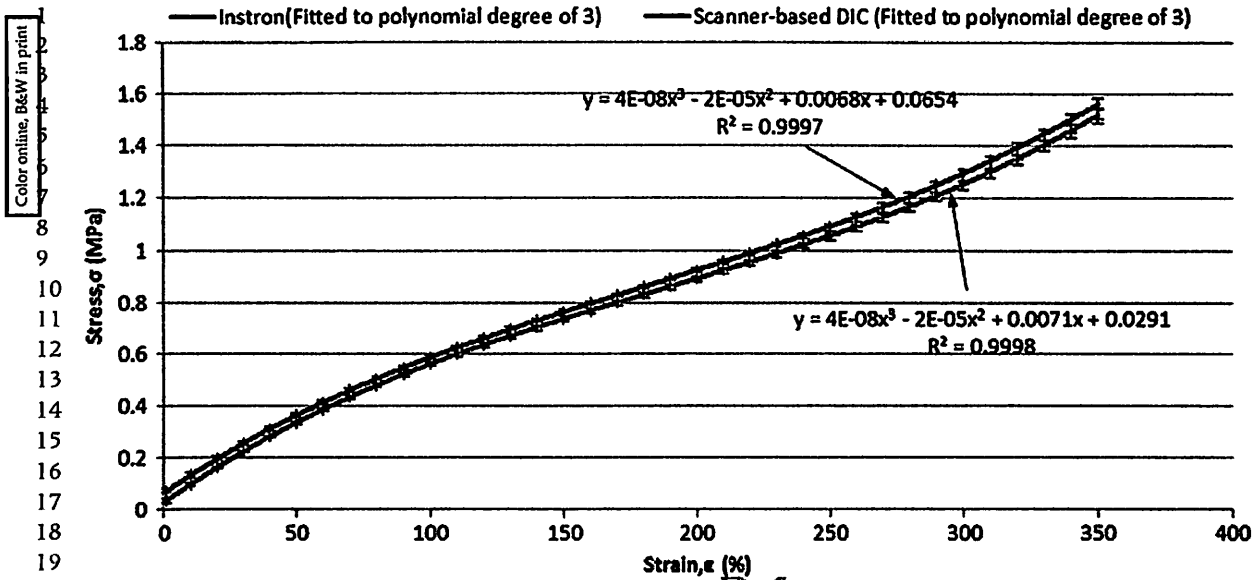


Figure 7 Comparison of stress–strain behavior between scanner-based DIC and Instron.

Table 4 Best-fit curve result comparison

Strain (%)	Specimen					Standard deviation	Average	From Instron	Error (%)
	1	2	3	4	5				
50	0.54	0.58	0.57	0.60	0.58	0.02	0.574	0.540	6.296
100	0.43	0.47	0.46	0.49	0.47	0.02	0.464	0.430	7.907
150	0.38	0.42	0.41	0.44	0.42	0.02	0.414	0.380	8.947
200	0.39	0.43	0.42	0.45	0.43	0.02	0.424	0.390	8.718
250	0.46	0.50	0.49	0.52	0.50	0.02	0.494	0.460	7.391
300	0.59	0.63	0.62	0.65	0.63	0.02	0.624	0.590	5.763
350	0.78	0.82	0.81	0.84	0.82	0.02	0.814	0.780	4.359

The results from this study show that the scanner-based DIC method is able to provide full-field displacement of the full gage length of the rubber specimen as well as the Young’s modulus of the material at various strains. This method can also be used to study homogeneity in rubber at large deformation from the strain map as well as hysteresis, creep, and stress relaxation effects in rubber and other elastomers.

Conclusion

The simple low-cost document scanner is proven to be a useful image acquisition device for 2-D DIC application for elastomeric materials like rubber. Unlike in the conventional DIC setup, the scanner-based DIC method does not use a CCD camera which

needs to be moved due to the limited field-of-view. External lighting and a high-resolution camera or accurate specimen-imaging device positioning are not required. Using the scanner-based DIC method the full-field in-plane displacements in an elastomeric rubber specimen were measured at different loads. A loading fixture was specially designed for this purpose and functioned as specimen clamping system. The reference points on the fixture enable the specimen to be located and cropped out automatically using image processing. From the displacement of each subset the strain experienced by the rubber specimen at different points was measured. Good agreements with the stress–strain behavior and Young’s modulus results were obtained, thus confirming that the common document scanner is a potential tool for low-cost DIC application.

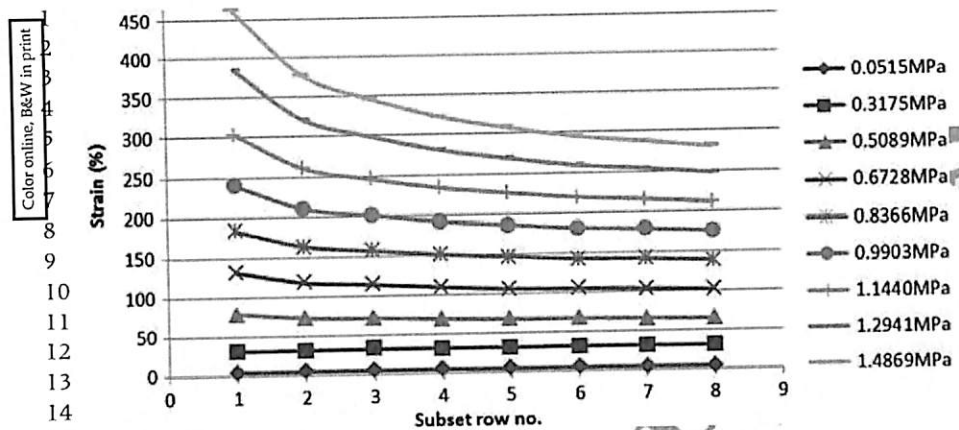


Figure 8 Plot of local strain values from the fixed end as stress values increase.

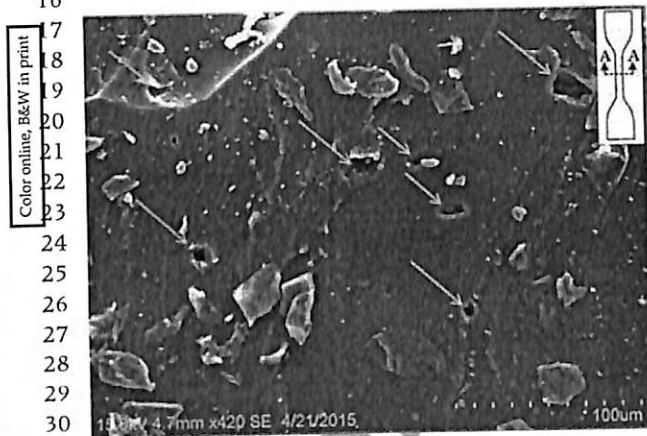


Figure 9 SEM micrograph taken in the cross-section area at central part of rubber specimen.

Acknowledgments

The authors would like to thank Universiti Sains Malaysia for offering the Research University research grant (Grant no. 1001/PMEKANIK/814182) for this study.

References

1. Passieux, J.-C., Bugarin, F., David, C., Périé, J.-N., and Robert, L., "Multiscale Displacement Field Measurement Using Digital Image Correlation: Application to the Identification of Elastic Properties," *Experimental Mechanics* 55: 121–137 (2015).
2. Ahn, B., and Nutt, S.R., "Strain Mapping of Al–Mg Alloy with Multi-scale Grain Structure Using Digital Image Correlation Method," *Experimental Mechanics* 50: 117–123 (2010).

3. Chen, J.L., Zhan, N., Zhang, X.C., and Wang, J.X., "Improved Extended Digital Image Correlation for Crack Tip Deformation Measurement," *Optics and Lasers in Engineering* 65: 103–109 (2015).
4. Tang, Z.Z., Liang, J., Xiao, Z.Z., and Guo, C., "Large Deformation Measurement Scheme for 3D Digital Image Correlation Method," *Optics and Lasers in Engineering* 50: 122–130 (2012).
5. Laraba-Abbes, F., Ienny, P., and Piques, R., "A New 'tailor-made' Methodology for the Mechanical Behaviour Analysis of Rubber-like Materials: I. Kinematics Measurements Using a Digital Speckle Extensometry," *Polymer* 44: 807–820 (2003).
6. Laraba-Abbes, F., Ienny, P., and Piques, R., "A New 'tailor-made' Methodology for the Mechanical Behaviour Analysis of Rubber-like Materials: II. Application to the Hyperelastic Behaviour Characterization of a Carbon-black Filled Natural Rubber Vulcanizate," *Polymer* 44: 821–840 (2003).
7. de Crevoisier, J., Besnard, G., Merckel, Y., et al., "Volume Changes in a Filled Elastomer Studied via Digital Image Correlation," *Polymer Testing* 31: 663–670 (2012).
8. Pan, B., Wu, D.F., and Xia, Y., "Incremental Calculation for Large Deformation Measurement Using Reliability-guided Digital Image Correlation," *Optics and Lasers in Engineering* 50: 586–592 (2012).
9. Jerabek, M., Major, Z., and Lang, R.W., "Strain Determination of Polymeric Materials Using Digital Image Correlation," *Polymer Testing* 29: 407–416 (2010).
10. Kangasrääsiö, J., and Hemming, B., "Calibration of a Flatbed Scanner for Traceable Paper Area Measurement," *Measurement Science and Technology* 20: 107003 (2009).
11. Kee, C.W., and Ratnam, M.M., "A Simple Approach to Fine Wire Diameter Measurement Using a High-resolution Flatbed Scanner," *The International*

- 1 *Journal of Advanced Manufacturing Technology* 40:
2 940–947 (2008).
- 3 12. Korin, I., Larrainzar, C., and Ipiña, J.P., "Crack
4 Length and Stable Crack Extension Measurements
5 from Images Acquired by Means of a Conventional
6 Flatbed Scanner," *Fatigue & Fracture of Engineering
7 Materials & Structures* 30: 876–884 (2008).
- 8 13. Lim, T.Y., and Ratnam, M.M., "Edge Detection and
9 Measurement of Nose Radii of Cutting Tool Inserts
10 from Scanned 2-D Images," *Optics and Lasers in
11 Engineering* 50: 1628–1642 (2012).
- 12 14. Ng, T.W., and Tajuddin, A., "Shadow Moiré
13 Topography Using a Flatbed Scanner," *Optical
14 Engineering* 41: 1908–1911 (2002).
- 15 15. van Dalen, G., "Determination of the Size
16 Distribution and Percentage of Broken Kernels of
17 Rice Using Flatbed Scanning and Image Analysis,"
18 *Food Research International* 37: 51–58 (2004).
- 19
- 20
- 21
- 22
- 23
- 24
- 25
- 26
- 27
- 28
- 29
- 30
- 31
- 32
- 33
- 34
- 35
- 36
- 37
- 38
- 39
- 40
- 41
- 42
- 43
- 44
- 45
- 46
- 47
- 48
- 49
- 50
- 51
- 52
- 53
16. ASTM D412-06a, *Standard Test Methods for Vulcanized
1 Rubber and Thermoplastic Elastomers-Tension*, ASTM
2 International, West Conshohocken, PA (2013).
- 3 17. Song, S., Chen, W., and Cheng, M., "Novel Model
4 for Uniaxial Strain-Rate-Dependent Stress-Strain
5 Behavior of Ethylene-Propylene-Diene Monomer
6 Rubber in Compression or Tension," *Journal of
7 Applied Polymer Science* 92: 1553–1558 (2004).
- 8 18. Pan, B., Qian, K.M., Xie, H.M., and Asundi, A.,
9 "Two-Dimensional Digital Image Correlation for
10 In-plane Displacement and Strain Measurement:
11 A Review," *Measurement Science and Technology* 20:
12 062001 (2009).
- 13 19. Bornert, M., Bremand, F., Doumalin, P., et al.,
14 "Assessment of Digital Image Correlation
15 Measurement Errors: Methodology and Results,"
16 *Experimental Mechanics* 49: 353–370 (2009).
- 17
- 18
- 19
- 20
- 21
- 22
- 23
- 24
- 25
- 26
- 27
- 28
- 29
- 30
- 31
- 32
- 33
- 34
- 35
- 36
- 37
- 38
- 39
- 40
- 41
- 42
- 43
- 44
- 45
- 46
- 47
- 48
- 49
- 50
- 51
- 52
- 53

QUERIES TO BE ANSWERED BY AUTHOR

IMPORTANT NOTE: Please mark your corrections and answers to these queries directly onto the proof at the relevant place. DO NOT mark your corrections on this query sheet.

Queries from the Copyeditor:

- AQ1.** Please confirm that given names (red) and surnames/family names (green) have been identified correctly
 - AQ2.** This figure is poor quality. Kindly resupply.
 - AQ3.** Please provide the supplier name and supplier location for the product Canoscan 5600F
 - AQ4.** Please clarify whether "strain-stress data" can be changed to "stress-strain data".
-



JABATAN BENDAHARI
PENYATA PERBELANJAAN SEHINGGA 7 MAC 2017
DEVELOPMENT OF LOW-COST RUBBER TENSILE PROPERTY TESTER USING DIGITAL IMAGE CORRECTION (DIC) AND FLATBED SCANNER

Tajuk projek
 Tempoh projek
 Taraf projek
 Ahli

15/12/2012 hingga 14/06/2016
 TAMAT TEMPOH (LAPORAN BELUM DITERIMA)
 MANI MARAN A/L RATNAM (KETUA PROJEK)
 HANAFAI BIN ISMAIL

YEN KIN SAM

Nombor akaun 1001.PMEKANIK.814182

Vot	Nama Vot	Peruntukan Projek	Perbelanjaan Terkumpul Sehingga Thn Lalu	Baki Peruntukan Tahun Lalu	Peruntukan Thn Semasa	Jumlah Peruntukan Thn Semasa	Tanggung Semasa	Bayaran Thn Semasa	Jum Belanja Thn Semasa	Baki Projek
111	GAJI	79,200.00	63,381.81	15,818.19	0.00	15,818.19	0.00	10,000.00	10,000.00	5,818.19
221	JALANAN & SARA HIDUP	4,000.00	1,986.47	2,013.53	0.00	2,013.53	0.00	0.00	0.00	2,013.53
227	BEKALAN BAHAN LAIN	4,000.00	9,796.40	(5,796.40)	0.00	(5,796.40)	0.00	1,407.10	1,407.10	(7,203.50)
228	PENYELENGGARAN KECIL	0.00	0.00	0.00	0.00	0.00	0.00	87.35	87.35	(87.35)
229	KHIDMAT IKTISAS	13,000.00	3,441.58	9,558.42	0.00	9,558.42	0.00	0.00	0.00	9,558.42
335	HARTA MODAL	5,700.00	3,229.00	2,471.00	0.00	2,471.00	0.00	0.00	0.00	2,471.00
552	PERBELANJAAN LAIN	0.00	0.00	0.00	0.00	0.00	0.00	53.46	53.46	(53.46)
Jumlah		105,900.00	81,935.26	24,064.74	0.00	24,064.74	0.00	11,547.91	11,547.91	12,516.83

Penyata ini adalah cetakan komputer tiada tandatangan diperlukan
 Penyata ini adalah dianggap tepat jika tiada maklumbalas dalam tempoh masa 14 hari dari tarikh penyata



BORANG PENYERAHAN ASET / INVENTORI

A. BUTIR PENYELIDIK

1. NAMA PENYELIDIK : Prof. Mani Maran a/l Ratnam
 2. NO STAF : AE50202
 3. PTJ : Pusat Pengajian Kejuruteraan Mekanik
 4. KOD PROJEK :
 5. TARIKH TAMAT PENYELIDIKAN : 14 Jun 2016

B. MAKLUMAT ASET / INVENTORI

BIL	KETERANGAN ASET	NO HARTA	NO. SIRI	HARGA (RM)
1.	Personal Computer (DELL OPTIPLEX 3010DT)	AK00007296	203971307	3,229.00
2.	CCD Flatbed scanner (CANON CANOSCAN 5600F SCANNER)	(Inventori)	ABEK05819	780.00

C. PERAKUAN PENYERAHAN

Saya dengan ini menyerahkan aset/ inventori seperti butiran B di atas kepada pihak Universiti:



(Mani Maran a/l Ratnam)

Tarikh: 04/08/17

D. PERAKUAN PENERIMAAN

Saya telah memeriksa dan menyemak setiap alatan dan didapati :

- Lengkap
 Rosak
 Hilang : Nyatakan.....
 Lain-lain : Nyatakan

Diperakukan Oleh :

.....

Tandatangan
 Pegawai Aset PTJ

Nama :
 Tarikh :

***Nota :** Sesalinan borang yang telah lengkap perlulah dikemukakan kepada Unit Pengurusan Harta, Jabatan Bendahari dan Pejabat RCMO untuk tujuan rekod.



RU(I) GRANT

COMPREHENSIVE TECHNICAL REPORT

Project title: Development of low-cost rubber tensile property tester using digital image correction (DIC) and flatbed scanner

Account Number: 1001/PMEKANIK/814182

Name of Research Leader:

Prof. Mani Maran a/l Ratnam

Name of Co-Researcher:

1. Prof. Hanafi Ismail
2. Ir. Dr. Yen Kin Sam

Name of Graduate/Student Assistants:

1. Goh Ching Pang
2. Neoh Boon Ping

CONTENTS

	Page
INTRODUCTION	
1.0 Research background	1
1.1 Research objectives	3
METHODOLOGY	
2.0 Overview	4
2.1 Preparation of natural rubber (NR) specimens and variables used in standard tensile test	4
2.2 Design criteria of the motorized loading rig	7
2.3 Preliminary tests of the motorized loading rig	17
2.3.1 Slip test of the clamping system	17
2.3.2 Force transmission efficiency test of loading system	17
2.3.3 Holding torque determination of the stepper motor	19
2.4 Preliminary tests of the flatbed scanner	20
2.4.1 Uniformity test of light intensity of flatbed scanner	20
2.4.2 Corrected scanning resolution test of flatbed scanner	20
2.5 Principle, variables, algorithm and experimental procedure of 2-D SB-DIC method	22
2.5.1 The DIC principle	22
2.5.2 Strain calculation and Poisson's ratio (PR) variables	23
3.5.2(a) Validation of Poisson's ratio	25
2.5.3 Experimental procedure for 2-D SB-DIC method	26
2.5.4 Algorithm of incremental 2-D SB-DIC method	27
3.5.4(a) Comparison between incremental 2-D SB-DIC and LaVision DIC methods	26
2.5.5 Principle and algorithm of single-step 2-D DIC method	31
2.5.5(a) Principle of single-step 2-D DIC method	32

2.5.5(b)	Single-step 2-D DIC algorithm	35
2.5.6	Reliability of the 2-D SB-DIC algorithm	38
2.6	Finite element modelling of the rubber specimens	39

RESULTS AND DISCUSSION

3.0	Overview	
3.1	Preliminaries of the 2-D SB-DIC method	42
3.1.1	Reliability test of clamping system	42
3.1.2	Determination of force transmission ratio of loading system	44
3.1.3	Holding torque determination of the stepper motor	44
3.1.4	Uniformity test of scanner light intensity	45
3.1.5	Corrected scanning resolution for nominal scanning resolution at 600 dpi	46
3.1.6	Reliability test of the DIC coding in simulation	46
3.1.7	Subset size selection in 2-D SB-DIC method	48
3.1.8	Randomness test of the speckle patterns	52
3.2	Incremental 2-D SB-DIC method	53
3.2.1	Comparison between grayscale- and binary-image based incremental 2-D SB-DIC methods	54
3.2.2	Displacement vector field of incremental 2-D SB-DIC method	56
3.2.3	Comparison of stress-axial strain curve and Young's modulus between the incremental 2-D SB-DIC method and standard tensile test machine	60
3.2.4	Comparison between incremental 2-D SB-DIC and LaVision DIC methods	65
3.2.5	Comparison of Poisson's ratio between incremental 2-D SB-DIC method and theoretical function	69
3.3	Single-step 2-D SB-DIC method	71
3.3.1	Displacement vector field of the single-step 2-D SB-DIC method	71

3.3.2	Comparison between single-step 2-D SB-DIC and incremental 2-D SB-DIC methods	74
3.3.3	Time comparison between the single-step 2-D SB-DIC and the incremental 2-D SB-DIC methods	76
3.3.4	FEM analysis on non-homogeneous strain distribution	79
CONCLUSION		82
REFERENCES		83

INTRODUCTION

1.0 Research Background

Two-dimensional digital image correlation (2-D DIC) method is a well-known optical full-field contactless method used for the in-plane displacement and strain mapping in materials subjected to loading. In contrast to the commercial mechanical properties characterization methods such as Instron which provides only the average strain value, the 2-D DIC method is capable of providing quantitative localized deformation measurement. The underlying principle of the DIC method is the comparison of the digital images of a specimen before and after deformation. A random speckle pattern is created on the specimen to enable the comparison. The speckle pattern acts as a deformation information carrier so that the displacement at a particular region on the loaded specimen can be detected. In order to obtain a clear and focused image so that the speckle patterns recorded are in good quality, the camera is placed in front of the specimen at an optimum distance. Due to the limited field-of-view (FOV) of the charge-coupled device (CCD) camera, the conventional 2-D DIC method can only be applied for low strain materials such as metals and ceramics (Dai et al., 1991, Coburn and Slevin, 1993).

To overcome the limited field-of-view and therefore larger full-field displacement and strain map, the experimental setup of the conventional 2-D DIC method was improved by moving the camera instead of fixing the camera relative to the loading mechanism (Laraba-Abbes et al., 2013a,b). The improved method was used to study the large deformation of carbon-black filled natural rubber (CB-NR). The CCD camera was mounted on a translation stage so that it moved according to the rubber specimen during loading. The full-field displacement was determined by re-constructing the displacement at each single stage. This approach enabled of 500% strain to be studied (maximum re-constructive FOV of 4.2 mm in length). This new technique then has been adopted by several researchers (Risbet et al., 2010, Wu et al., 2011a, de Crevoisier et al., 2012) to study high strain materials with maximum re-constructive FOV of $70 \times 10 \text{ mm}^2$ (Wu et al., 2011a). Although the moving camera 2-D DIC method was successfully applied on large strain materials; this method, however, has three main disadvantages: (a) the need of precise alignment between the moving camera and the inspected specimen subjected to loading. The camera mounted on the translation stage moves according to the previous displacement value. A slight misalignment can cause image de-correlation (b) the need of uniform illumination of the external lighting thorough the experiment. The concept of the 2-D DIC method is to find the intensity changes between the images before and after deformation, a non-uniform illumination caused by improper experimental setup introduces noise on the digitized image. The noise introduced on the digitized speckle pattern reduces the correlation accuracy, (c)

vibration caused by the translation stage. A high performance translation stage need to be installed to reduce the vibration effect imposed by the motor used to drive the CCD camera. The vibration causes the misalignment of the camera relative to the loaded specimen.

The incremental 2-D DIC algorithm has been used to measure the large displacement from a sequence of images. In a large deformation measurement, however, the measurement of large deformations using the same reference image leads to significant errors (Han et al., 2012). This is because the shape and the size of the speckle pattern in the large deformed images are different from that in the reference image. Thus, an updating of reference image method was introduced by changing the reference view when the deformation is too large ($\geq 20\%$ strain) (Tang et al., 2012). In this approach, the displacement field is determined incrementally by considering two consecutive images in sequence. Although the incremental 2-D DIC algorithm is able to provide reliable displacement and strain measurement for large strain materials; this method, however, introduces accumulated errors during the displacement measurement process (Tang et al., 2012). This is because the reference subset used for the tracking process in the current image is dependent upon the tracking accuracy in the previous image. A slight error introduced during correlation calculation in the previous image is brought forward to the next tracking process in the following images since the process is continuous and uninterrupted. In addition, the time taken for image acquisition and correlation calculation process is long.

The use of full-field displacement and strain mapping method in mechanical characterization of rubber is important in rubber manufacturing industries, such as surgical glove and automotive tyre manufacturing. Defects such as uneven-thickness, fish eye and cracks which will cause pinhole and tear on the finished products are impossible to be detected and analysed using the conventional standard tensile test such as Instron. The defectively manufactured products might cause permanently disabled or fatality due to bacterial contamination using torn surgical glove. Thus, quality control and functional tests on rubber product are important to make sure that the finished goods meet the quality specifications. Therefore, the implementation of 2-D DIC method on rubber inspection is important as it is able to provide localized deformation information where the undesirable defects mentioned above can be detected and analysed.

In order to map the large deformation in rubber without using the moving camera technique, the low-cost and commonly available 2-D flatbed scanner is introduced in this research. The 2-D flatbed scanner is able to provide larger field-of-view and equipped with uniform built-in lighting. Besides, it is capable of providing digitized information of flat surfaces with high scanning resolutions approaching those of high-resolution and expensive CCD cameras. The advantages of using a flatbed scanner as an imaging device are the ability to capture large deformation of large strain materials such as rubber without any

changes of experimental setup, it is relatively low cost, high resolution and the built-in lighting system. Several researchers have used the common flatbed scanner for various metrological applications such as paper area measurement (Kangasrääsiö et al., 2009), measurement of fine wire diameter (Kee and Ratnam, 2008), determination of size distribution of broken rice kernels (van Dalen, 2004), characterizing frost damages of concrete (Wang et al., 2016) and measurement of nose radii of cutting inserts (Lim and Ratnam, 2012). However, the potential of combining the 2-D DIC method and the flatbed scanner to obtain the full-field in-plane displacement of large strain material has yet to be explored. Thus, a new technique in 2-D DIC experimental setup coupled with a new 2-D DIC algorithm is introduced to address the main problems which are presented in the following section.

1.1 Research Objectives

The objectives of this research are as follows:

1. To develop a two-dimensional scanner-based digital image correlation (2-D SB-DIC) method for in-plane displacement and strain mapping for large deformation on natural rubber.
2. To compare the stress-axial strain relationship obtained from the 2-D SB-DIC method with those obtained from a tensile test machine.
3. To develop a single-step 2-D SB-DIC algorithm to determine the in-plane displacement and strain undergone by natural rubber specimens and compare the strain data with the result obtained from the incremental 2-D SB-DIC method.
4. To verify the single-step 2-D SB-DIC method in non-homogeneous strain measurement by comparing the strain maps between the single-step 2-D SB-DIC method and finite element modelling.

METHODOLOGY

2.0 Overview

The procedure for the preparation of the rubber specimens and the variables used in standard tensile test are outlined in Section 2.1. The design criteria of the motorized loading rig are discussed in Section 2.2. The preliminary tests of the motorized loading are presented in Section 2.3 in terms of effectiveness test of the clamping system, force transmission efficiency test and the determination of the holding torque required for the stepper motor used.

The uniformity test of the illumination provided by the flatbed scanner and the procedure to obtain the corrected scanning resolution at a particular height above the scanner platen is explained in this Section 2.4. The principle of the DIC method and the variables used in the experiment are outlined in Section 2.5. The procedures for conducting the experiments on the rubber specimen by using the conventional incremental 2-D SB-DIC and the proposed single-step 2-D SB-DIC are discussed in this section. The algorithms of the incremental 2-D SB-DIC and the procedure for conducting the standard 2-D DIC method (LaVision) are also explained in this section. The principle and the algorithm of the proposed single-step 2-D SB-DIC are discussed in this section. The reliability test of the DIC program in detecting the displacement of a white speckle is explained in the last part of this section. The finite element modelling (FEM) of the rubber specimen is discussed in Section 2.6. Lastly the chapter summary is presented in Section 2.7.

2.1 Preparation of natural rubber (NR) specimens and variables used in standard tensile test

The composition of the rubber specimen and their function are shown in Table 2.1. The elastomer used was natural rubber (Standard Malaysia Rubber L-grade, SMR L) supplied by MARDEC Berhad, Malaysia. Due to its high molecular weight render to high viscosity of the raw natural rubber, the raw natural rubber was masticated using two-roll mill of 160 mm working diameter of roller and 320 mm of working length of roller for 2 minutes to soften it. Rolling ensures all the compositions can be dispersed homogeneously into the rubber matrix. All the compositions shown in Table 3.1 except for sulfur (vulcanization agent) were added in and the mixing was continued for another eight minutes at $70\pm 5^{\circ}\text{C}$. Sulfur was added last for two minutes to prevent premature vulcanization. The zinc oxide and the stearic acid act as activator system to activate the network formation of the compositions during vulcanization process. Due to the slow vulcanization process by using the sulfur, the N-cyclohexyl-benzothiazyl-sulphenamide (CBS) was used as an accelerator to speed up the

vulcanization process. N-isopropyl-N'-phenyl-p-phenylenediamine (IPPD) acts as an antioxidant agent to prevent ozone, flex crack and also a good protecting agent for oxygen, light and heat which will affect the material properties of the rubber.

The vulcanizing conditions, namely time (t_{90}) and temperature, were determined using Monsanto Moving Die Rheometer (MDR 2000E; Alpha Technologies; Akron, OH; US) at 150 °C according to ASTM: D2084-11. The vulcanization time (t_{90}) used for preparation of the vulcanized samples was the optimum time at which the rheometer torque increased to 90% of the total torque change on the cure curve of the sheets. The vulcanization times obtained was 6 minutes. The uncured compound was then placed into a rectangular mold of 2 mm thickness and compressed under pressure of 10 MPa at 150°C in a hot press machine (SD50(1S) Rubber Moulding Machine; Shinn Dwo Machinery Co., Ltd; Guang-Dong; China) with the vulcanization times determined from the rheometer.

Table 2.1 Compositions of the unfilled natural rubber specimen

Compositions	Function	Parts per Hundred Rubber (PHR)	Rate	Weight (g)
SMR L (Standard Malaysia Rubber L-grade)	Large deformation domain	100	2.77	277
Zinc Oxide	Activator	1.5	2.77	4.16
Stearic Acid	Activator	1.5	2.77	4.16
N-cyclohexyl-benzothiazyl-sulphenamide (CBS)	Accelerator	1.9	2.77	5.27
N-isopropyl-N-phenyl-p-phenylenediamine (IPPD)	Antioxidant	2.0	2.77	5.54
Sulfur	Vulcanization Agent	1.6	2.77	4.43
Total		108.5	2.77	300.56

The vulcanizates in sheet form were cut into dumbbell-shaped specimens according to ASTM: D412-06a (Die C) as shown in Figure 3.1 with gauge section dimensions of 33 mm× 6 mm× 2 mm. Tensile properties of the five dumbbell-shaped rubber specimens were determined for validation purpose on an Instron 3366 (Instron Ltd; High Wycombe; UK) tensile test machine at a crosshead speed of 500 mm/min at room temperature. Another five dumbbell-shape rubber specimen were used in the tensile test using the 2-D scanner-based DIC method. The specimen with a through-hole geometry was prepared using a hole-punch with diameter of 20 mm while the specimen with a through-square hole geometry was prepared using a 19 mm chisel to test the ability of the proposed single-step 2-D SB-DIC method in measuring the heterogeneous strain distribution as shown in Figure 2.2.

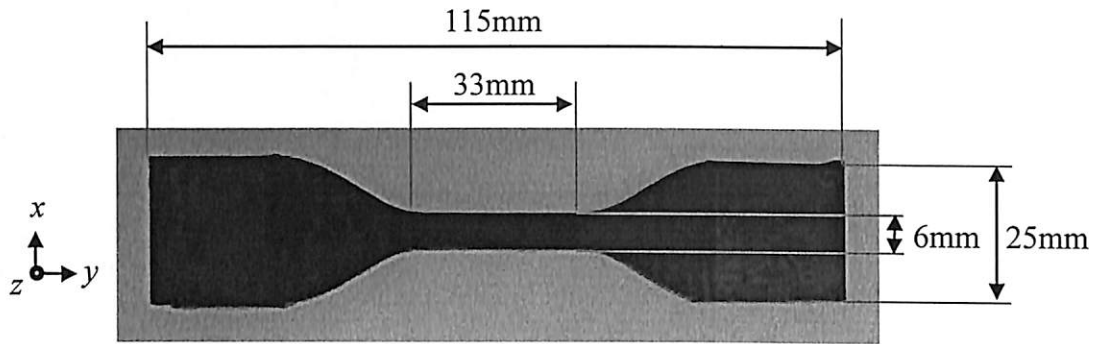


Figure 2.1 Dumbbell-shaped rubber specimen

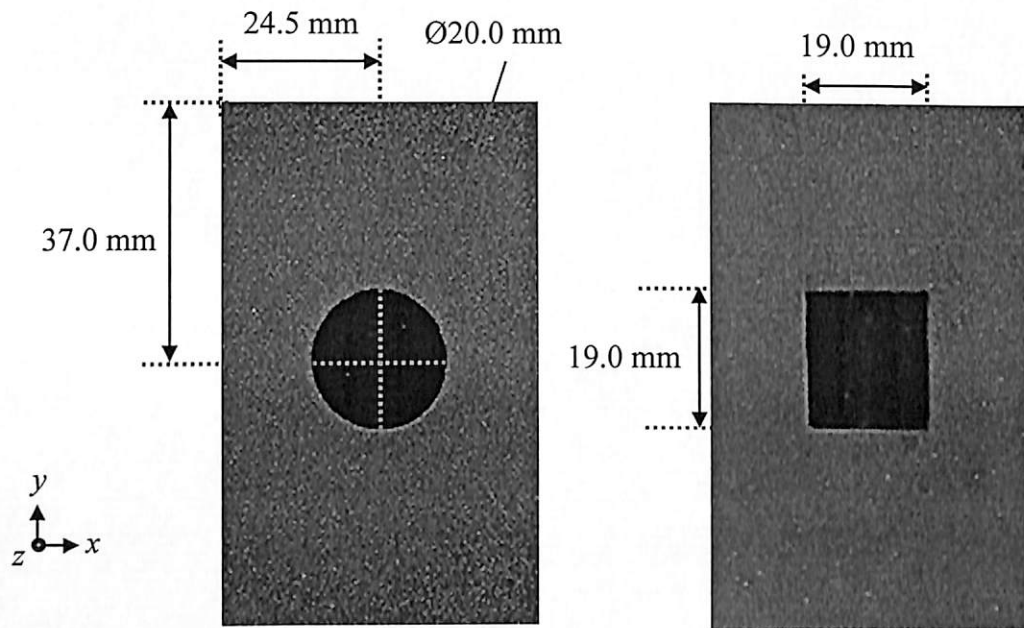


Figure 2.2 Circular hole-containing and square hole-containing rubber specimens

The thickness and the width of the rubber specimens at three different locations were measured by using coordinate measuring machine (CMM) (Model: Crysta-Plus M443, Mitutoyo America Corporation, USA) and profile projector (Model: CPJ-3015Z, Rational Precision Instrument Co., Ltd, China), respectively to obtain the cross sectional area. The cross sectional area of the dumbbell-shaped rubber specimen was used to obtain the engineering stress, σ in the standard tensile test by using the following equation:

$$\sigma = \frac{F}{A} \quad (2.1)$$

where F is the load applied onto the rubber specimen and A is the cross sectional area of the rubber specimen. The cross sectional area was obtained by using the following equation:

$$A = \bar{T} \times \bar{W} \quad (2.2)$$

where \bar{T} is the mean thickness and \bar{W} is the mean width of the dumbbell-shaped rubber specimen measured at three different locations. The original gauge length used to obtain the engineering axial strain, ϵ_a^e in the standard tensile test was 50.0 mm. Although the gauge length of the dumbbell-shaped rubber specimen is 33.0 mm (Figure 3.1), "extra" gauge length at the fillet region of the dumbbell-shaped rubber specimen was taken into account since the grip region did not fully cover the non-gauge length region. The engineering axial strain was obtained by using the following equation:

$$\epsilon_a^e = \frac{(l_f - l_i)}{l_i} = \frac{\Delta l}{l_i} \quad (2.3)$$

where l_f is final length, l_i is original gauge length and Δl is the elongation.

3.2 Design criteria of the motorized loading rig

In this research, a flatbed scanner (Model: Canoscan 5600F, Woodhatch, Reigate, Surrey, UK) was used as an image acquisition system to replace the conventional charge-coupled device camera in the 2-D DIC method. The outer dimensions of the flatbed scanner were measured by using vernier caliper (Mitutoyo, Japan, 200 × 0.02 mm) and ruler (sensitivity of 1 mm). Six crucial criteria were defined and discussed in detail before the motorized loading rig is fabricated. The motorized loading rig was designed (Figure 3.3) customary to fit the shape of the flatbed scanner (i.e. parallel orientation between the rubber specimen and the scanner platen due to the plane-horizontal design of the flatbed scanner) while considering all of the criteria which met the experimental requirements and the conditions during tensile test:

(i) Effectiveness of the clamping system.

There is no slippage between the clamping system (part number: 1 and 3 in Figure 2.3) and the rubber specimen during loading. The clamping system must be able to clamp the rubber specimen firmly without slippage during the loading. Slippage of the rubber specimen can cause additional deformation due to the translation motion, thus, introducing systematic error and reducing the accuracy of the displacement measurement. Therefore, the design of the clamping system and its reliability to clamp the rubber specimen through the experiment is extremely important as a slight of slippage will introduce undesirable deformation into the displacement measurement.

A clamping system consisting of an upper clamp set and a lower clamp set was designed to clamp the rubber specimen as shown in Figure 2.4. Each of the clamp sets consisted of a "male" clasper with two bolts and a "female" clasper. The internal surfaces of

the “male” and “female” clampers that contacts with the rubber specimen were designed to be “zig-zag” shape to increase the friction force between the clampers and the rubber specimen as shown in Figure 2.5. These uneven surfaces of the clampers act as an interlock system to prevent the surfaces of the rubber specimen slides from the clampers. An experiment was conducted to investigate the effectiveness of the clamping system (refer to Section 2.3.1).

(ii) Loading mechanism of motorized loading rig

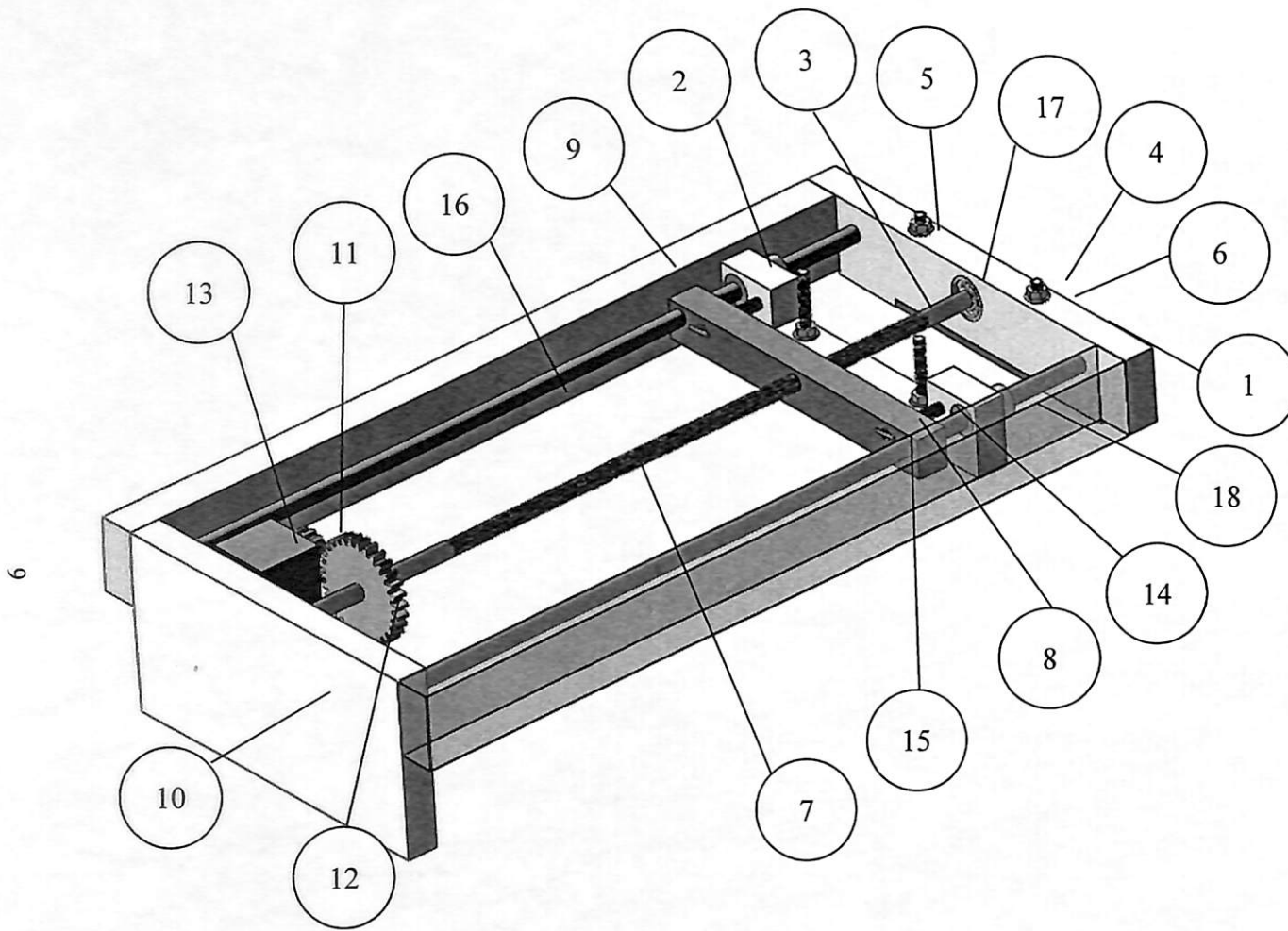
The rubber specimen must be loaded only in one direction (i.e. the tensile loading is uniaxial). The focus of this work is to determine the mechanical properties of the rubber specimen in uniaxial tensile test. Thus, movement in any other direction is not allowed because the movement will cause extra deformations (rotation and shear deformation) which reduce the accuracy of the displacement measurement.

The design of the loading system and the loading mechanism are shown in Figure 2.6. Firstly, a pre-setting stepper motor was used to drive the gear train ratio of 2:1. The parameters such as number of rotations and frequency were pre-set by using the microcontroller which was interfaced to the stepper motor driver. The stepper motor driver which was interfaced to the stepper motor sent the pulses of electric current to the stepper motor once the command was given. The motion of the gear train rotated the leadscrew attached to the driven gear. The downward force (F_a) is exerted by the load applicator when the lead screw rotates in the counter-clockwise (CCW) direction.

The restoring forces F_s in the springs, which were attached between the load applicator and the lower clamp set, are exerted in the direction opposite to the load applicator movement. Due to the action-reaction pair principle, the restoring force in the rubber specimen F_r and the downward force F_a exerted by the load applicator are of equal magnitudes. Thus, the force applied onto the rubber specimen F_r was determined by calculating the total restoring forces in the two springs using the following equation:

$$F_r = k_{eq}.x_{avg}. \quad (2.4)$$

where the equivalent spring constant $k_{eq} = k_1 + k_2$. The spring constants k_1 and k_2 were determined using a universal testing machine (Model: Instron 3367; Instron Ltd; High Wycombe, UK). The average extension x_{avg} of the two springs during the loading of the rubber specimen in the 2-D SB-DIC setup was determined using the image processing steps outlined in criteria (iv).



1. Top "female" clamber/top frame
2. Bottom "female" clamber
3. "Male" clamber
4. Bolt
5. Nut
6. Washer
7. Leadscrew
8. Load applicator
9. Side frame
10. Bottom frame
11. Driver gear
12. Driven gear
13. Stepper motor
14. Spring
15. Spring's hook
16. Sliding rod
17. Ball bearing
18. Linear bearing

Figure 2.3 Isometric view of the motorized loading rig

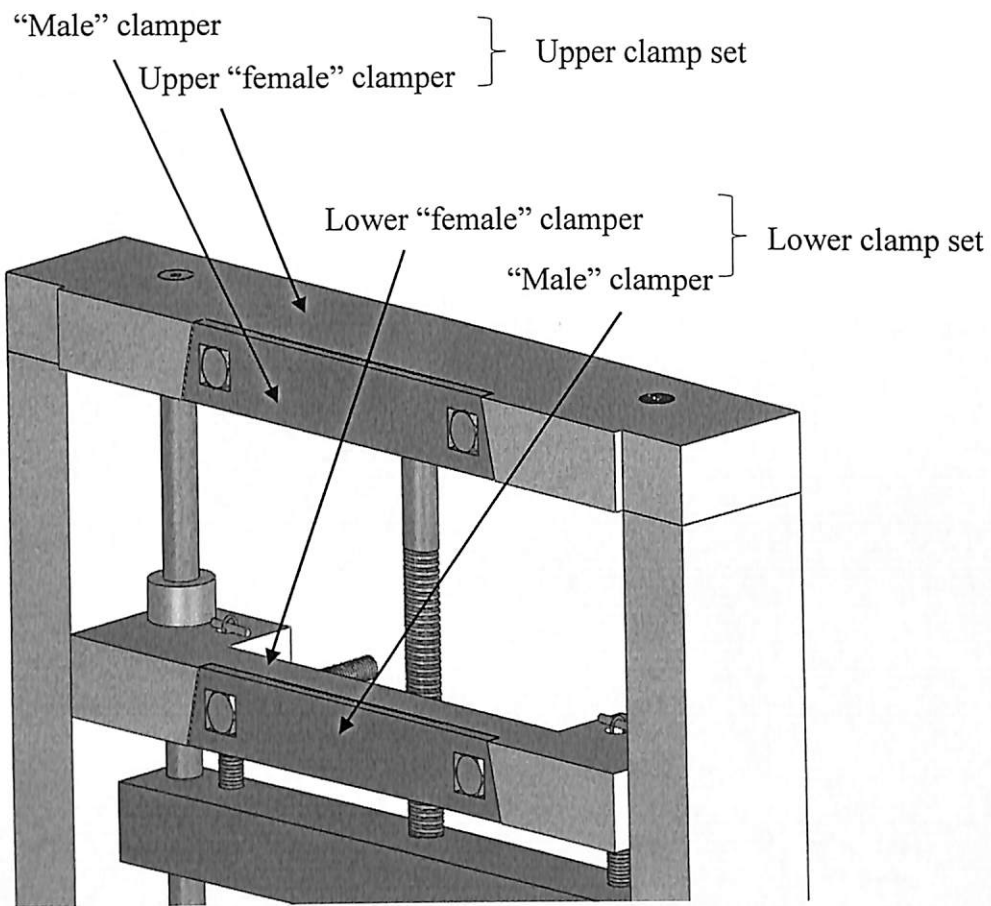


Figure 2.4 Clamping system of the motorized loading rig

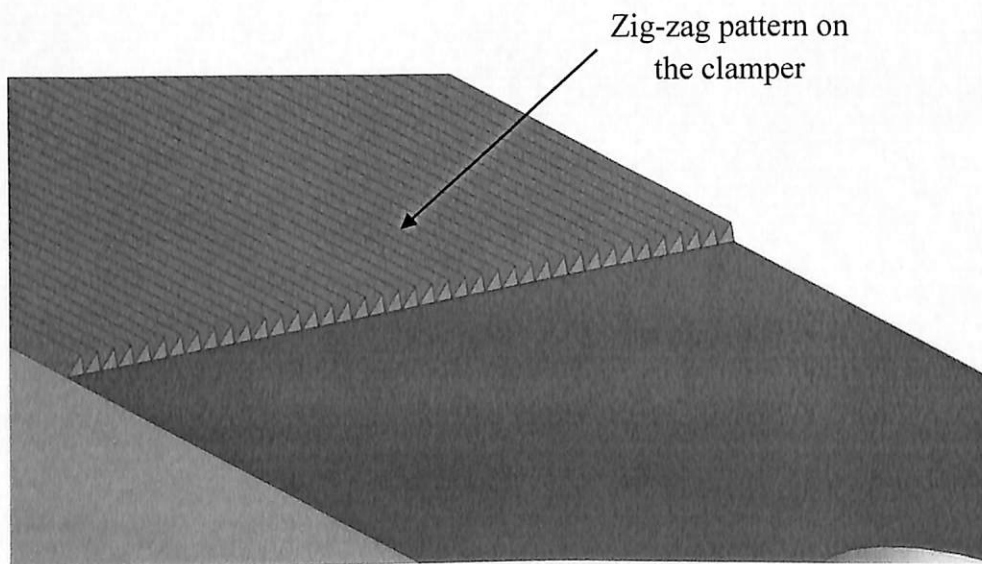


Figure 2.5 Zig-zag pattern on the clammer

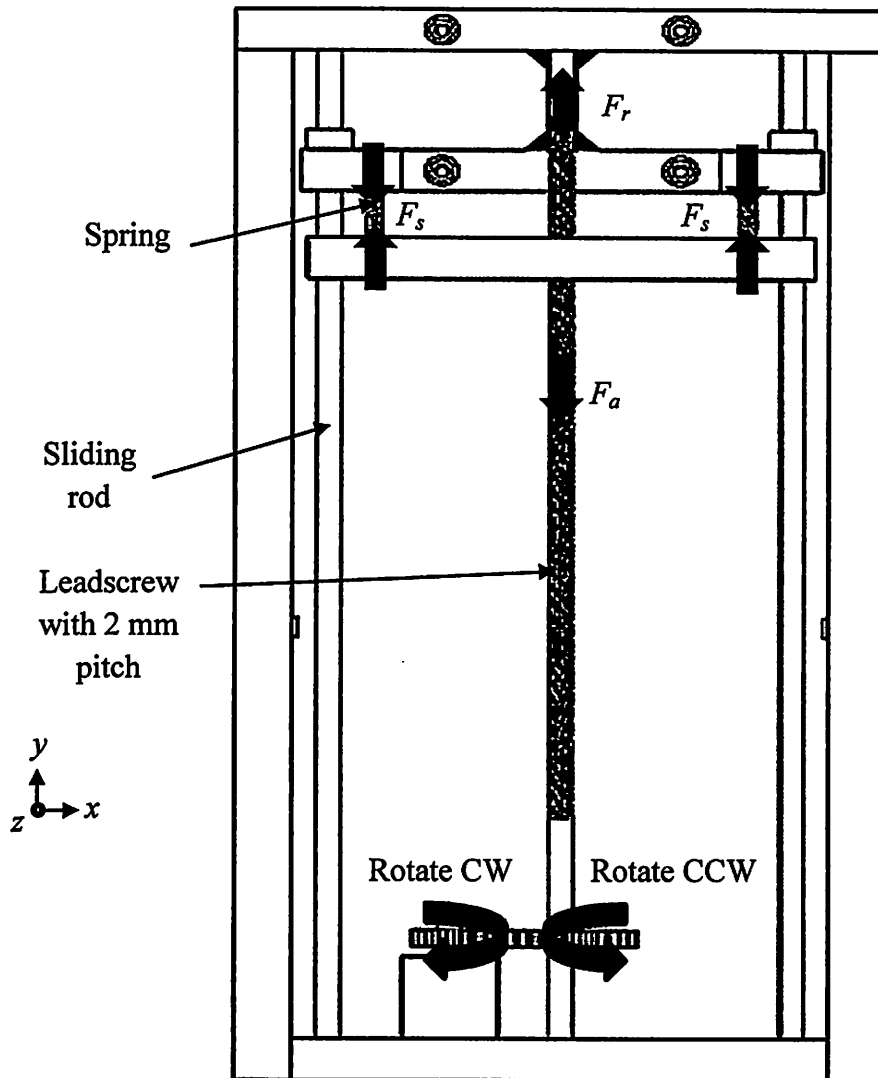


Figure 2.6 Schematic design of the loading mechanism for the motorized loading rig

To ensure that the load applicator and the lower clamp set move in only one direction which is in axis along to the loading direction, two sliding rods were attached to both sides of the load applicator and the lower clamp set as shown in Figure 2.6. Both ends of the two sliding rods were fixed at the top and bottom frames. The rotational motion in all the directions and translational motion in the perpendicular axis to the loading direction were constrained. Hence, the loading system and the clamping system have only one degree of freedom which is the y -axis movement.

(iii) of clamping-loading system on scanner platen

There is no contact between the lower surfaces of the lower clamp set and the load applicator relative to the scanner platen. During loading, the clamping system and the loading system are moving parallel to the scanner platen. Contact occurs if the gaps

between the lower surfaces of the clamping system and the loading system relative to the scanner platen are negligible small or none. The touching induces frictional force and affects the movement of the clamping system and the loading system during the loading, thus, affecting the quality of the scanned image during scanning process. A gap of 1.0 mm was designed to separate the lower surfaces of the lower lamp set and the load applicator relative to the scanner platen so that no contact occurred during the loading (Figure 2.7). After the fabrication of the motorized loading rig, the gap was measured using a vernier caliper. The gap obtained was 1.24 mm.

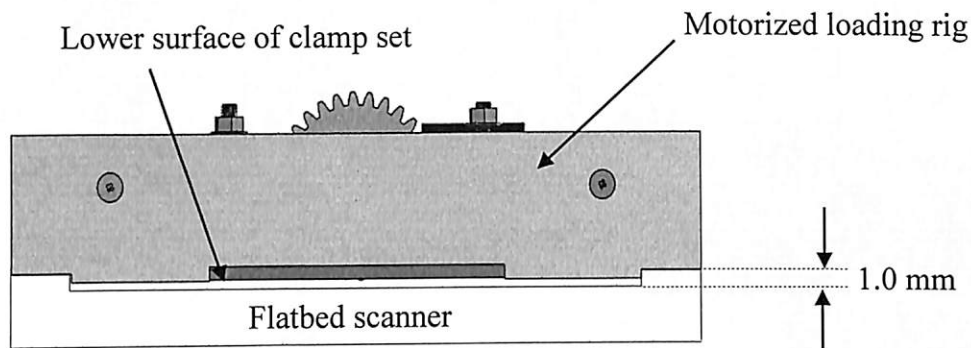


Figure 2.7 Top view of the motorized loading rig.

(iv) Determination of spring distance using image processing

The force applied onto the rubber specimen is one of the important parameter to obtain the load applied and stress data. Thus, the loading system of the motorized loading rig must be able to provide the force applied information. In order to obtain the load applied value, the spring displacement of the motorized loading rig must able to be read first. This was done by attaching the white markers on the lower surfaces of the lower "male" clasper and the load applicator as shown in Figure 2.8. The lengths of the springs before and after each loading were computed by using image processing based on the white rectangular markers shown in the Figure 2.8. The y -coordinates of the top left corner of both markers "B1" (y_1) and bottom left corner of marker "B2" (y_2) were obtained by using the 'bounding box' command in MATLAB. The extension of each spring was determined by subtracting y_1 from y_2 . The average spring extension in pixels unit was converted into millimetres using a calibrated factor and the load applied to the specimen was determined using Eq. (2.4).

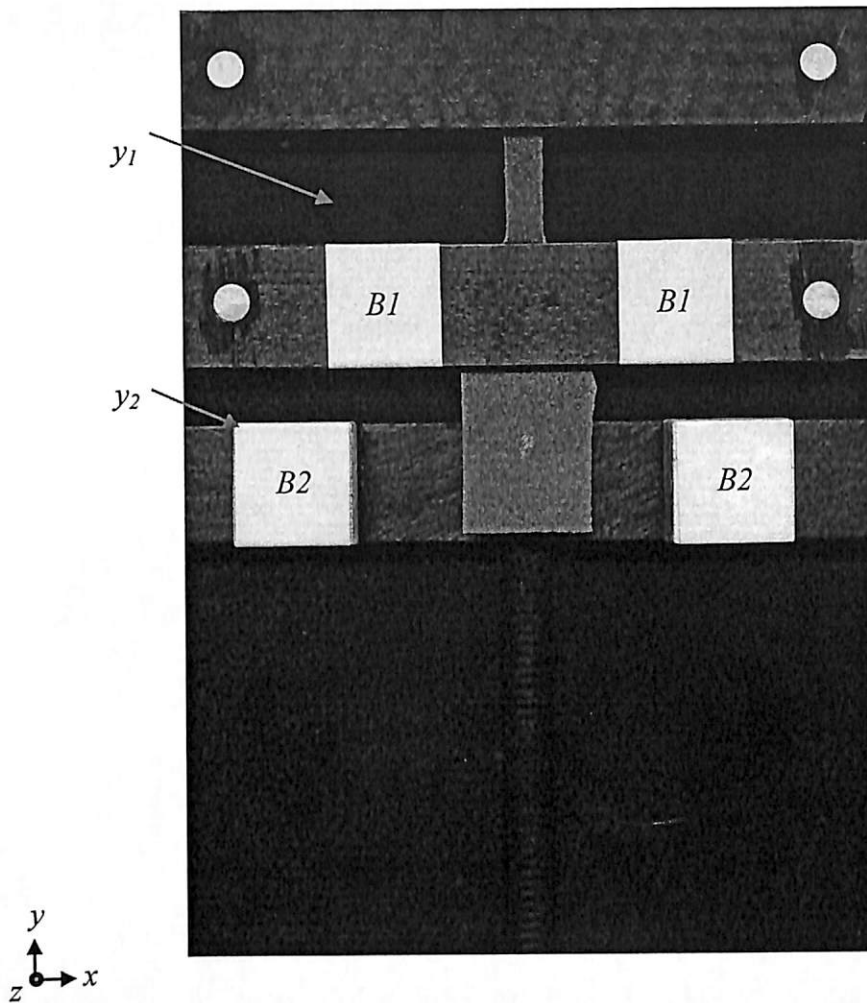


Figure 2.8 Scanned image showing white markers used to provide the spring distance

(v) In-plane displacement during loading

The out-of-plane movement happens if the surface of the rubber specimen is not parallel relative to the platen glass of the flatbed scanner. The out-of-plane movement leads to additional in-plane displacement due to the change in magnification of the acquired image. To eliminate the out-of-plane movement during loading, the gaps between the lower surfaces of the "female" clampers for both clamp sets relative to the scanner platen must be the same. A gap of 5.0 mm was designed to separate the lower surface of the "female" clampers relative to the scanner platen as shown in Figure 2.9. The positions of the two sliding rods and the leadscrew were designed precisely to support the lower clamp set so that gap of the lower surface of the "female" clamber for upper clamp set relative to the scanner platen is same as the gap of the lower surface of the "female" clamber for the lower clamp set relative to the scanner platen. After the fabrication of the motorized loading rig, the distances between the lower surfaces of the "female" clampers for both clamp sets relative

to the scanner platen were measured by using vernier caliper. The result showed that both heights gave the same value which was 5.12 mm.

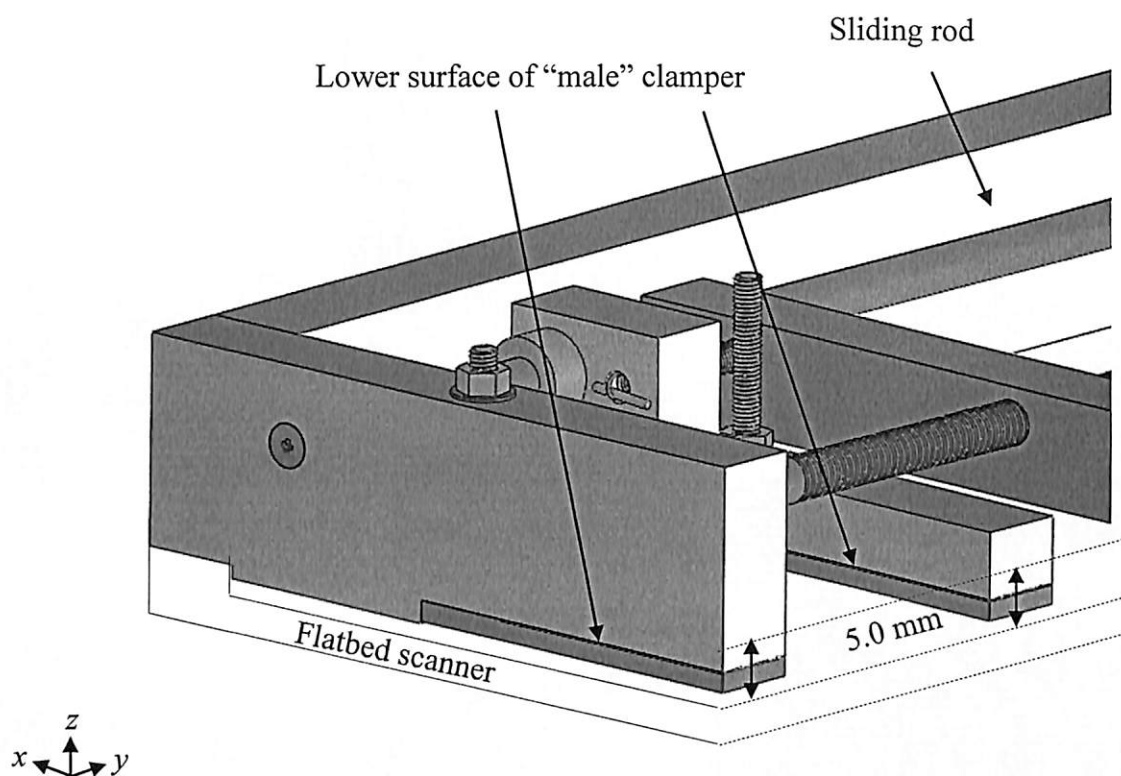


Figure 2.9. 5.0 mm gap separating the lower surface of “female” clampers relative to the scanner platen.

(vi) No backlash of the loading system

In the 2-D SB-DIC method, the loading system must be able to be paused so that the rubber specimen can be captured by the scanner. The backlash effect will cause blur images to be captured due to the movement of the rubber specimen during the image acquisition process, thus, reducing the measurement accuracy during image correlation process. Therefore, the selection of the motor used to load the rubber specimen is extremely important. Stepper motor was chosen in this work is due to its high holding torque. The high holding torque is required to hold the rubber specimen without backlash effect when the loading is paused during the scanning process. The stepper motor used in the work is MO-STEP-17PM-J342U-Minebea hybrid unipolar stepper motor, which is small in size and cheaper compared to the other types of stepper motors available in the market. The stepper motor was run by direct current of 12 V 2000 mA from an adapter, and was programmed to run at a frequency of 600 Hz. From the graph of Torque vs. Speed Characteristics of the stepper motor obtained from its data sheets, the rated pull-in torque that can be produced at 600 Hz is about 160 mNm with supply voltage of 24 V. The power output is directly proportional to the voltage supply, and so is the turning torque. Converting into the

conditions of the design of this work, which used 12 V, the rated pull-in torque of the stepper motor is about 80 mNm at rotating speed of 600 Hz.

A driver circuit (SD028 stepper motor driver) is required for precisely controlling the current in each motor phase so that accurate number of sequenced steps of the stepper motor can be achieved. The stepper motor driver consists of a circuit designed to drive both bipolar and unipolar stepper motors. The driver system controls and sends pulses of electric current to the stepper motor, controlling the motions and rotations of the motor. When a signal is sent from the control circuit connecting to the stepper motor driver, the stepper motor driver reads the signal, processes it and sends the signals of electric current pulses to the stepper motor. Different phases of the pulses sent actuate different polarity in the stepper motor, thus, rotating the shaft of the stepper motor into position.

Since it is necessary for the stepper motor to rotate to specific number of rotation, a PR7 microcontroller was chosen to complete the task, where the microcontroller can be programmed to control the stepper motor through a stepper motor driver. The microcontroller consists of a PIC (Programmable Interface Controller), PIC16F876A, which is mainly designed to program controls of stepper motor, and a circuit that supports the features of the PIC to control the stepper motor. The microcontroller is an 8 bit microcontroller with 22I/O, operating with 5V and at 20MHz. A programmer cable is required when programming the PIC, interfacing with computer connected to it. While writing program into the PIC, power supply is needed for the PR7 microcontroller board to be functioning. Though if the programming process is completed, the programmer cable no longer had to be connected to the microcontroller board.

There are four built in buttons on the PR7 microcontroller board which were programmed to control and send different command back to the PIC. The command was then processed into distinct current signals of 0 and 1, and sent to the stepper motor driver to control the motions of the stepper motor. Figure 2.10 shows the flowchart which runs when the PR7 microcontroller PCB is switched on and connected to the stepper motor and its driver.

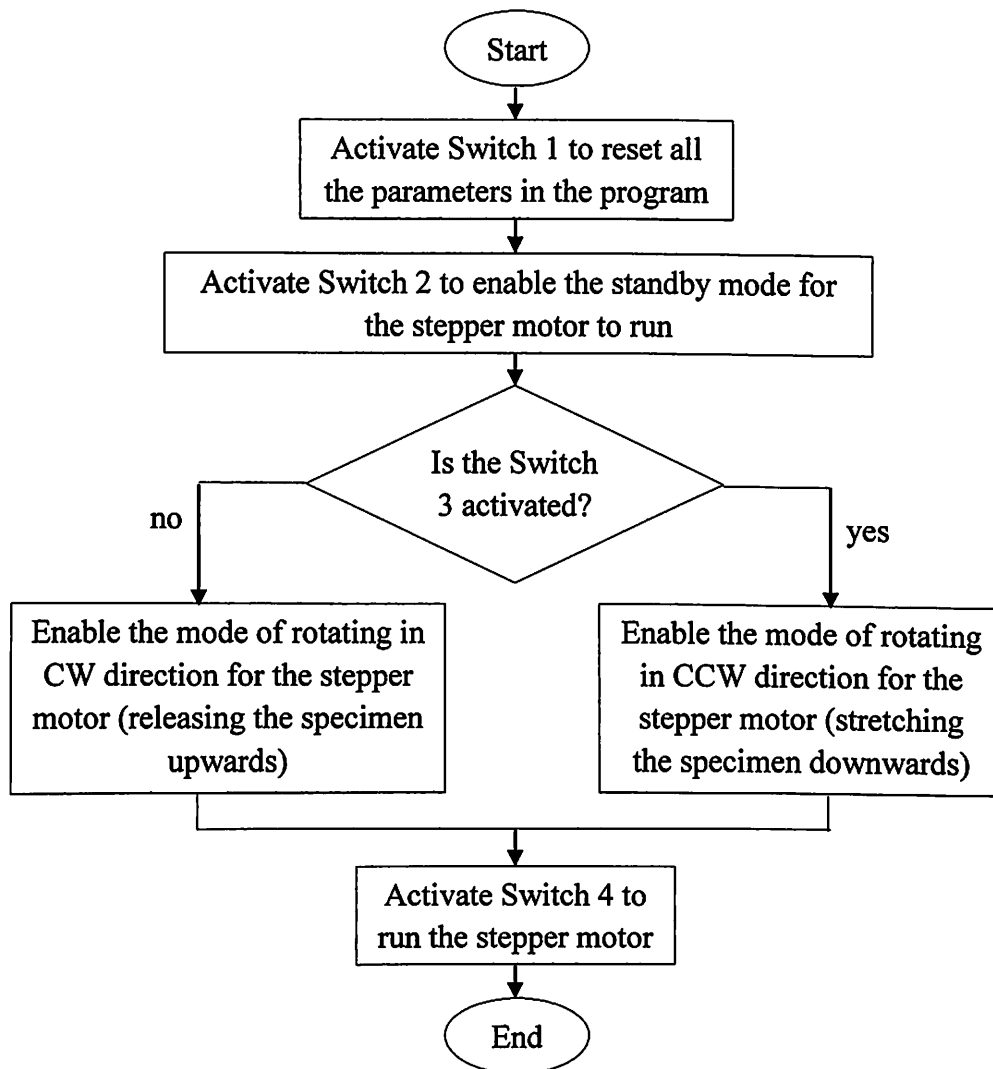


Figure 2.10 Flowchart for controlling the stepper motor

When started, the program reads the number of rotations, which was inserted into the program earlier using MPLAB IDE v8.60. Switch 1 was activated to reset all the current stated parameters in the program to its original setting. Then Switch 2 was activated to set the stepper motor driver to enable mode, which will enable the motor to run. Then, the program checks for any signal from the Switch 3, which defines the direction of motor rotation. When Switch 3 is not activated, the mode for the stepper motor to rotate in clockwise (CW) is enabled which the load applicator is moving upwards (releasing the coil springs). Otherwise, the mode for the stepper motor to rotate in counter-clockwise (CCW) direction and stretching the coil springs is enabled. The stepper motor starts to rotate if the Switch 4 is activated. The reset button on the PCB is required to be activated again if another set of run is to be performed, to release the spring back to its original length and set the parameter back to their original states.

2.3 Preliminary tests of the motorized loading rig

The preliminaries of the motorized loading rig was assessed in terms of the effectiveness of the clamping system, the force transmission efficiency and the holding torque required of the stepper motor used. A test was conducted to investigate the effectiveness of the clamping system (Section 2.3.1) and the force transmission efficiency of loading system (Section 2.3.2). Also, the required holding torque to hold the rubber specimen at static condition is determined by using the screw jack principle as explained in Section 2.3.3.

2.3.1 Slip test of the clamping system

Ensuring good clamping is crucial because a small slippage in the rubber specimen will cause large errors in the displacement and strain values. The DIC method was used to investigate the presence of slippage in the rubber specimen. A standard procedure was adopted to tighten the wing nuts when mounting the rubber specimens. The wing nuts were at first rotated through two rotations by hand and then tightened by another two rotations using a tool. The loading fixture was then placed on the scanner and the rubber specimen having a speckle pattern was stretched to the maximum length of the platen glass of flatbed scanner. The stretched specimen was scanned as the reference image. Another nine images were scanned every ten minutes without disturbing the experiment setup. The experiment was repeated for another two different rubber specimens. The slipping displacements were then computed using the DIC method. The size of cropped image was 2325×1115 pixel. The three subsets used to compute the slipping displacements were the top (i.e. from pixel 557 to 607), center (i.e. pixel 1138 to 1188) and bottom (i.e. 1720 to 1770) regions. The subset size is 51×51 pixels.

2.3.2 Force transmission efficiency test of loading system

The force applied on the rubber specimen was determined by the restoring force induced by the springs attached to the load applicator and the lower clamp set. However, it is not possible to transmit the restoring force of springs fully to the rubber specimen since some of the forces will be lost due to friction in the moving parts of the loading rig. Therefore, a test was conducted to obtain the force transmission ratio which was used as a scaling factor to obtain the net force applied to the rubber. A calibrated spring ($k= 282.2$ N/m) was clamped as a specimen to determine the output force as shown in Figure 2.11. The loading fixture was placed on the flatbed scanner without applying any load. Next, ten rotations were applied to the motor to load the spring and image of the loading rig with the stretched springs was scanned. The loading and scanning process were repeated until a total of six images

were scanned. This experiment was repeated for another two sets of readings using the same springs.

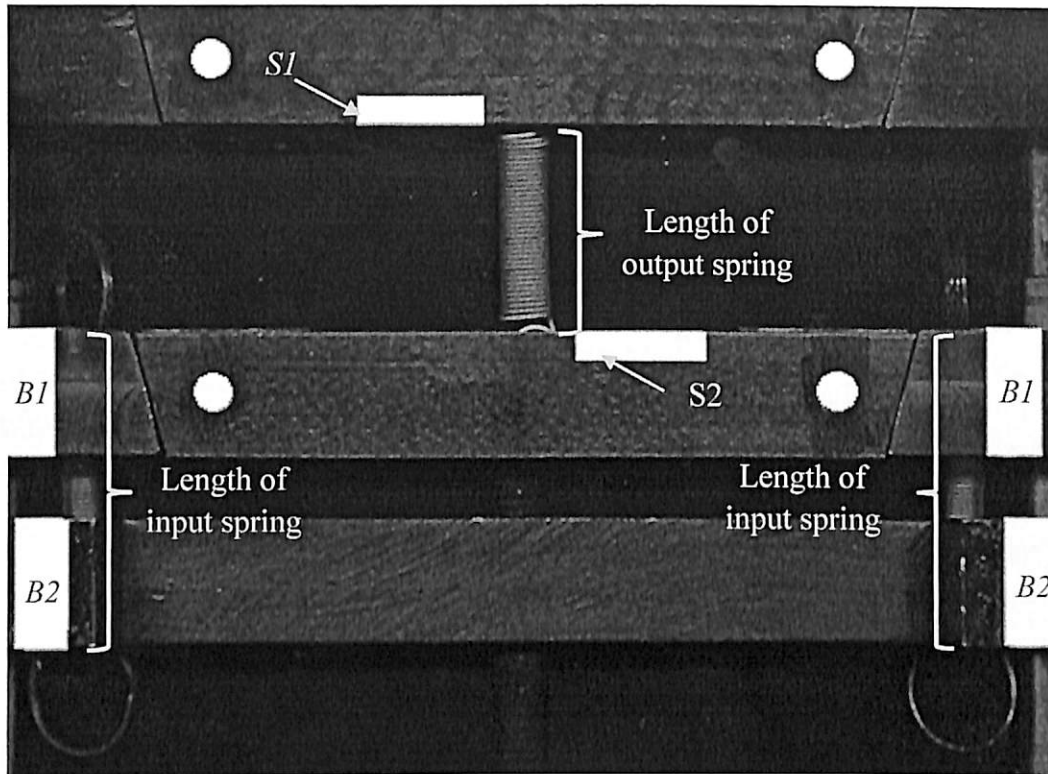


Figure 2.11 Scanned image showing white markers used to obtain spring distances in image processing

The markers $S1$ and $S2$ were used to determine the length of the output spring by subtracting the y -coordinate at the top left of marker $S2$ with the y -coordinate at bottom right of marker $S1$. Meanwhile, the length of the input spring was determined by subtracting the y -coordinate at top left corner of marker $B1$ by the y -coordinate at bottom left corner of marker $B2$. Then, the force applied by the two parallel springs (also known as input force) was determined by using Eq. (2.4) while the output force was determined by using following equation:

$$F_{out} = k_{out}x_{out} \quad (2.5)$$

where k_{out} is the spring constant of the output spring and x_{out} is the extension for the output spring during the loading. The force transmission ratio was obtained by dividing the output force by the input force.

2.3.3 Holding torque determination of the stepper motor

The maximum output torque induced by the driven gear to rotate the leadcrew and drive the clamping system was calculated by using the screw jack principle. Screw jack is used to overcome a heavy pressure or raise a heavy load, W_r by a much smaller force applied at the handle. Neglecting the friction, the force applied, F_h to move the handle multiplied by the distance through which it moves in one complete turn is equal to the weight lifted times the pitch of the leadscrew (Bird, 2003). In one complete turn at the end of the handle describes a circle of circumference $2\pi r$, where r is the distance of the handle from the centre of the leadscrew to the end point of the handle. Thus, the work done to move the handle with radius r is represented by:

$$W_r l = F_h 2\pi r \quad (2.6)$$

Also, the output torque of the induced on handle of the the screw jack is represented as (Serway and Jewett., 2014):

$$\tau_o = F_h r \quad (2.7)$$

Meanwhile the relationship between the input torque and the output torque in the gear train of the loading system for motorized loading rig is (Bird, 2003):

$$\tau_o = \tau_i \times GR \quad (2.8)$$

where τ_i is the input torque (torque induced by the stepper motor) and GR is the gear ratio. The heavy load, W_r for the screw jack is analogy to the maximum load applied onto the rubber specimen (F_a or F_r shown in page 47) at 350% strain in the motorized loading rig. By rearranging the Eq (3.6), Eq.(2.7) and Eq.(3.8) the input torque induced by the stepper motor is reduce to

$$\tau_i = \frac{F_r l}{2\pi GR} \quad (2.9)$$

The F_r was obtained by averaging the load applied onto the rubber specimen at 350% axial strain which was obtained from the standard tensile test. The holding torque determination is given in Section 4.1.3 (page 93). The maximum input torque must be less than 80 mNm (theoretical value obtained from datasheet) so that no backlash effect occurs when the loading was paused.

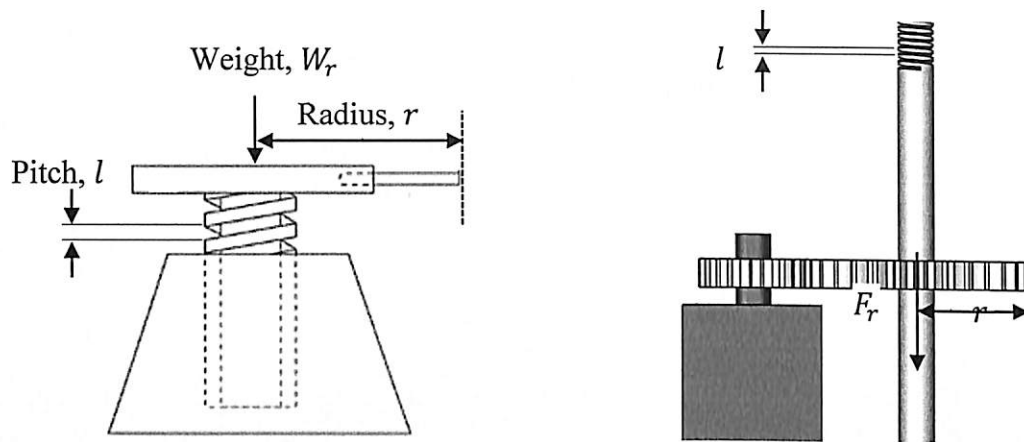


Figure 2.12 Analogy of the screw jack principle and motorized loading rig

2.4 Preliminary tests of flatbed scanner

The uniformity of the illumination during image acquisition is one of the important factors to achieve high accuracy in displacement and strain measurement. This is because the variation of the light intensity affects the speckle pattern before and after deformation in the image processing. This in turn reduces the accuracy of the speckle pattern matching and the displacement measurement. A test was conducted to investigate the uniformity of the light intensity provided by the flatbed scanner as explained in Section 3.4.1. Moreover, due to the gaps separating the surfaces of the white markers (used to determine the force applied) and the lower surface of the rubber specimen relative to the scanner platen, experiments were conducted to obtain the corrected scanning resolution which later used in spring distance and displacement measurement (Section 2.4.2).

2.4.1 Uniformity test of light intensity of flatbed scanner

A standard fixed frequency target (Figure 3.13) was placed above of the scanner platen. The standard fixed frequency target was scanned at scanning resolution of 600 dpi. The scanned image was then processed using MATLAB R2014. The scanned image was first binarized using a threshold value of 0.5. The light intensity profiles at eight regions were then measured and plotted using "improfile" command.

2.4.2 Corrected scanning resolution test of flatbed scanner

Since there are 1.24 mm (refer to Section 2.2 criteria (iii)) and 3.06 mm of gaps separating the surfaces of the white markers and the lower surface of the rubber specimen relative to the scanner platen, respectively, the corrected scanning resolution at these

heights were determined. The height of the lower surface of the rubber specimen relative to the scanner platen was obtained by deducting the average thickness of the dumbbell-shaped rubber specimen which was 2.06 mm (measured by using CMM) by the gap between the lower surface of the “female” clampers relative to the scanner platen which was 5.12 mm (Section 3.2 criteria (v)) A standard fixed frequency target was placed 1.24 mm and 3.06 mm above of the platen glass of the flatbed scanner by using 4 sets of gauge blocks. The gauge blocks were first cleaned by soft cloth and wrung together to obtain the desired height. Then the standard fixed frequency target was scanned at scanning resolution of 600 dpi. The scanned image was then processed using MATLAB for determining the corrected scanning resolution. In image processing, the scanned image was binarized with a threshold value of 0.5. Then three different sizes of dots (large, medium and small) on the scanned images were cropped out independently (Figure 2.14). The centroids of the dots in every row and column for the three different sizes of dots were determined using ‘regionprops’ command. The distance between the first dot and the last dot in the horizontal direction was determined by subtracting the x -coordinate of the centroid for the first dot by the x -coordinate of the centroid for the last dot. Meanwhile the distance between the first dot and the last dot in the vertical direction was determined by subtracting the y -coordinate of the centroid for the first dot by the y -coordinate of the centroid for the last dot. Since the distances are in pixels unit, the corrected scanning resolution in dpi unit, $R_{corrected}$ was obtained by using the following equation:

$$R_{corrected} = \frac{d_{pixel}}{S/25.4} \quad (2.10)$$

where d_{pixel} is the distance in pixels unit and S is the square length in mm unit. The mean corrected scanning resolution $\bar{R}_{corrected}$ was obtained by averaging the total corrected scanning resolution determined from every rows and columns. To convert the distance in mm unit, d_{mm} the following equation was use:

$$d_{mm} = \frac{d_{pixel}}{\bar{R}_{corrected} / 25.4} \quad (2.11)$$

Distortion test of the flatbed scanner was also carried out by using the corrected scanning resolution obtained at height of 3.06 mm above the platen glass. The distortions in x - and y -directions are obtained by determining the deviation of the corrected scanning resolution for the first and thirteen columns (y -direction) and rows (x -direction) of centroidal distance.

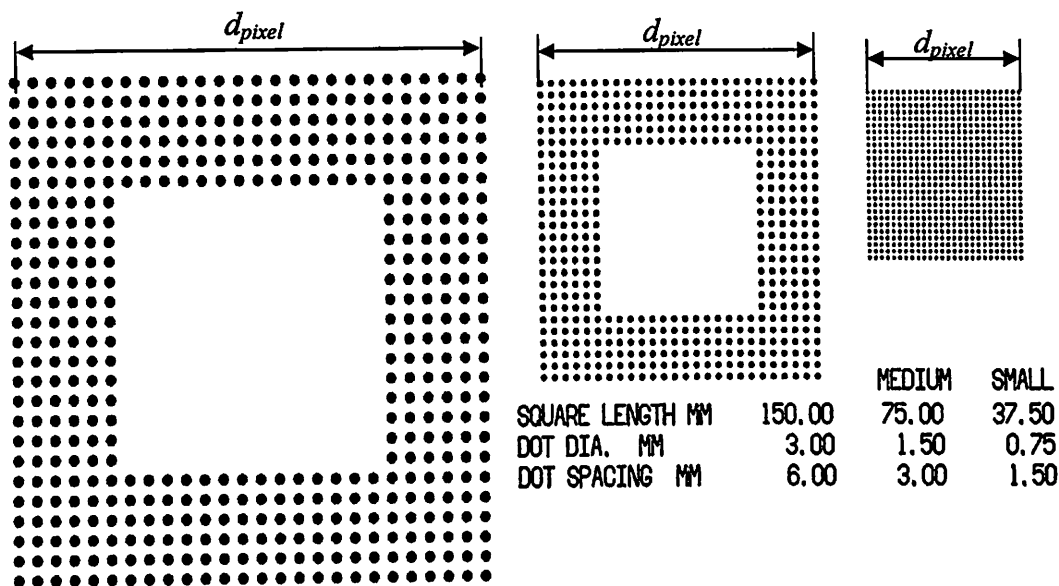


Figure 2.14 Three independent dot sizes used to obtain the corrected scanning resolution

2.5 Principle, variables, algorithm and experimental procedure of 2-D SB-DIC method

The DIC principle is discussed in Section 3.5.1. The variables used for strain and the Poisson's ratio calculation in the 2-D SB-DIC method are presented in Section 3.5.2. The theoretical Poisson's function used to validate the Poisson's ratio obtained from the incremental 2-D SB-DIC method is also explained under this section. The experimental procedure and the algorithms for the 2-D SB-DIC method used to obtain the displacement field in rubber specimen are outlined in Section 3.5.3 to Section 3.5.5. The reliability test of the DIC algorithm in detecting a white speckle is presented in Section 3.5.6.

2.5.1 The DIC principle

In the DIC method the random speckle pattern in a predefined reference subset is correlated with the deformed image. Figure 3.15 shows simulated speckle images before and after deformation. A square reference subset with predefined size 31×31 pixels centred at point f is first selected. The tracking process is carried out to find the location of a subset centred at point g that gives the highest correlation coefficient. The displacement and direction from the point f to g gives the in-plane displacement vector. The correlation coefficient is computed by using either the cross-correlation (CC) criterion or the sum-squared difference (SSD) correlation criterion (Pan et al., 2009). In this work, the following normalized cross-correlation criterion (NCC) was adopted:

$$C_{NCC} = \sum_{i=-M}^M \sum_{j=-M}^M \left[\frac{f(x_i, y_j)g(x'_i, y'_j)}{\left(\sqrt{\sum_{i=-M}^M \sum_{j=-M}^M [f(x_i, y_j)]^2} \right) \left(\sqrt{\sum_{i=-M}^M \sum_{j=-M}^M [g(x'_i, y'_j)]^2} \right)} \right] \quad (2.12)$$

where $f(x_i, y_j)$ is the pixel value in the reference image while $g(x'_i, y'_j)$ is the pixel value in the deformed image.

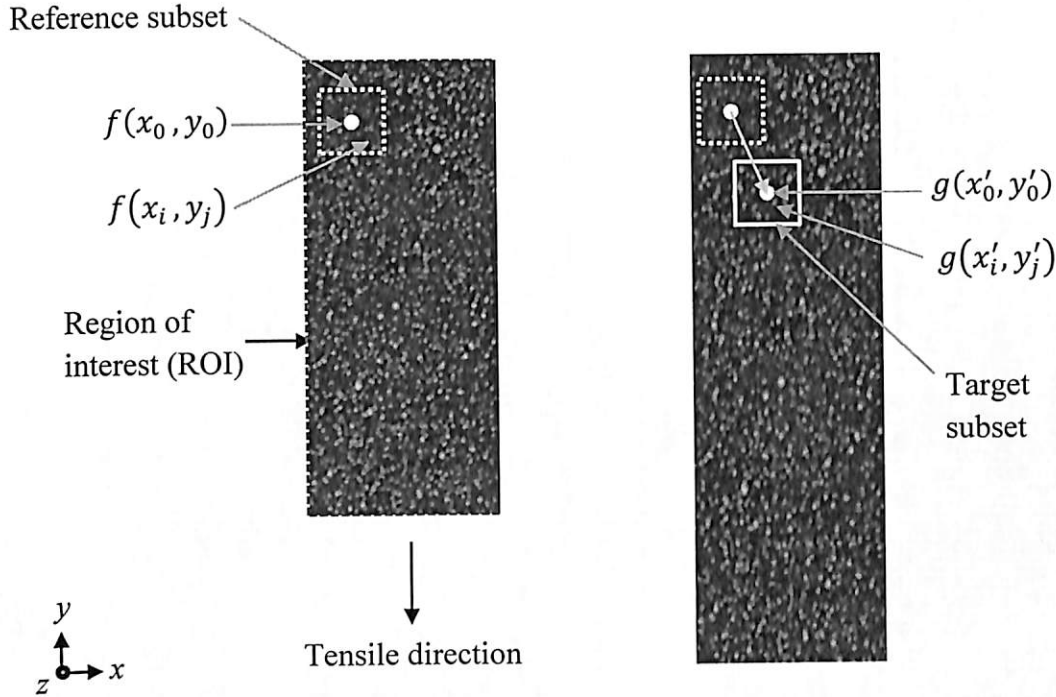


Figure 2.15 Principle of the DIC method

2.5.2 Strain calculation and Poisson's ratio (PR) variables

The engineering strain ϵ_a^e in the axial direction and lateral direction ϵ_l^e for the 2-D SB-DIC method were calculated using the following equations (Starkova and Aniskevich, 2010):

$$\epsilon_a^e = \frac{\Delta l}{l_{is}} = \frac{l_{fs} - l_{is}}{l_{is}} = \frac{l_{fs}}{l_{is}} - 1 = \lambda_1 - 1 \quad (2.13)$$

$$\epsilon_l^e = \frac{\Delta w}{w_{is}} = \frac{w_{fs} - w_{is}}{w_{is}} = \frac{w_{fs}}{w_{is}} - 1 = \lambda_2 - 1 \quad (2.14)$$

where l_{is} is the initial length given by the distance of the centroid of each subset from the reference end, l_{fs} is the corresponding final length, Δw is width contraction, w_{is} is the initial width given by the distance between center points of each subset from the center position of the rubber specimen, w_{fs} is the corresponding final width, λ_1 is the axial stretch ratio which is defined as the ratio of final length to initial length and λ_2 is lateral contraction ratio which is

defined as final width to initial width. The definition of the variables used in DIC local strain measurement is shown in Figure 2.16.

The Poisson's ratio (ν^e) of the material based on the engineering strain is calculated using following equation:

$$\square \nu^e = - \frac{\varepsilon_l^e}{\varepsilon_a^e} = - \frac{\lambda_2 - 1}{\lambda_1 - 1} \quad (2.15)$$

Meanwhile, the Poisson's ratio (ν^t) based on the true strain is calculated using following equation:

$$\nu^t = - \frac{\varepsilon_l^t}{\varepsilon_a^t} \quad (2.16)$$

where ε_l^t and ε_a^t are the true lateral strain and true axial strain respectively. Since,

$$\varepsilon_l^t = \int_{w_{is}}^{w_{fs}} \frac{dw}{w} = \ln \frac{w_{fs}}{w_{is}} = \ln \left(\frac{w_{is} + \Delta w}{w_{is}} \right) = \ln (1 + \varepsilon_l^e) \quad (2.17)$$

and

$$\varepsilon_a^t = \int_{l_{is}}^{l_{fs}} \frac{dl}{l} = \ln \frac{l_{fs}}{l_{is}} = \ln \left(\frac{l_{is} + \Delta l}{l_{is}} \right) = \ln (1 + \varepsilon_a^e) \quad (2.18)$$

therefore Eq. (3.16) is reduces to

$$\nu^t = - \frac{\ln (1 + \varepsilon_l^e)}{\ln (1 + \varepsilon_a^e)} = - \frac{\ln \lambda_2}{\ln \lambda_1} \quad (2.19)$$

The global axial strain and lateral strain of the specimen were obtained by averaging all the local strains in the specimen for each load applied.

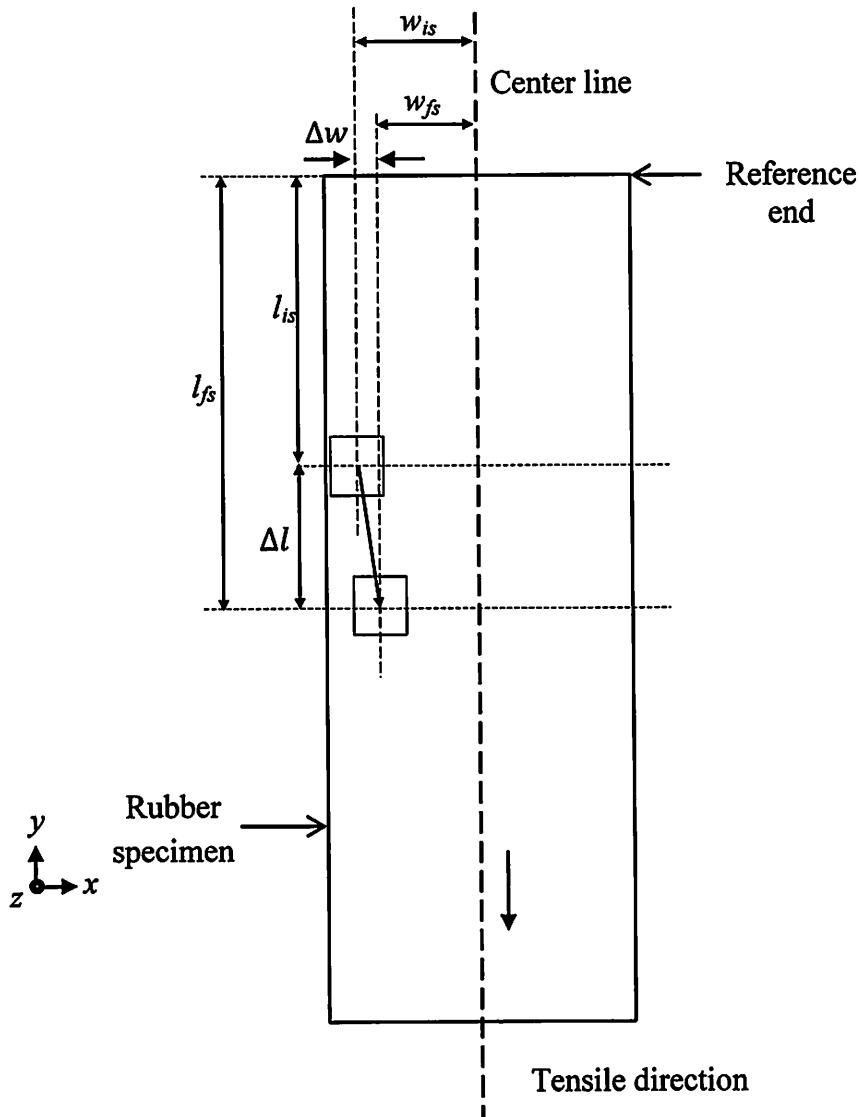


Figure 2.16 Variables used in local strain measurement for 2-D DIC method

2.5.2(a) Validation of Poisson's ratio

The Poisson's ratio of rubber is commonly reported in the literature as a constant, i.e. 0.5 (Han et al., 2012, Starkova and Aniskevich, 2010, Pritchard et al., 2013). However, this value depends on the types of stretch ratio measured. Starkova and Aniskevich (2010) proved that all stretch ratio measures give the same value of Poisson's ratio (0.5) at infinitesimal strain ($\epsilon_a^e \ll 1$). However, at large deformation the Poisson function should be used for analysis instead of the constant Poisson's ratio. In this research, Poisson's ratio based on engineering strain and true strain obtained from the 2-D DIC method were validated with the stretch-dependent Poisson's ratio proposed by Starkova and Aniskevich (2010). In the case of incompressibility assumption of the rubber specimen, $\lambda_2 = \lambda_3$ and $\lambda_1 \lambda_2 \lambda_3 = 1$, where λ_3 is the lateral contraction ratio in thickness. Therefore,

$$\lambda_2 = (\lambda_1)^{-1/2} \quad (2.20)$$

From Eq(s). (3.15) and (3.20), the Poisson function based on engineering strain in terms of the the axial stretch ratio is obtained as follows:

$$\square v^e = - \frac{(\lambda_1)^{-1/2}-1}{(\lambda_1)-1} = \frac{1}{(\lambda_1)+(\lambda_1)^{1/2}} \quad (2.21)$$

The Poisson function given by Eq. (3.21) was plotted to validate the experimental result using incremental 2-D SB-DIC method. Unlike the Poisson function based on engineering strain, the Poisson's ratio is a constant value based on the true strain with the isotropic incompressibility assumption. From Eqs. (3.13), (3.14), (3.16) and (3.20), the Poisson's ratio based on true strain v^t is given as:

$$v^t = - \frac{\ln(\lambda_1)^{-\frac{1}{2}}}{\ln(\lambda_1)} = 0.5 \quad (2.22)$$

2.5.3 Experimental procedure for 2-D SB-DIC method

The experimental setup of the 2-D SB-DIC method is shown in Figure 3.17. The flowchart of the tensile test for the rubber specimen by using 2-D SB-DIC method is shown in Figure 2.18.

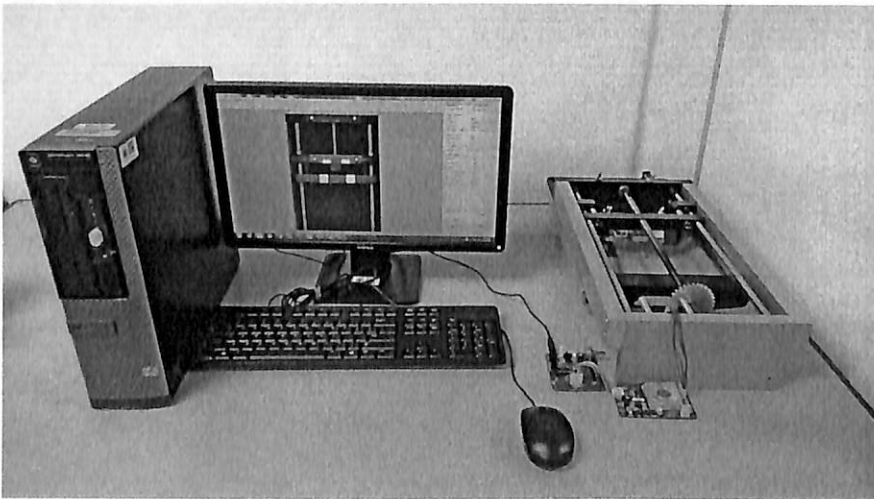


Figure 2.17 Experimental setup of the 2-D SB-DIC method

The speckle pattern was produced on the rubber specimens by using a matt-white aerosol spray (Type: 32 Baltic White, SAMURAI paint, Kuala Lumpur, Malaysia). The rubber specimen was then dried at room temperature for one hour. The rubber specimen with speckle pattern (Figure 2.19) was clamped onto the motorized loading rig. The motorized loading rig was placed on the flatbed scanner. Pre-loading was applied to the rubber

specimen to prevent sagging. The pre-load applied was then added into the force applied (Eq. (2.4)) at a particular loading stage. The pre-loaded rubber specimen was scanned and the image was saved by using PhotoStudio 5.5. The rubber specimen was then stretched incrementally by applying small loads (2 rotations of driver gear equivalent to 3-5% strain of the original length). The load applied was controlled by the stepper motor. The deformed rubber specimen was scanned (i. e. 600 dpi corresponding to an image resolution of 0.0432 mm/pixel) and the image was saved.

The loading and scanning were continued in stages until the load applicator has reached the lower edge of the platen glass. The total time taken for loading and scanning was 55 minutes. Using this approach a total of 76 images including the reference image were scanned for a maximum strain of 350%. At the maximum strain the extended length of the specimen is 112.5 mm. The loading and scanning were done manually. The strain rate used was 0.045 s^{-1} which was determined by dividing the maximum global strain by the total time taken for the loading. The scanned images were then saved and the image correlation process was started by using the conventional 2-D DIC algorithm and the proposed single-step 2-D DIC algorithm which are discussed in detail in Section 2.5.4 and Section 2.5.5.

The loading and scanning were continued in stages until the load applicator has reached the lower edge of the platen glass. The total time taken for loading and scanning was 55 minutes. Using this approach a total of 76 images including the reference image were scanned for a maximum strain of 350%. At the maximum strain the extended length of the specimen is 112.5 mm. The loading and scanning were done manually. The strain rate used was 0.045 s^{-1} which was determined by dividing the maximum global strain by the total time taken for the loading. The scanned images were then saved and the image correlation process was started by using the conventional 2-D DIC algorithm and the proposed single-step 2-D DIC algorithm which are discussed in detail in Section 2.5.4 and Section 2.5.5.

2.5.4 Algorithm of incremental 2-D SB-DIC method

A flowchart of the algorithm used to process the scanned image is shown in Figure 3.20. Firstly, the total number of scanned images is counted. A variable "v" keeps track of the number of images read and processed. A zeros array of size 198 rows and 75 columns is created to store the result. The reference image and the deformed image were then cropped out using auto-cropping algorithm as shown in Figure 2.21.

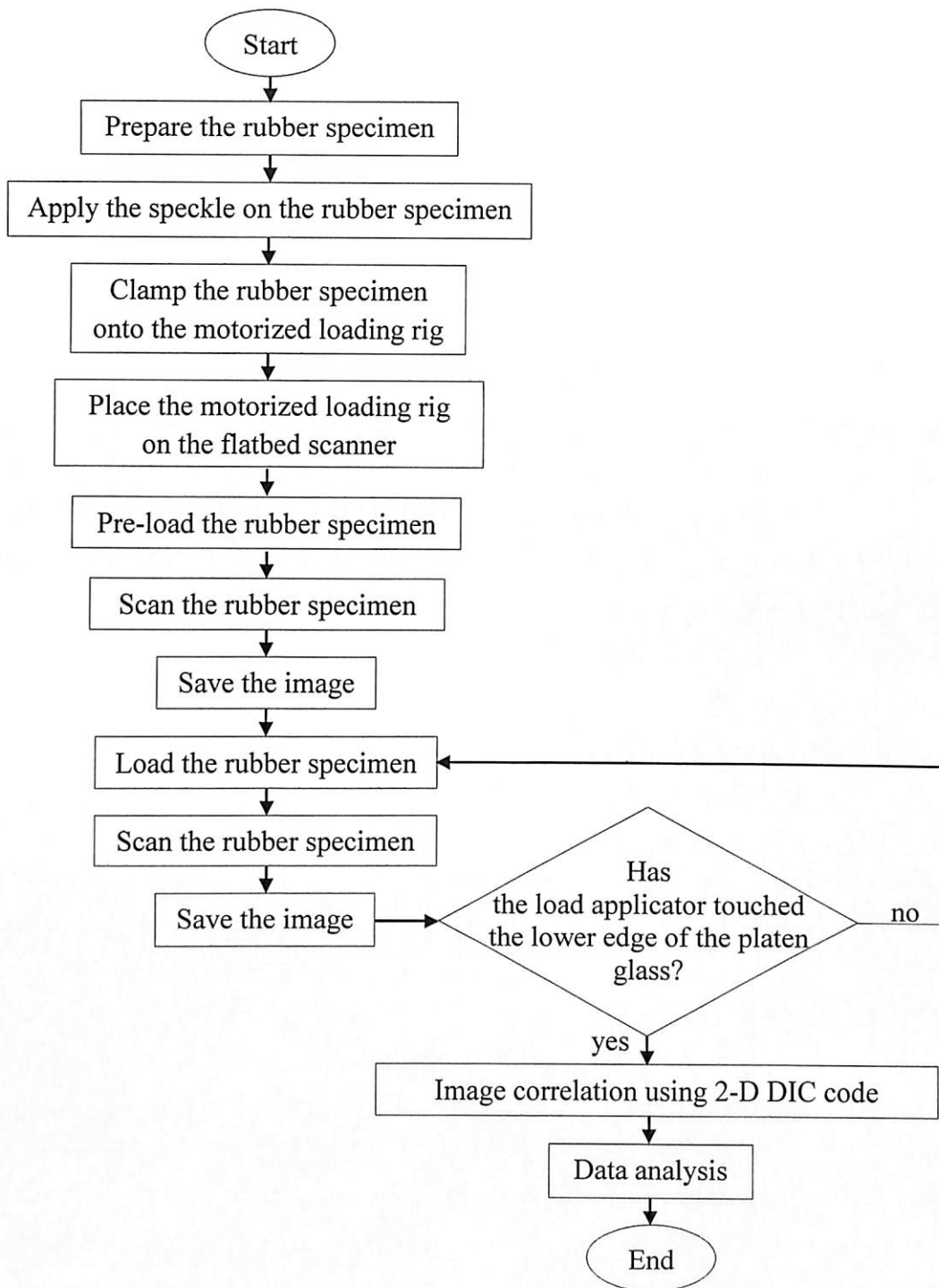


Figure 2.18 Flowchart of the 2-D SB-DIC experiment.

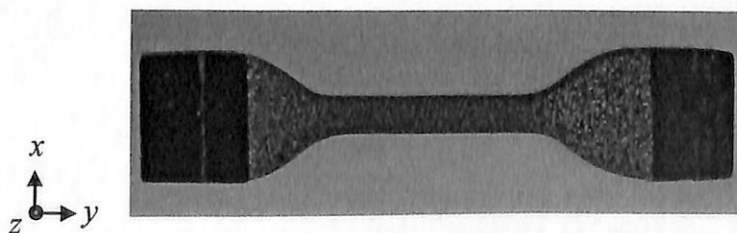


Figure 2.19 Rubber specimen with speckle pattern

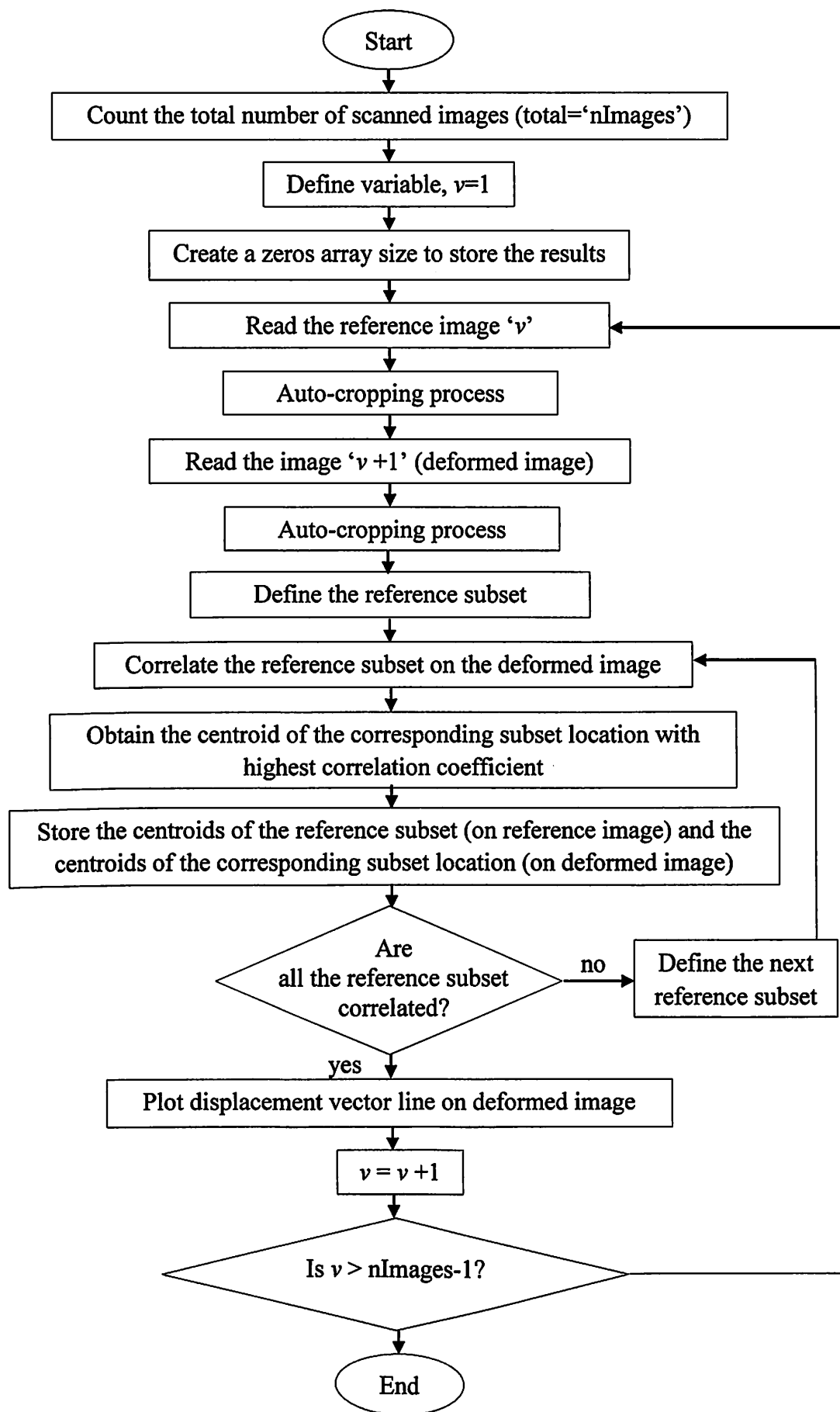


Figure 2.20 Flowchart of the incremental SB-DIC method

The images were binarized using a threshold value T_h of 0.5. Four circular dots are kept for the auto-cropping process by removing the rectangular white markers and noise using “bwareaopen” command. The centroids of the four circular dots are then determined for the purpose of creating an auto-cropping window using “regionprops” command. Figure 2.22 shows the region of interest (ROI) of an auto-cropped image after binarization

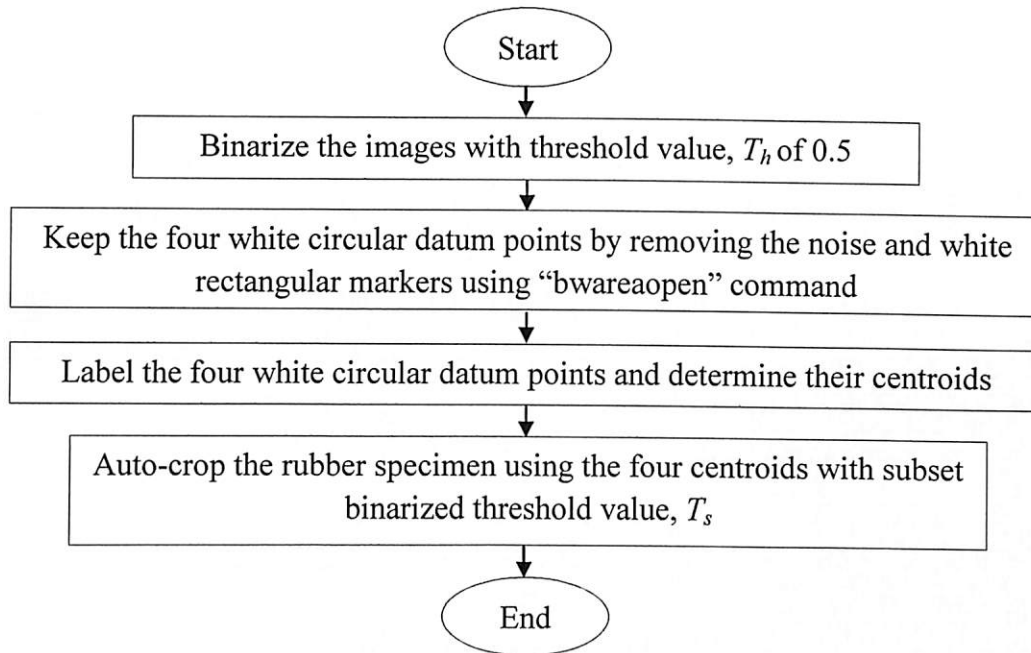


Figure 2.21 Flowchart of the auto-cropping process

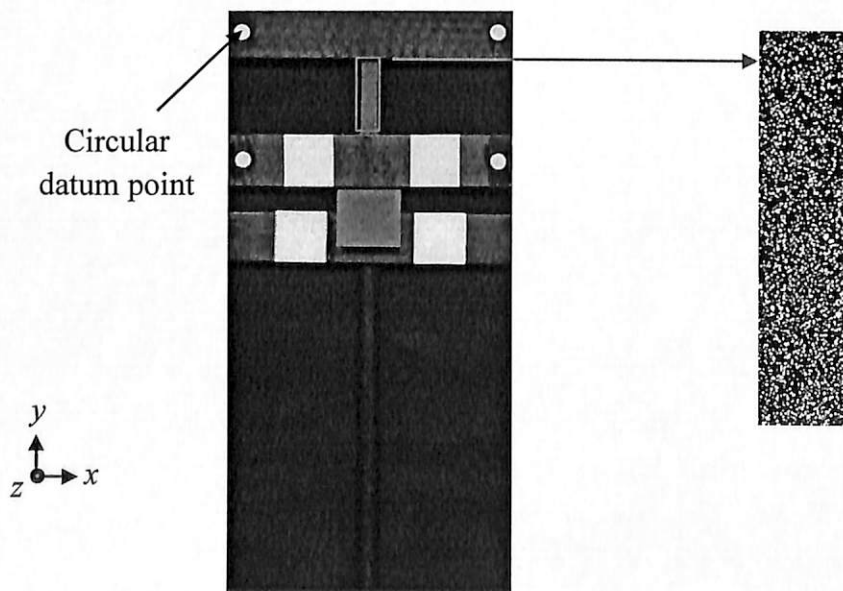


Figure 2.22 Auto-cropping of the ROI

Next, a 31×31 pixels of reference subset is defined on the reference image and each subset is correlated with the image after loading. The scanning process is started from the left of first row followed by the subsequent rows until the bottom right corner of last row. The

highest correlation coefficient and the center point in pixel coordinates of the corresponding subset with highest correlation coefficient are determined. The coordinate and the correlation coefficient are stored in the zeros array. The matching process is repeated for another sixty-five subsets (6 subsets in x-direction and 11 subsets in y-direction). The reference subset is stepped in the horizontal and vertical directions by 20 pixels and 50 pixels, respectively. Finally, the full-field displacement map is drawn by using the stored center points having the highest correlation coefficient before and after deformation. The second image used as the deformed image in the first incremental matching process is used as a new reference image to correlate with the third image (second deformed image). The process was completed once the last scanned image was correlated and full-field displacement map is drawn.

An experiment was conducted to compare the performance of the 2-D SB-DIC method by using grayscale and binary images. The procedure for the tensile test for the grayscale-image based incremental 2-D SB-DIC method was same as the binary-image based incremental 2-D SB-DIC method but the binarization process in the auto-cropping step was skipped (last step in Figure 3.21). The performance in terms of the matching accuracy and the time consumed were compared. The time was measured using the stopwatch.

2.5.4(a) Comparison between incremental 2-D SB-DIC and LaVision DIC method

A standard 2-D DIC method was performed so that the displacement field obtained from the incremental 2-D SB-DIC is able to be compared with the displacement field obtained from the standard 2-D DIC method. A dumbbell-shaped rubber specimen with white speckle pattern on it (Figure 3.19) was clamped onto the Instron 3367 (gauge length of 25 cm). The strain rate of the tensile test was same as the strain rate used in the 2-D SB-DIC method which is 0.045 s^{-1} . In order to record the deformation during the tensile test, images were taken using a camera aligned perpendicular relative to the front surface of the rubber specimen. The camera (LaVision imager pro X) features a resolution up to 29 million dpi equipped with a lens of 105 mm focal length (micro-nikkor) was used in the LaVision DIC method. The working distance between the camera and the specimen was optimized to 27 cm so that clear image is obtained and the study area is about $25 \times 6 \text{ mm}^2$. The rubber specimen was loaded up to 33% axial strain and a total number of 1000 images were acquired for the entire experiment (one reference image and the left are deformed images).

The DaVis 8.1.1 software is used to analyse the images and provide the displacement field and strain data for the deformation of the rubber specimen. A total of 153 reference subsets were used to trace the deformation on the deformed image. The subset size of the reference subset is 31×31 pixels with subset step of 31 pixels and 51 pixels in horizontal and vertical directions, respectively. The stress applied onto the rubber specimen

was obtained from the Instron while the strain data was obtained by averaging the total strain from each local subset. The DIC program used to compute the displacement data was the incremental 2-D DIC algorithm. The comparison of the displacement field and the stress-strain data between the incremental 2-D SB-DIC and LaVision DIC method are given in Section 2.2.4.

2.5.5 Principle and algorithm of single-step 2-D SB-DIC method

The principle of the proposed single-step 2-D SB-DIC method is discussed in detail in Section 2.5.5(a) while the algorithm to process the images using the single-step 2-D SB-DIC is outlined in Section 2.5.5(b).

2.5.5(a) Principle of single-step 2-D SB-DIC method

In the conventional 2-D DIC method the size of the target subset on the deformed image is the same as that of the reference subset during the correlation process. This method is accurate only when the displacement of rigid body translations and small deformations were analysed. For large deformations the reference subset size must be deformed or reshaped in order to track its corresponding location in the deformed image. Figure 2.23 illustrates the image and its reference subset at the un-deformed and deformed states. The yellow dotted box is the reference subset of size $x_0 \times y_0$ which is deformed to $x' \times y'$. The deformed reference subset is then used to track the position with the highest similarity on the deformed image.

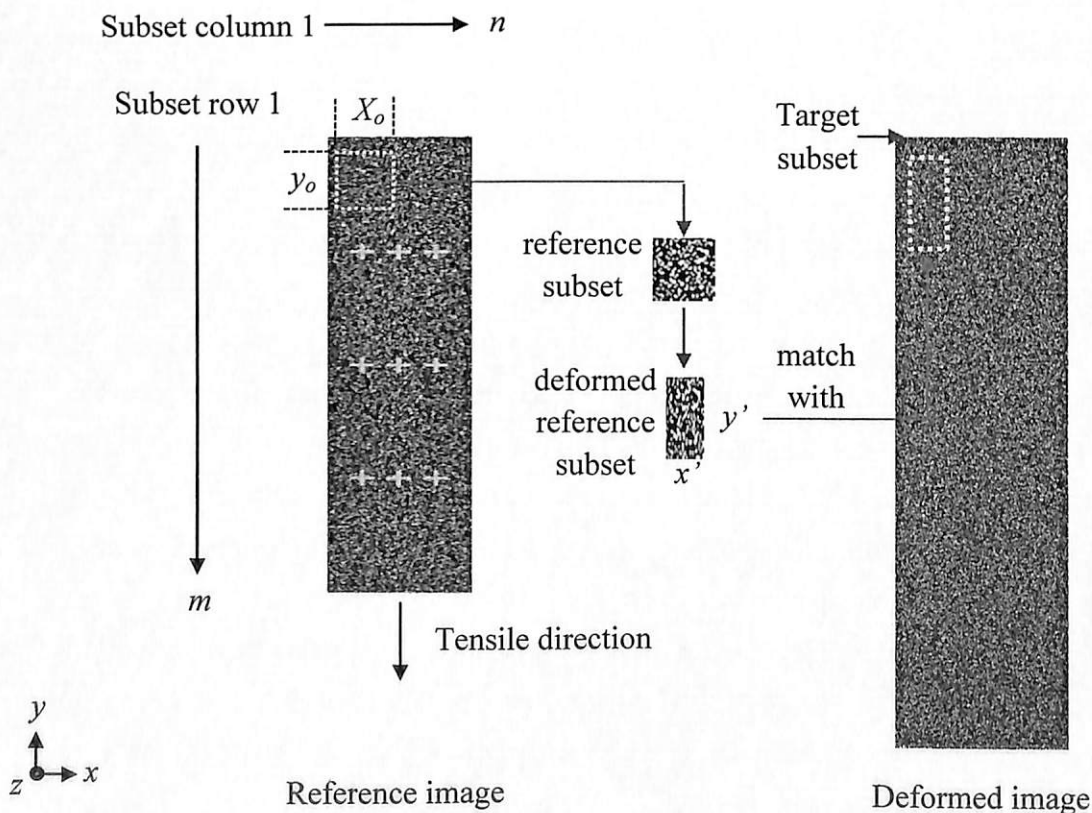


Figure 2.23 Schematic diagram of working principle for the single-step 2-D SB-DIC method

In order to obtain the 2-D deformation matrix, F to deform the reference subset the size of the reference subset was first represented by a vector \mathbf{a} which can be resolved into two components (i.e. i - and j -components) as shown in Figure 2.24. The reference subset is then assumed to be subjected to a uniform deformation F . The size of the deformed reference subset is represented by vector \mathbf{b} . Vectors \mathbf{a} and \mathbf{b} are given by,

$$\mathbf{a} = x_0 \hat{i} + y_0 \hat{j} \quad (2.23)$$

$$\mathbf{b} = x' \hat{i} + y' \hat{j} \quad (2.24)$$

Thus, the mapping of the reference subset's vector to the deformed reference subset's vector is given by

$$\mathbf{b} = \mathbf{F} \cdot \mathbf{a} \quad (2.25)$$

where F is the 2-D deformation factor which can be represented in the matrix form as

$$\mathbf{F} = \begin{bmatrix} \lambda_2 & 0 \\ 0 & \lambda_1 \end{bmatrix} \quad (3.26)$$

where λ_1 is the elongation deformation factor (equivalent to axial stretch ratio) and λ_2 is the lateral contraction deformation factor (equivalent to lateral contraction ratio).

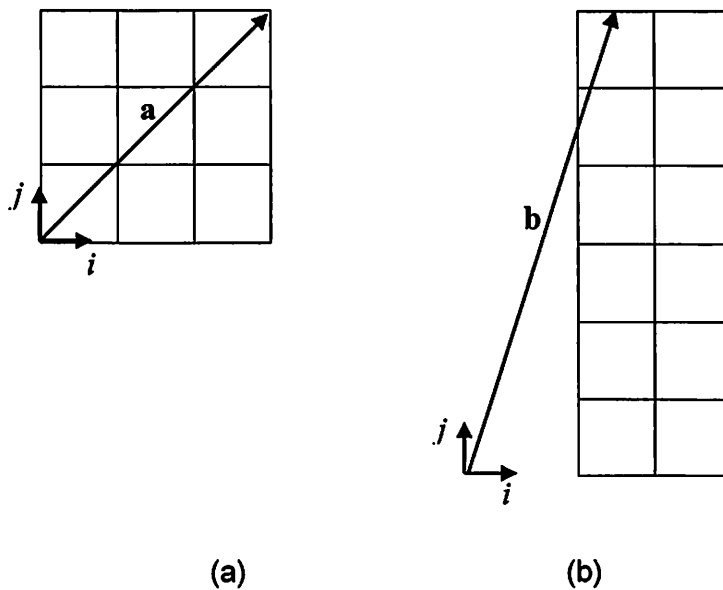


Figure 2.24 Vectors of (a) reference subset and (b) deformed reference subset

From Eqs. (2.23), (2.24), (2.25) and (2.26), the deformed reference subset can be represented in the matrix form as

$$\begin{bmatrix} x' \\ y' \end{bmatrix} = \begin{bmatrix} \lambda_2 & 0 \\ 0 & \lambda_1 \end{bmatrix} \begin{bmatrix} x_o \\ y_o \end{bmatrix} \quad (2.27)$$

A third order polynomial function was derived from the fitted mean stress-axial stretch ratio curve obtained from the standard tensile tests as shown in Figure 3.25. The third order polynomial function (Eq. (3.28)) was then inserted into the MATLAB program.

$$a\lambda_1^3 + b\lambda_1^2 + c\lambda_1 + d - \sigma = 0 \quad (2.28)$$

where a , b , c , d are constants and σ is engineering stress. The polynomial function has one real root and two complex conjugate roots by using cubic polynomial discriminant theorem when a particular of stress value was provided (Irving and Ronald, 2004). Command was given into the MATLAB to discard the two complex conjugate roots while the real root was saved. The saved real root is the elongation deformation factor λ_1 used to obtain the Poisson's ratio, ν^e .

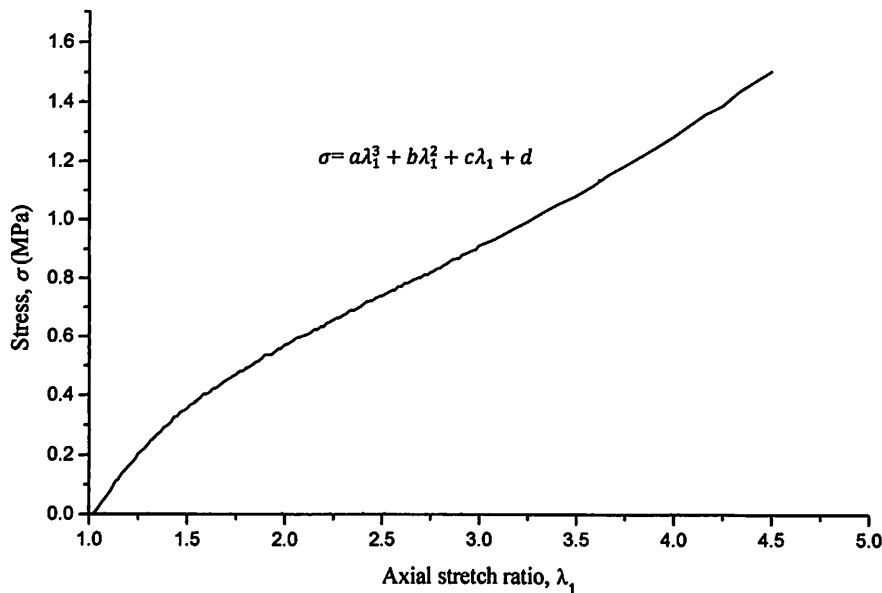


Figure 2.25 Stress-axial stretch ratio curve obtained from standard tensile machine

The lateral contraction deformation factor λ_2 was obtained from the equation derived from the theoretical Poisson function based on the engineering strain in terms of the axial stretch ratio. For a material which is incompressible, such as rubber, Eq. (2.21) is the Poisson function based on the engineering strain in term of the axial stretch ratio. As the elongation deformation factor λ_1 is obtained from the Eq. (2.28) when the stress applied on the specimen is known, the Poisson's ratio ν^e can be determined from the Eq. (3.21). Also the Eq. (3.15) is the Poisson's ratio of any material. At a particular point where $\lambda_1 = \lambda'_1$, the

Poisson's ratio $\nu^e = \nu^{e'}$. By rearranging Eq. (3.15), the lateral contraction ratio λ'_2 at a particular stress value, σ' is reduced to

$$\lambda'_2 = 1 - [\nu^{e'}(\lambda'_1 - 1)] \quad (2.29)$$

Hence, the equation for the deformed reference subset (from Eq. (3.27)) in matrix form is given by

$$\begin{bmatrix} x' \\ y' \end{bmatrix} = \begin{bmatrix} 1 - [\nu'(\lambda'_1 - 1)] & 0 \\ 0 & \lambda'_1 \end{bmatrix} \begin{bmatrix} x_o \\ y_o \end{bmatrix} \quad (2.30)$$

2.5.5(b) Single-step 2-D SB-DIC algorithm

A flowchart of the algorithm used to process the scanned images is shown in Figure 3.26. A zeros array of 198 rows and 2 columns is created to store the results. The first image (reference image) was read and the ROI of the image is cropped out by using auto-cropping algorithm (Figure 3.21). The pre-load force value was obtained by using the Eq. (3.4). Next the deformed image at a particular stage was read. The ROI of the deformed image is obtained by using auto-cropping algorithm. Then the force applied on the rubber specimen at that particular stage was obtained using the Eq. (3.4). The net force value was then determined by subtracting the pre-load force value with the force applied value at that particular stage. The stress value was then obtained by using the Eq. (3.1). The deformation factors were obtained by using the Eq. (3.28) and Eq. (3.29). Later, a reference subset was defined and cropped from the reference image. The deformation factor matrix obtained early was used to deform the reference subset.

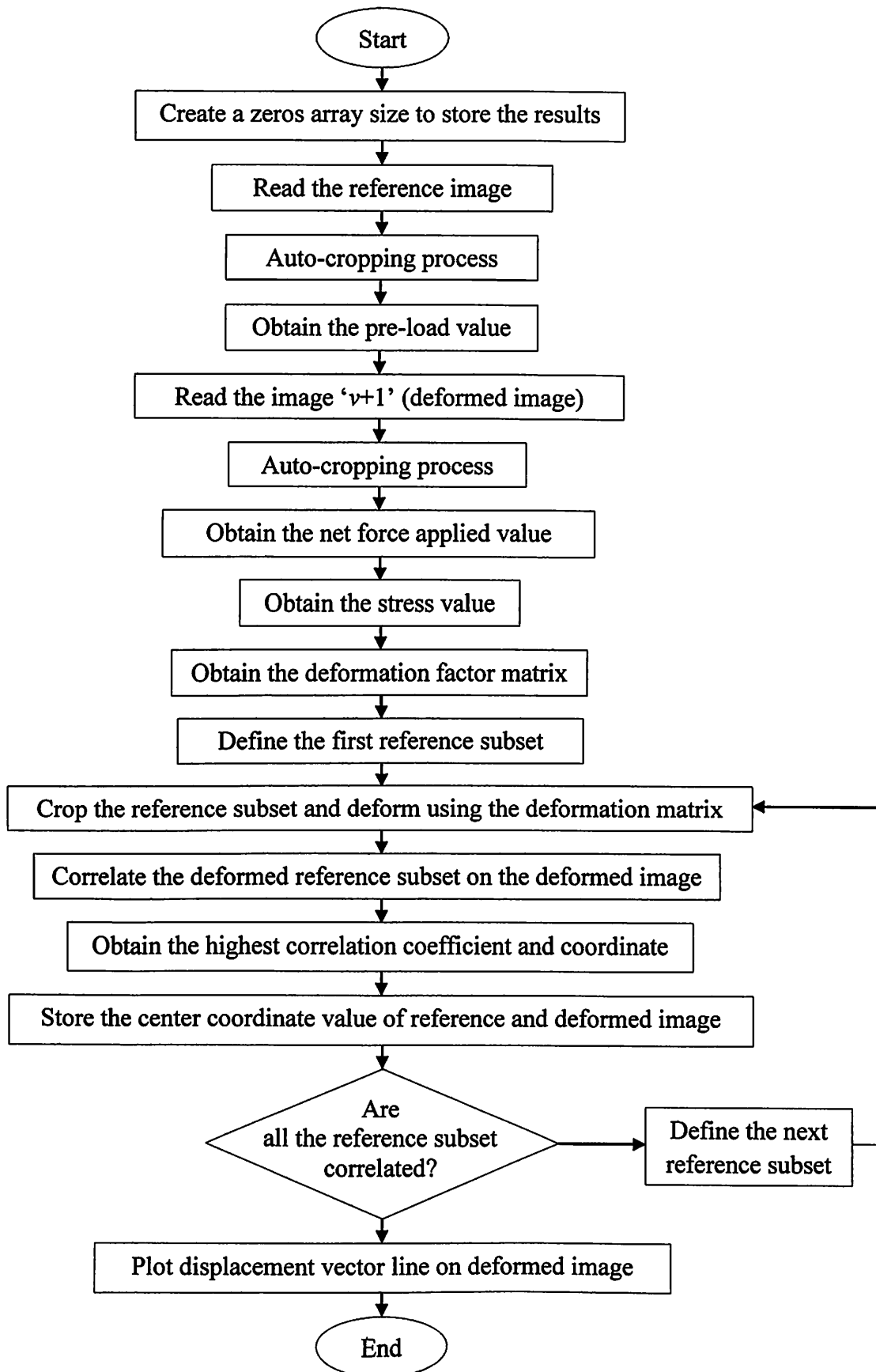


Figure 2.26 Flowchart of single-step 2-D SB-DIC method

Then, the scanning process was started from the left of first row followed by the subsequent rows until the bottom right corner of last row. The highest correlation coefficient and the center point in pixel coordinate of the subset with highest correlation coefficient are determined and stored in the zeros array. The matching process was repeated for another sixty-five subsets (6 subsets in x-direction and 11 subsets in y-direction). All the reference subsets are deformed using the same deformation factor matrix. The reference subset was stepped in the horizontal and vertical directions by 20 pixels and 50 pixels, respectively. Finally, the full-field displacement map was drawn by using the stored center points having the highest correlation coefficient before and after deformation.

The difference between the conventional incremental 2-D DIC method and the proposed single-step 2-D DIC method is illustrated in Figure 3.27. Only two images are needed (one reference image and one deformed image) to obtain the displacement field and strain field in the proposed single-step SB-DIC method. The reference subset is deformed by using deformation factor to correlate in the deformed image. Meanwhile in the conventional incremental 2-D SB-DIC method, the reference subset which correlate in the deformed image is updating from stage to stage until the last deformed image. Therefore, a large series of deformed images are needed in order to obtain displacement and strain map for large deformation measurement. Besides, the displacement data for the subsequent deformed image is solely dependent on the displacement determined from the early stage. The final full-field displacement at a particular loading stage is determined by totalling up the displacement data for every subset at every loading stage.

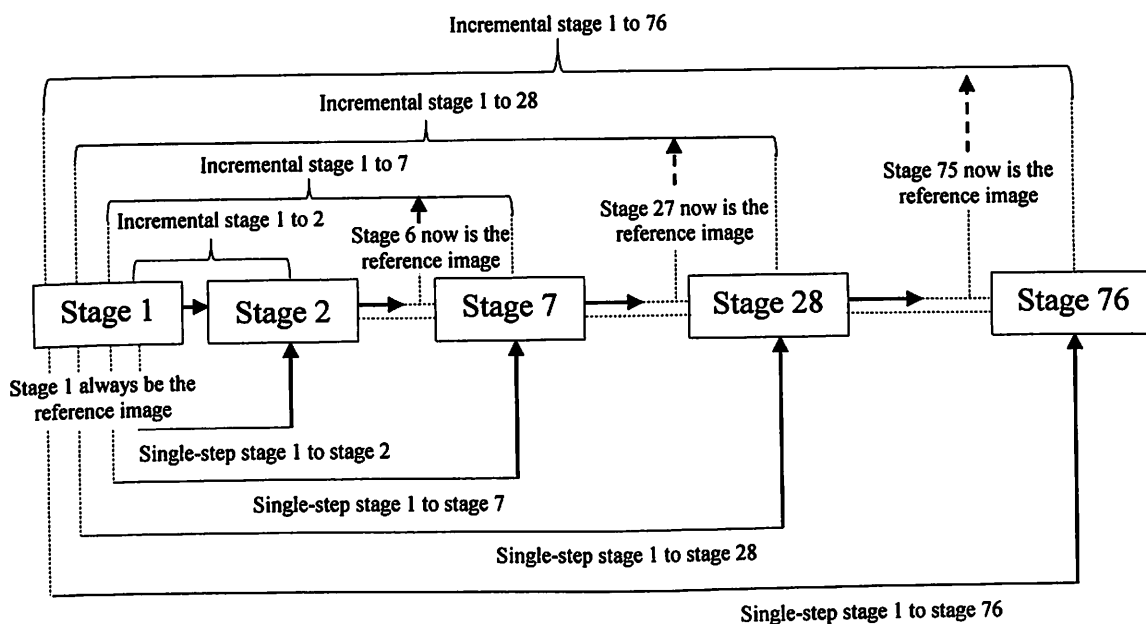


Figure 2.27 Comparison of conventional incremental SB-DIC method and proposed single-step SB-DIC method

2.5.6 Reliability of the 2-D SB-DIC algorithm

A simulation test was conducted to access the reliability of the 2D SB-DIC algorithm in searching the speckle pattern. Six images (450×150 pixels) were created by using photo editing software (Microsoft Paint) as shown in Figure 3.28. Each of the images contains one white circular dot with an area of 324 pixels. The first image was used as the reference image and the rest were assumed to be “deformed” image. The white dot in the “deformed” image was subjected to translation motion. The translation motion was done randomly. A subset size of 31×31 pixels which contains the circular dot was created at the first image to correlate the corresponding position at the five deformed image. The centroids coordinate of the dot at the reference image was [38.5, 56.05].

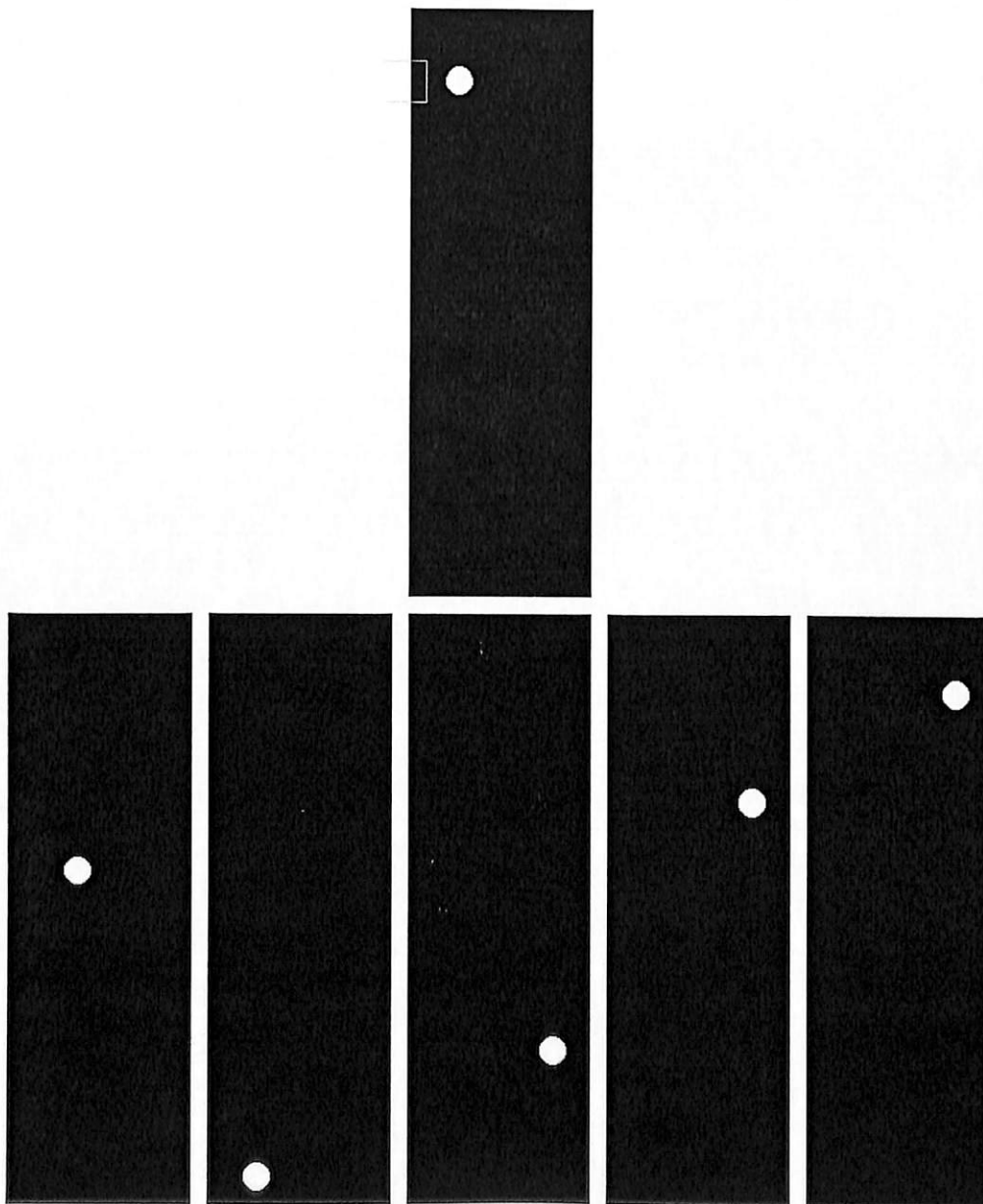


Figure 3.28 Reference image with a white circular dot and five deformed image with randomly translated white circular dots

2.6 Finite element modelling of rubber specimens

Engineering materials such as metals are classified as linear elastic material whereby the strain can be obtained at a particular stress value given that the stiffness of the material is known. However, rubber-like materials are considered as non-linear elastic materials which undergo strains that are several orders of magnitude higher than the linear elastic materials. Thus, the strain energy density function or constitutive hyperelastic models need to be defined in order to obtain the desired stress-strain relationship. Three principle stretch ratios, namely λ_1 , λ_2 , and λ_3 , are used in defining the constitutive hyperelastic models. The three strain invariants in term of stretch ratios used to define the constitutive hyperelastic models are (Odgen et al., 2004):

$$\begin{aligned} I_1 &= \lambda_1^2 + \lambda_2^2 + \lambda_3^2 \\ I_2 &= (\lambda_1\lambda_2)^2 + (\lambda_2\lambda_3)^2 + (\lambda_3\lambda_1)^2 \\ I_3 &= \lambda_1^2\lambda_2^2\lambda_3^2 \end{aligned} \quad (2.31)$$

The third invariant I_3 is equal to 1 if a material is incompressible (Laraba-Abbes et al., 2005).

The constitutive hyperelastic model is denoted as W which can be either a direct function of the principle stretch ratios or a function of the strain invariants, i.e. $W = W(I_1, I_2, I_3)$ or $W = W(\lambda_1, \lambda_2, \lambda_3)$. The engineering strain ε_a^e can be determined based on W :

$$\varepsilon_a^e = \frac{dW}{d\sigma} \quad (2.32)$$

In this research, three different constitutive hyperelastic models which are commonly used in rubber applications were used to describe the stress-strain relationship of a single-ended dumbbell-shaped rubber model with gauge dimensions of 33 × 6 × 2 mm using SolidWorks 2013 (Cosmos Non-linear Simulation Analysis) as shown in Figure 2.29. Mooney-Rivlin two-parameter, Mooney-Rivlin five-parameter and Odgen three-parameter models were chosen to fit the mean stress-strain data obtained from the standard tensile test (*Instron 3366*). The Mooney-Rivlin two-parameter and Mooney-Rivlin five-parameter models are defined as (Laraba-Abbes et al., 2005):

$$W_{(MR2)} = C_1 (I_1 - 3) + C_2 (I_2 - 3) \quad (2.33)$$

$$W_{(MR5)} = C_1 (I_1 - 3) + C_2 (I_2 - 3) + C_3 (I_1 - 3) (I_2 - 3) + C_4 (I_1 - 3)^2 + C_5 (I_1 - 3)^3 \quad (2.34)$$

where C_1 , C_2 , C_3 , C_4 and C_5 are material constants which were generated in Cosmos non-linear simulation analysis itself given that the stress-strain data obtained from the standard tensile test was inputted into material properties of rubber model.

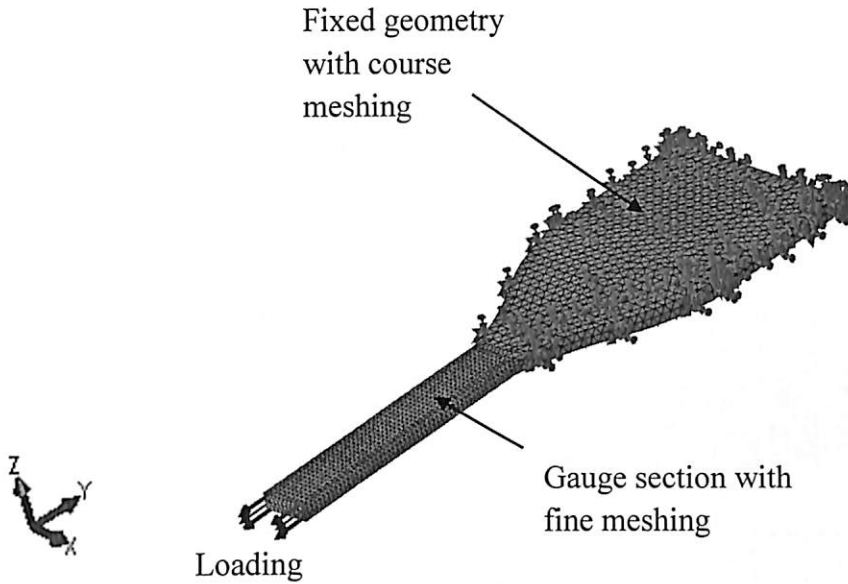


Figure 2.29 Single-ended dumbbell-shaped model used in finite element modelling

Meanwhile the Odgen three-parameter model which is the only model which is expressed in terms of the principle stretch ratio is defined as (Odgen et al., 2004):

$$W_{(Odgen)} = \sum_{i=1}^n \frac{\mu_i}{\alpha_i} (\lambda_1^{\alpha_i} + \lambda_2^{\alpha_i} + \lambda_3^{\alpha_i} - 3) \quad (2.35)$$

where μ_i and α_i are material constants which were generated in Cosmos non-linear simulation analysis itself given that the stress-strain data obtained from the standard tensile test was inputted into material properties of rubber model. The best model which has the best-fit with the mean stress-strain curve from the standard tensile tests was used to characterize the two rubber models containing a circular hole (Figure 3.30 (a)) and square hole (Figure 3.30 (b)) respectively. The dimensions of the models were same as the dimensions of the rubber specimens used in tensile tests as shown in Figure 3.2. The equation used to determine the resultant strains for the 2-D SB-DIC method is defined as:

$$\varepsilon_{resultant,dic}^e = \sqrt{(\varepsilon_a^e)^2 + (\varepsilon_l^e)^2} \quad (2.36)$$

Meanwhile, the equation used to obtain the resultant strains for the FEM in SolidWorks 2013 (Cosmos Non-linear Simulation Analysis) is defined as (SolidWorks Strain Components, 2013):

$$\varepsilon_{resultant,FEM}^e = 2 \times \sqrt{(\varepsilon_1 + \varepsilon_2)/3} \quad (2.37)$$

where

$$\varepsilon_1 = 0.5 [(\varepsilon_l^e - \varepsilon^*)^2 + (\varepsilon_a^e - \varepsilon^*)^2 + (\varepsilon_{lt}^e - \varepsilon^*)^2] \quad (2.38)$$

$$\varepsilon_2 = [(\gamma_1)^2 + (\gamma_2)^2 + (\gamma_3)^2]/4 \quad (2.39)$$

$$\varepsilon^* = (\varepsilon_l^e + \varepsilon_a^e + \varepsilon_{lt}^e)/3 \quad (2.40)$$

γ_1 is the shear strain in y-direction on yz-plane, γ_2 is the shear strain in z-direction on yz-plane, γ_3 is the shear strain in z-direction on xz-plane and ε_{lt}^e is the lateral contraction strain in thickness. The resultant strain maps obtained from the finite element modelling were used to verify the results of the rubber specimens containing a circular hole and a square hole respectively obtained from the single step SB-DIC method.

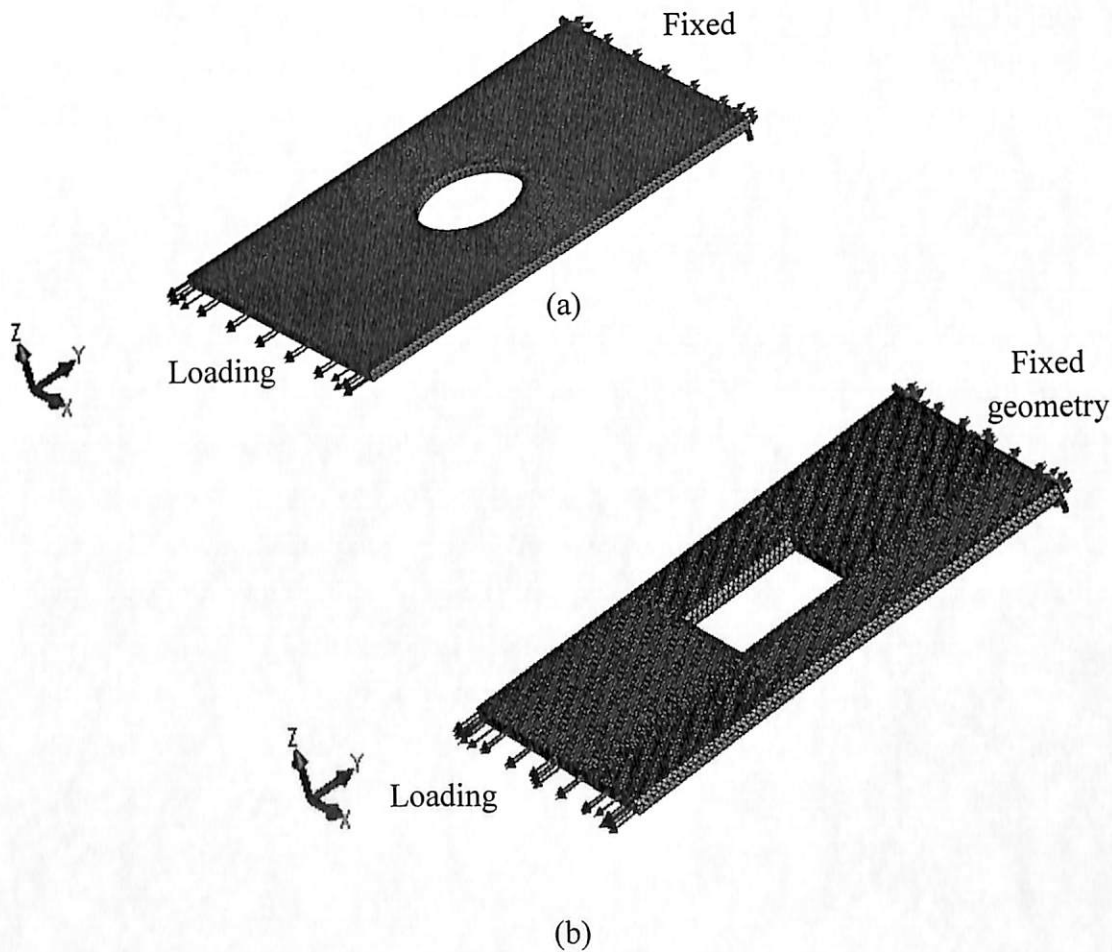


Figure 2.30 (a) Circular hole-containing rubber model and (b) square hole-containing rubber model used in finite element

RESULTS AND DISCUSSIONS

3.0 Overview

The results and the discussions of the research are presented in this chapter. The results of preliminaries for the motorized loading rig, flatbed scanner and the DIC coding before the 2-D SB-DIC experiments were presented and discussed in Section 3.1. The results of the displacement vector field and stress-axial strain curve obtained by using the incremental 2-D SB-DIC method are discussed in Section 3.2. The comparison of the stress-axial strain curve and the Young's modulus between the incremental 2-D SB-DIC method and the standard tensile test are presented in this section. The results of the Poisson's ratio based on engineering and true strains are discussed in the last part of this section.

The displacement vector field obtained by using the single-step 2-D SB-DIC method is presented in Section 4.3. The comparisons of the axial strain value, normalized cross-correlation coefficient and the time taken between the single step 2-D SB-DIC and the incremental 2-D SB-DIC methods are also discussed in this section. Lastly, the selection of the hyperelastic models used in the FEM analysis is discussed. The comparison of the resultant strain field between the single-step 2-D SB-DIC and FEM methods is presented in the last part of this section. Finally, the chapter summary is presented in Section 3.4.

3.1 Preliminary tests of the 2-D SB-DIC method

The results of the six preliminary tests of the 2-D SB-DIC experiment which are: (i) reliability test of the clamping system, (ii) determination of the average force transmission ratio of the loading system, (iii) determination of the holding torque required by the stepper motor to hold the rubber specimen, (iv) uniformity test of the light intensity provided by the flatbed scanner, (v) corrected scanning resolution of nominal scanning resolution of 600 dpi at 1.0 mm and 5 mm away from the scanner platen and (vi) simulation test of DIC coding in detecting the deformation of white speckle are outlined from Section 3.1.1 to 3.1.6. Two experimental conditions in the DIC method which are the subset size selection and randomness test of the white speckle pattern are discussed in Section 3.1.7 and Section 3.1.8.

4.1.1 Reliability test of clamping system

The effectiveness of the clamping system to clamp the rubber specimen without slippage was investigated and the result is shown in Figure 4.1. The figure shows that the average displacement of the subset centroid, s in y -direction for three rubber specimens in 90 minutes. The average displacement of the subset centroid was obtained by averaging the

displacements of the three local subsets located at the top, centre and bottom region of the scanned image. The result shows that there is no movement in the rubber specimens for the first 70 minutes. An average displacement of 0.028 mm occurs at 80 minutes and it increases to 0.056 mm at 90 minutes due to the creep effect of the rubber itself (Serope and Steven, 2006). Since the total time for loading and scanning process for completing a single incremental 2-D SB-DIC experiment is 55 minutes, the clamping system is concluded to be firm enough to clamp the specimen and the slippage effect can be neglected as the experiment for the incremental 2-D SB-DIC method was done within 55 minutes.

To avoid extra displacement induced from the creep effect from adding into the pure tensile displacement measurement, the optimum scanning resolution used for the scanning process was fixed at 600 dpi. This is because the total time taken in loading the specimen and scanning process by using the nominal scanning resolution of 600 dpi for a single experiment is 55 minutes during which the creep effect has not taken place. For scanning resolutions above 600 dpi, the total time taken in loading and scanning process to complete a single experiment exceeded 80 minutes, e.g. 118 minutes for 700 dpi. Thus, the scanning resolution of 600 dpi was used for all of the experiment.

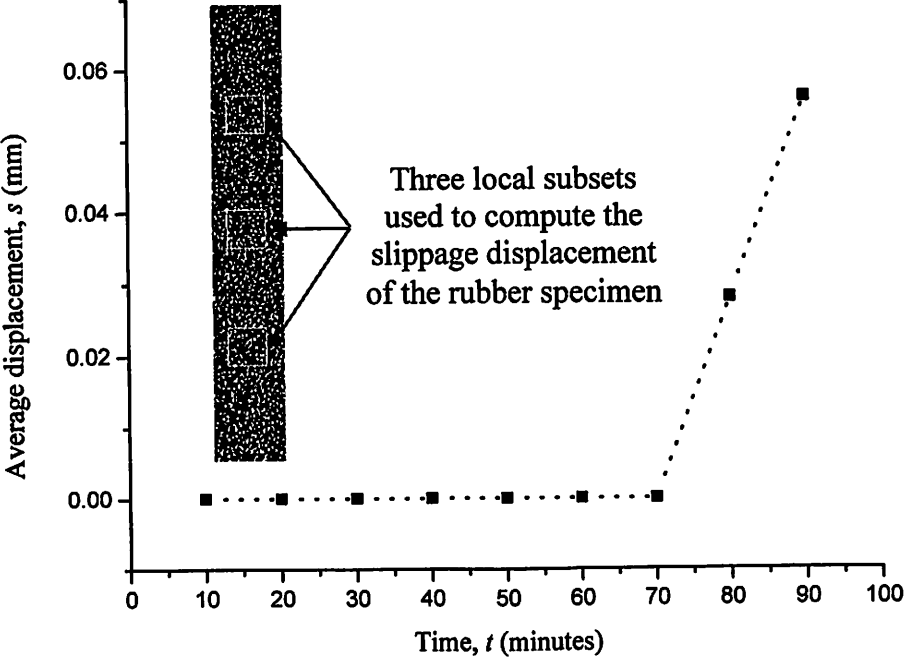


Figure 3.1 Average slippage displacements of subset centroid for rubber specimen at static in 90 minutes

3.1.2 Determination of force transmission ratio of loading system

The efficient of the force transmission for the loading system was investigated and the result is shown in Table 4.1. Table 4.1 shows the force transmission ratios for the three sets of experiment. The output forces are lower than the input force since some forces were lost due to the friction in the sliding rods on the linear bearing. The force transmission ratios for the three sets of experiment are in the range of 0.94-0.99. The average force transmission ratio obtained was 0.97. This value was used as a correction factor to obtain the net force, F_{nr} applied onto the rubber specimen by using the following equation:

$$F_{nr} = 0.97 F_r \quad (3.1)$$

where the F_r is the force applied onto the rubber specimen before applying the correction factor.

Table 3.1 Average of force transmission ratio

No. of driver gear rotation	Input force (N)			Output force (N)			Force transmission ratio		
	1	2	3	1	2	3	1	2	3
10	3.50	2.71	2.58	3.36	2.57	2.48	0.96	0.95	0.96
20	4.39	4.47	3.52	4.26	4.43	3.38	0.97	0.99	0.96
30	5.32	5.46	4.45	5.21	5.35	4.36	0.98	0.98	0.98
40	6.37	6.37	6.37	6.12	6.12	6.31	0.96	0.96	0.99
50	7.23	8.30	7.27	7.16	8.22	6.91	0.99	0.99	0.95
60	8.50	10.28	10.12	7.99	10.07	9.72	0.94	0.98	0.96
Average							0.97		

3.1.3 Holding torque determination of the stepper motor

The input holding torque of the stepper motor for the 2-D SB-DIC experiment must be less than the theoretical holding torque of the stepper motor obtained from the datasheet (80 mNm, refer to Section 3.3.3 page 58) so that no backlash effect occurs when the loading was paused for image scanning process. The input holding torque induced when the loading was paused is calculated by using the Equation (3.9) (Page 59).

$$T_i = \frac{F_r l}{2\pi GR} = \frac{87(2)}{2\pi(2)}$$

$$= 13.85 \text{ mNm}$$

The weight value F_r is the average load to be applied onto the rubber specimen at 350% axial strain which was obtained from the standard tensile test. From the calculation, the input torque induced on the stepper motor at 350% axial strain is 13.85 mNm which is about six times lower than the theoretical holding torque obtained from the datasheet. Therefore, it is concluded that the stepper motor is able to hold the rubber specimen without backlash effect at 350% axial strain.

3.1.4 Corrected scanning resolution for nominal scanning resolution at 600 dpi

Figure 4.3 shows the corrected scanning resolution of the flatbed scanner in y-direction at a height of 1.24 mm from the scanner platen. Three different dot sizes of the multi-frequency target were used to obtain the average corrected scanning resolution. The average corrected scanning resolution obtained was 600.02 dpi which is 0.003% deviation from the nominal scanning resolution of 600 dpi. Only the corrected scanning resolution in the y-direction was calculated since the springs used to provide the force applied information were stretched in only the y-direction.

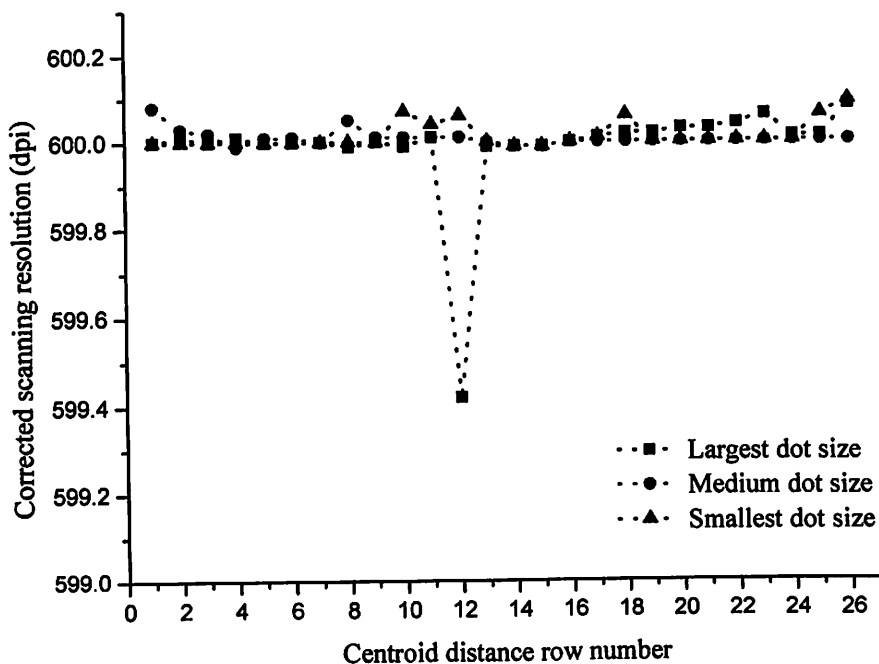


Figure 3.3 Corrected scanning resolution in y-direction at height of 1.24 mm above the scanner platen

Figure 3.4 shows the corrected scanning resolution in the x- and y-directions at height of 3.06 mm above from the scanner platen. The average scaling factors for the three different dot sizes in x- and y-directions were 588.19 dpi and 600.03 dpi respectively, which

are 1.97% and 0.005% deviations from the nominal scanning resolution of 600 dpi. The scaling factors for the 1.24 mm and 3.06 mm above from the scanner platen were used to obtain the dimension in *mm* unit by using the Eq. (3.11) (page 62). Based on the scanner distortion test no distortion was observed in the y-directional scanning whereas a slight distortion of only 0.137% was found in the x-directional scanning for the first and thirteen rows of the centroidal distances.

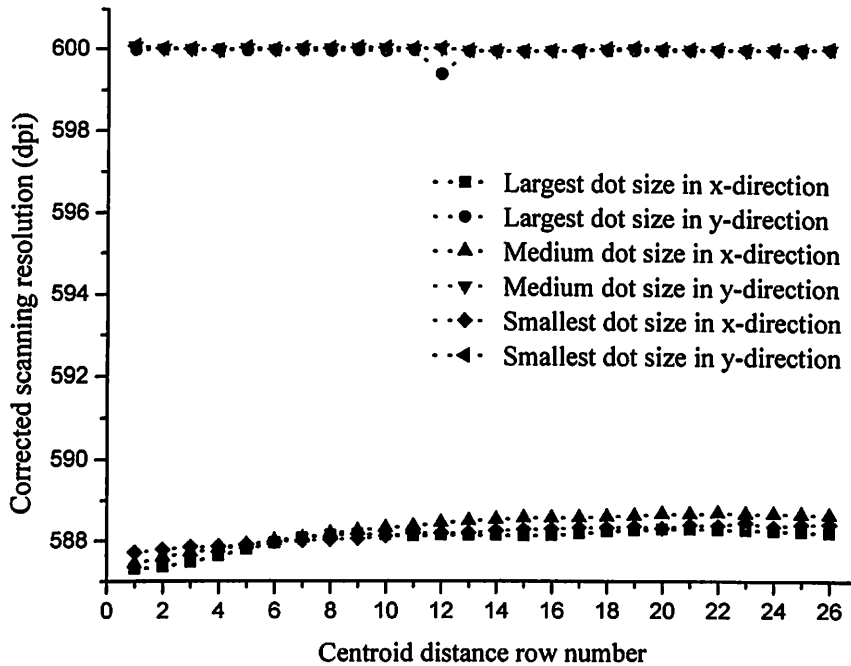


Figure 3.4 Corrected scanning resolution in x- and y-directions at height of 3.06 mm away from the scanner platen

3.1.5 Reliability test of the DIC coding in simulation

Figure 4.5 shows the successful correlation of the white speckle from the reference location to five different translated locations. The red-cross symbol indicates the centroid of the white speckle and the yellow line shows the displacement of the white speckle. Figure 3.6 shows the normalized cross-correlation coefficient distributions of the successful match for the first deformed image. The white speckle on the deformed image at the centroid location of [55,198] was successfully detected with normalized cross-correlation coefficient of one (perfect match). Table 3.2 shows the centroid locations of the white speckles for the five deformed images before and after the correlation. The results show that all the white speckles which were translated randomly were successfully detected with normalized cross-correlation coefficient of one. Thus, it is shown that the DIC coding is reliable to be used in detecting the deformation of the white speckle.

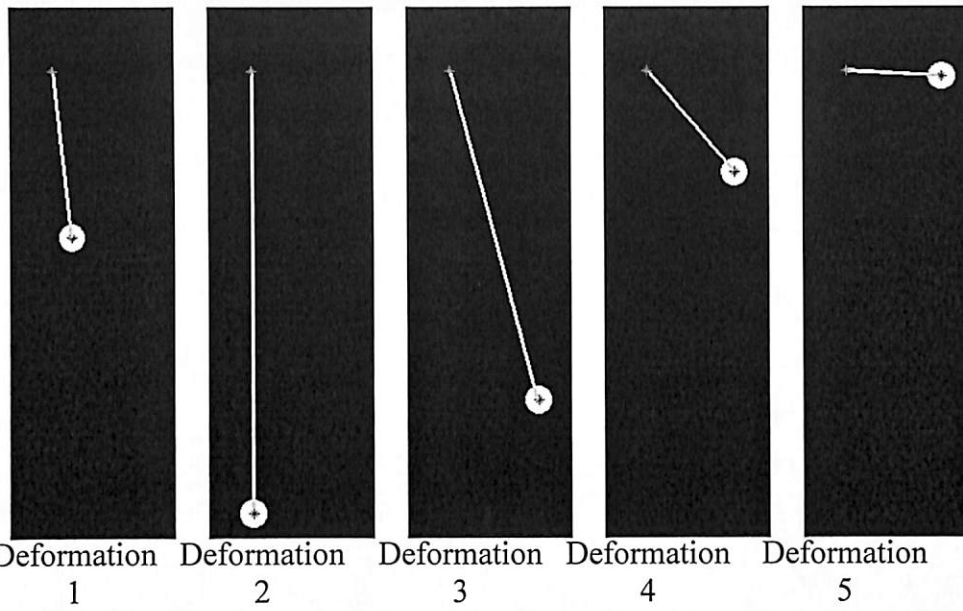


Figure 3.5 Successful tracking of the white speckle at different locations

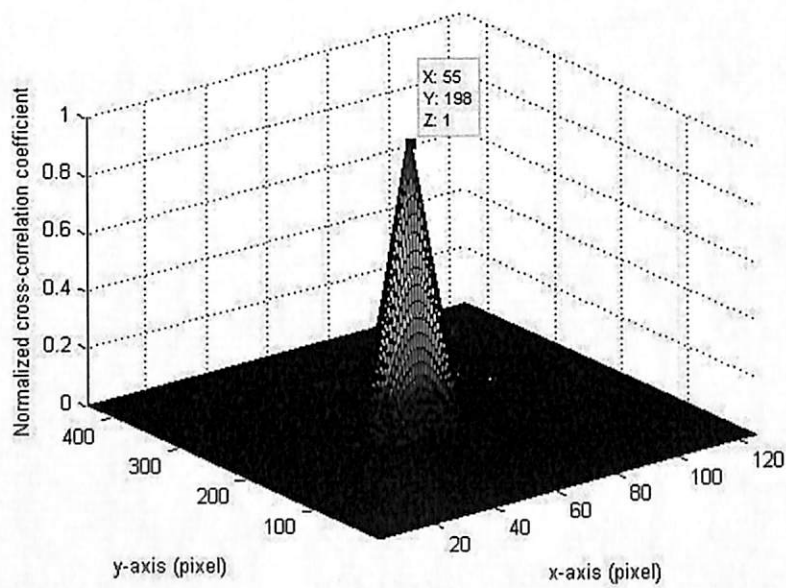


Figure 3.6 Normalized cross-correlation coefficient distributions of the successful match for first deformed image

Table 3.2 Comparison of the centroid locations between the white speckle before and after correlation

Deformed image	Centroid of white speckle	Detected centroid of white speckle	Normalized cross-correlation coefficient
1	[55,198]	[55,198]	1
2	[39,430]	[39,430]	1
3	[111,334]	[111,334]	1
4	[111,142]	[111,142]	1
5	[118,61]	[118,61]	1

3.1.6 Subset size selection in 2-D SB-DIC method

A test was carried out to investigate the subset size selection for the 2-D SB-DIC experiment. A reference and a deformed image (3.42% at 0.038 MPa) were used in the test. Eight different reference subset sizes of 11×11, 21×21, 31×31, 41×41, 51×51, 61×61, 71×71 and 81×81 pixels were defined in the reference image. A total of sixty-six reference subsets with the predefined subset size were used to correlate in the deformed image. The effect of the subset size on the average normalized cross-correlation coefficient is shown in Figure 3.7. The average normalized cross-correlation coefficient is 0.57 for the subset size of 11×11 pixels. More than half of the reference subsets fail to detect their corresponding deformation locations in the deformed image for the subset size of 11×11 pixels as shown in Figure 3.8 (i). The number of successful matches of the reference subsets increases when the subset size was increased to 21×21 pixels with average normalized cross-correlation coefficient of 0.68 (Figure 3.7) and Figure 3.8 (ii). For the subset sizes above 31×31 pixels, all the reference subsets successfully detect their corresponding deformation location at the deformed image with mean normalized cross-correlation coefficient of 0.83-0.84 as shown in Figure 3.7 and Figure 3.8 (iii).

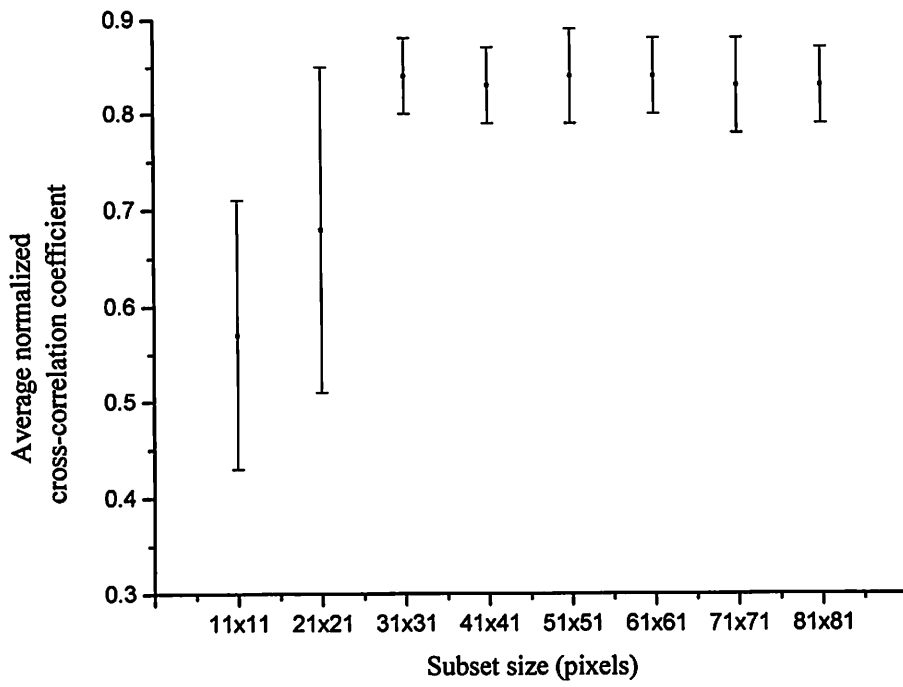


Figure 3.7 Effect of subset size on the average normalized cross-correlation coefficient

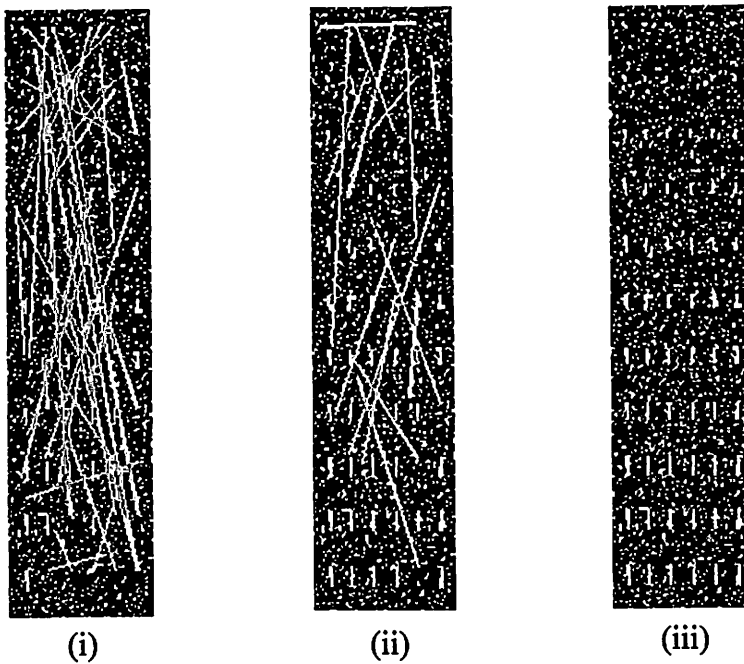


Figure 3.8 Erroneous displacement fields at subset sizes of (i) 11x11 (ii) 21x21 pixels and (ii) perfect match for all of reference subsets at subset sizes over 31x31 pixels

The de-correlation of the reference subset in the deformed image is due to the dimensions of the bounding box containing a white speckle in x- and y-directions is larger than the reference subset size. The dimensions of the bounding box containing a white speckle in x- and y-directions is between 1-29 pixels and 1-27 pixels respectively as shown in Figure 3.9 which is larger than the reference subset size, e.g. 11×11 and 21×21 pixels. The bounding box is defined as the smallest rectangle that contains a white speckle (element) as shown in Figure 3.10. As the dimensions of the bounding box containing a white speckle is larger than the reference subset size (either in only x- or y-direction or in both directions), de-correlation of the reference subset in the deformed image occurs due to the insufficient white speckle information used to track the deformation.

Two main reasons whereby the insufficient speckle information occurs when the size of the white speckle inside the bounding box is larger than the reference subset size are (i) some of the white speckles pattern inside the reference subset lie outside the boundary of the reference subset and (ii) the reference subset contained mostly or totally white speckle pattern. Therefore, it is concluded that the de-correlation of the reference subset in the deformed image occurs when the reference subset size is less than the size of the white speckle pattern. This finding agreed with the research done by Bornert et al. (2009) who reported that the size of the subset chosen depends largely on the size of the speckle pattern generated on the specimen.

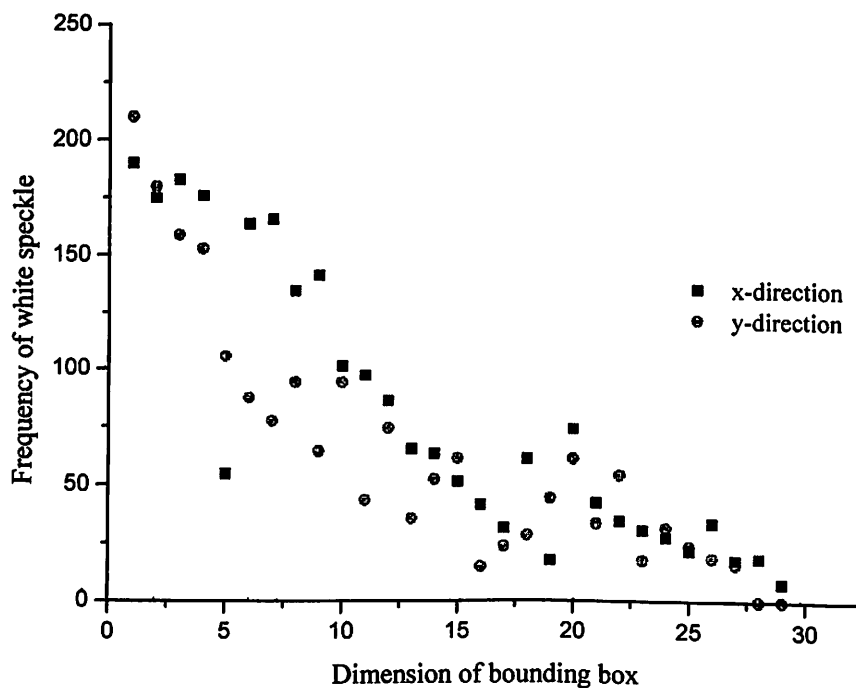


Figure 3.9 Frequency of white speckle in x- and y- directions of bounding box

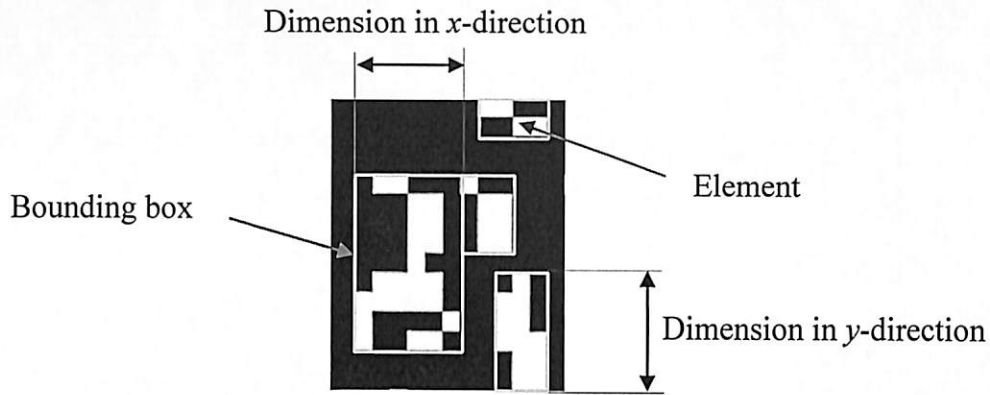


Figure 3.10 Definition of element, bounding box and size of the element

From the Figure 3.7 and Figure 3.8, it can be concluded that the larger subset size provides more accurate result, but the use of large subsets size slows down the matching process as shown in Figure 3.11. As a compromise between the DIC programme code running time t_c and accuracy the subset size 31×31 pixels was used in the 2-D SB-DIC experiments. Although the subset size can be predefined when the maximum size of the speckles is known, there is no standard procedure to obtain the desired speckle sizes which are always less than the predefined subset size. Nevertheless, there are two solutions to ensure that the subset contains adequate white speckles which are: (i) adjusting the subset size according to the maximum size of the white speckle with fixed binarization threshold value and (ii) adjusting the binarization threshold value with fixed subset size. The first method, however, is time consuming as higher subset size consumes more time in DIC programme code running time if large speckles are generated on the specimen. Moreover, it is not practical if the subset size is adjusted according to the maximum size of the white speckle if only few of the white speckles are bigger than others. The latter solution is done by adjusting the binarization threshold value until the maximum size of the white speckle inside bounding box is within the subset size in both x - and y -directions. This method consumes lesser time than the first solution and the adjusted binarization threshold value will not affect the correlation process since both of the reference image and deformed image are binarized using the same threshold value. Therefore, the second method was used for all of 2-D SB-DIC experiments.

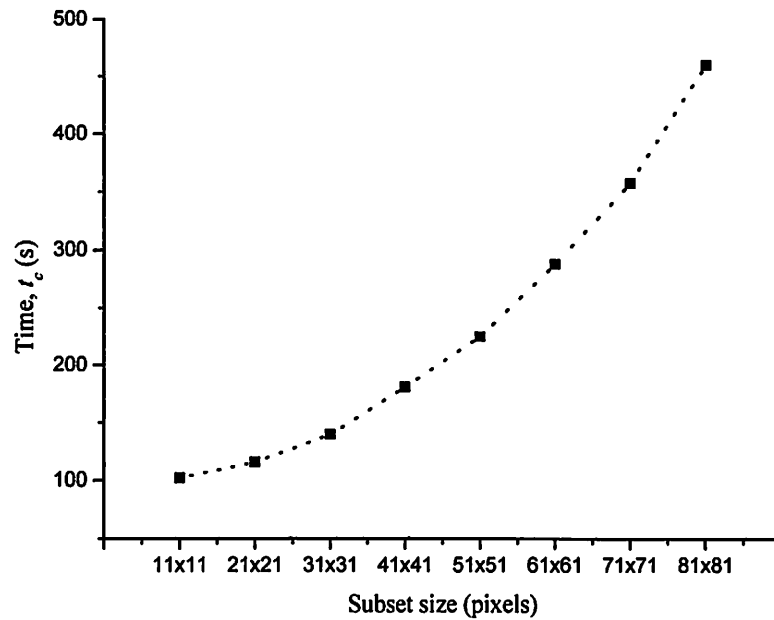


Figure 3.11 Effect of subset size on DIC programme code running time

3.1.7 Randomness test of the speckle patterns

A randomness test was conducted at each of the rubber specimen (five dumbbell-shaped rubber specimens and two rubber specimens containing circular hole and square hole) before the correlation process to avoid mis-match due to the exactly same speckle pattern existing at two or more locations on the same rubber specimen. Randomness test was done by correlating the reference subset on the same reference image. The conditions of the correlation process which are the total number of reference subset, subset size and subset step were same as the one used in the 2-D SB-DIC experiments. The correlation started from the top left corner to the bottom right corner on the reference image. To detect the possibility of exactly same speckle patterns occurring in any other area beside than the reference subset itself, the scanning step was skipped by 31 pixels when reference subset has reached the region of the reference subset itself on the reference image during scanning process. The speckle pattern in the reference image is said to be not random and unique if there is other area which the normalized cross-correlation coefficient is near to 1.

The average of the highest similarity degree (i.e. normalized cross-correlation coefficient) of the speckle pattern is shown in Figure 3.12. The first five rubber specimens were the dumbbell-shaped rubber specimen used in the incremental 2-D SB-DIC method and the specimen number 7 and 8 were the rubber specimens containing circular hole and square hole used in the validation of non-homogeneous strain distribution experiments by using single-step 2-D SB-DIC method. The results show that the average normalized cross-

correlation coefficients for all the rubber specimens were in the range of 0.31-0.51. Meanwhile the maximum normalized cross-correlation coefficient was only 0.63 for rubber specimen 3. Thus, it can be concluded that the speckle patterns in each reference subset for all the rubber specimens used in the 2-D SB-DIC experiments are random and unique.

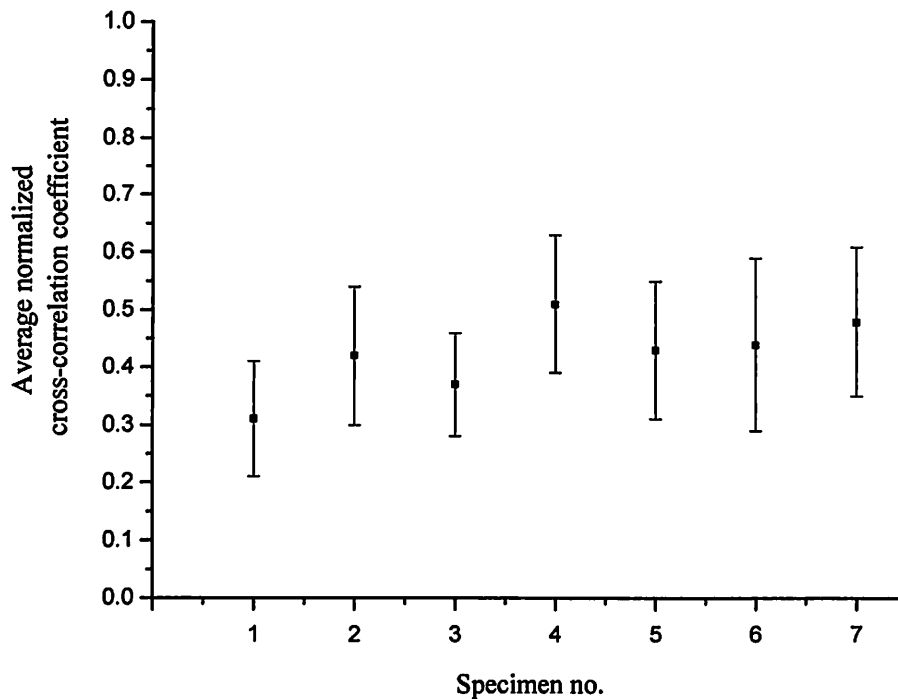


Figure 3.12 Average normalized cross-correlation coefficients of self-correlation for rubber specimens used in the 2-D SB-DIC experiments

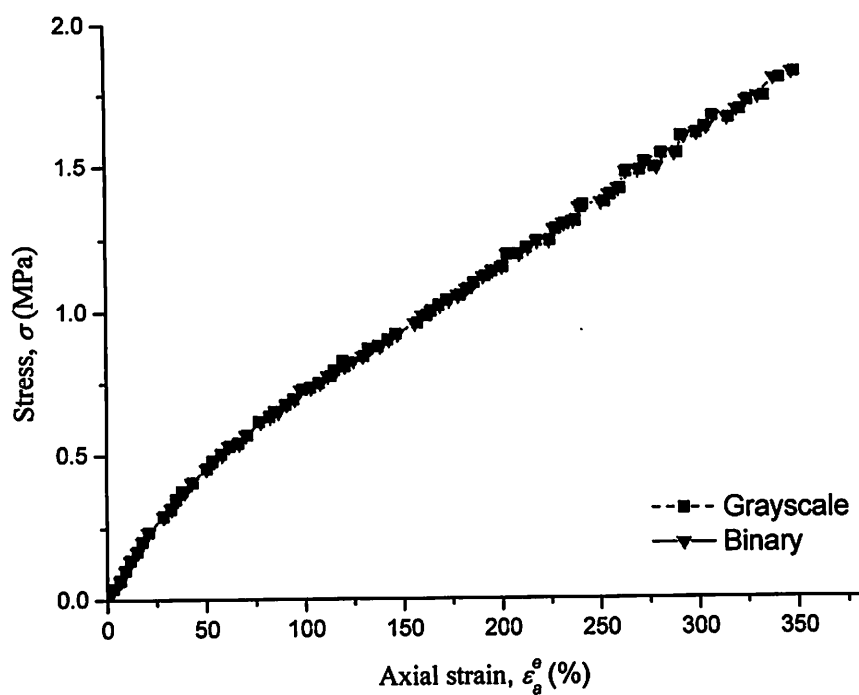
3.2 Incremental 2-D SB-DIC method

The comparisons between the grayscale- and binary-image based incremental 2-D SB-DIC methods in term of stress-axial strain curve, normalized cross-correlation coefficient and DIC programme code running time are presented in Section 4.2.1. The displacement vector field obtained by using the incremental 2-D SB-DIC method is discussed in Section 4.2.2. The comparisons of the stress-axial strain curve, tangent modulus and secant modulus between the incremental 2-D SB-DIC and the standard tensile test methods are discussed in Section 4.2.3. To validate the reliability of the incremental 2-D SB-DIC method in obtaining the displacement vector field and axial strain data, comparisons were made between the incremental 2-D SB-DIC method and the standard DIC software which are discussed in Section 4.2.4. The comparison of the Poisson's ratio based on engineering and true axial strains between the theoretical result and the incremental 2-D SB-DIC method is presented in the final part of this section.

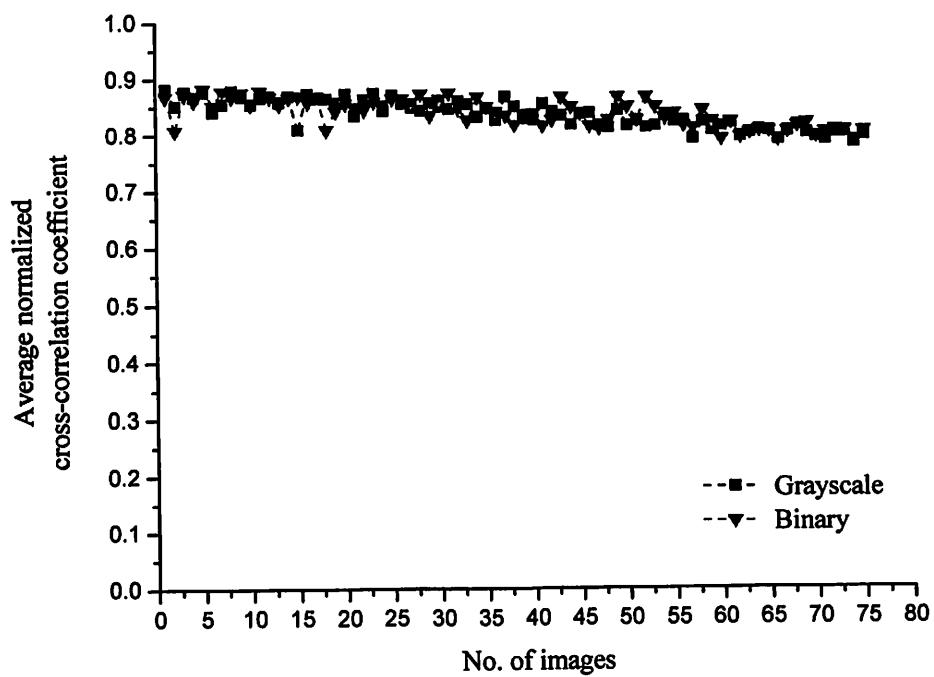
3.2.1 Comparison between grayscale- and binary-image based incremental 2-D SB-DIC methods

Figure 3.13(a)-(b) shows the comparison between the grayscale- and binary-image based incremental 2-D SB-DIC methods in term of stress-axial strain curve and normalized cross-correlation coefficient at each loading stage. The axial strain data was obtained by averaging the total axial strain for 66 reference subsets. The result shows that the stress-axial strain curves for the grayscale- and binary-image based incremental 2-D SB-DIC methods overlap each other. The average normalized cross correlation coefficient of the grayscale- and binary-image based incremental 2-D SB-DIC methods are 0.838 and 0.835 respectively, which is only 0.36% of deviation. The decreasing trend of the normalized cross-correlation coefficient in the grayscale- and binary-image based incremental 2-D SB-DIC methods is due to the significant changes of the speckle pattern in the deformed image compared to the one in the reference image when the deformation increases. From the Figure 4.13, it can be concluded that there is no significant difference of using either grayscale- or binary-image based 2-D SB-DIC method in correlation process and strain determination.

For the comparison in term of DIC programme code running time, the grayscale-based incremental 2-D SB-DIC methods consumed much longer time at each loading stage compared to binary-image based incremental 2-D SB-DIC methods for the entire experiment as shown in Figure 4.14. The difference of the DIC programme code running time between the grayscale- and binary-image based incremental 2-D SB-DIC methods increases quadratically from stage 1 to stage 76. The total DIC programme code running time taken of the grayscale- and binary-image based incremental 2-D SB-DIC methods are 34522 s and 30094 s, respectively. Thus, a total of 74 minutes were saved in programme code execution by using the binary-image based incremental 2-D SB-DIC method for the entire 76 stages. Therefore, it is concluded that the binary-image based 2-D SB-DIC method is able to provide the equally accurate strain result and high normalized correlation coefficient as the grayscale-image based 2-D SB-DIC method but with lesser DIC programme code running time. Thus, the binary-image based 2-D SB-DIC method was used for the rest of the work in this research.



(a)



(b)

Figure 3.13 Comparison of (a) stress-axial strain curve and (b) average normalized cross-correlation coefficient between grayscale and binary images using incremental 2-D SB-DIC method

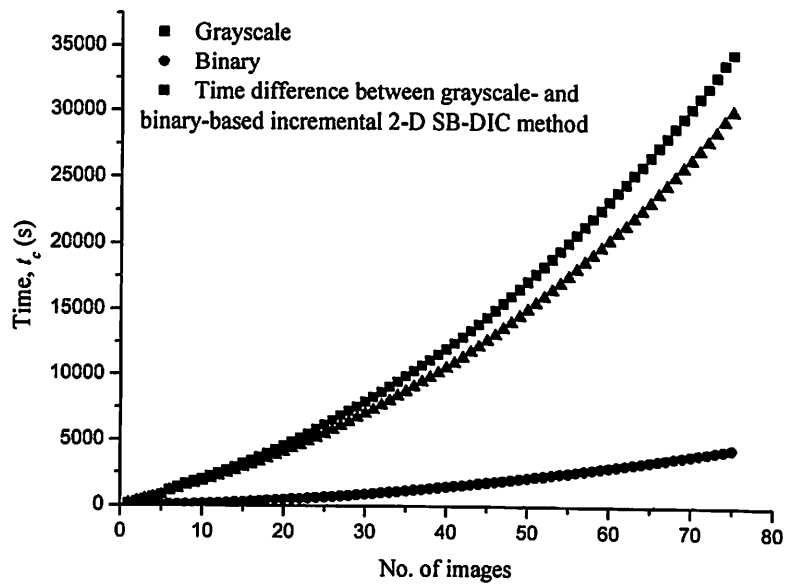


Figure 3.14 Comparison of DIC programme code running time between grayscale and binary images using incremental 2-D SB-DIC method

4.2.2 Displacement vector field of incremental 2-D SB-DIC method

The 2-D displacement vector field superimposed onto the specimen and plotted separately is shown in Figure 3.15. Only the displacement vector field for the first rubber specimen was shown as the rest of the specimens show the same displacement vector plots. The relative displacement vector was plotted with respect to the final location on the deformed image. At lower load (0.19 MPa) (Figure 3.15(a)) the displacement vector field can be seen clearly but most of the vectors overlapped at higher load (0.58 MPa) as seen in Figure 3.15(b). All of the displacement vector fields overlapped each other at the loads between 1.14-1.82 MPa (Figure 4.15(c)-(d)). This is because the displacements of reference subsets were higher than the predefined center position of reference subset in the subsequent rows. The asymmetry of displacement vector field between the left and right sides of the specimens observed in Figure 3.15(a)-(b) is caused by the slight offset of the specimen axis compared to the clamp axes. This offset will not affect the strain data as the magnitude of each vector component in the tensile direction was used in the strain computation.

The 3-D representatives of the 2-D displacement vector fields in Figure 3.16(a)-(d) provide a better visualization of the deformation of the elastomeric material. The results show that all the displacement vector fields are directed to the loading direction and move towards inside the centre line of the rubber specimen. No mismatch of the reference subset

was seen in Figure 3.16(a)-(d). Thus, the strain data obtained by using the Eq. (3.13) for all the reference subsets were averaged and the result is discussed in the following section.

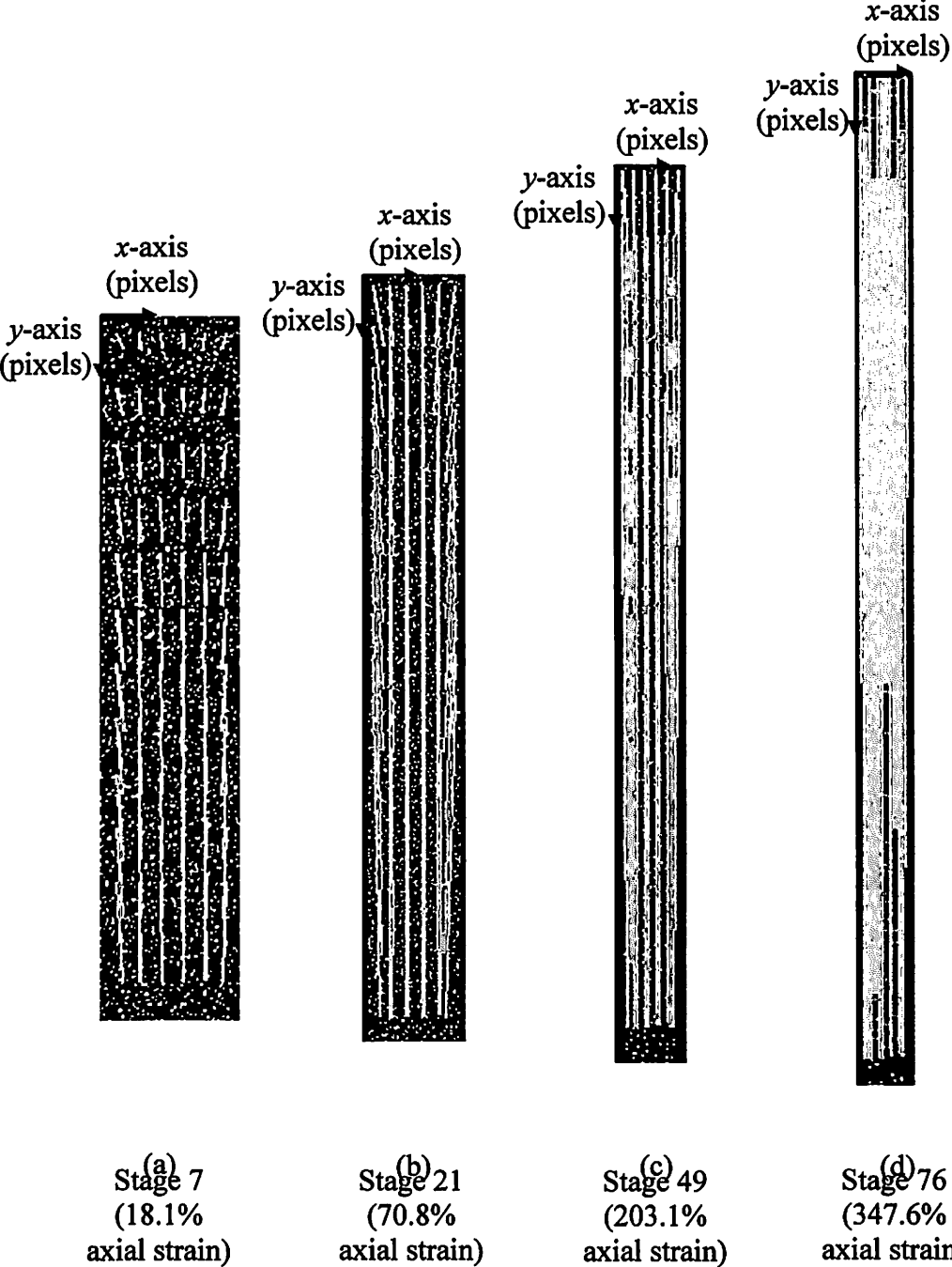
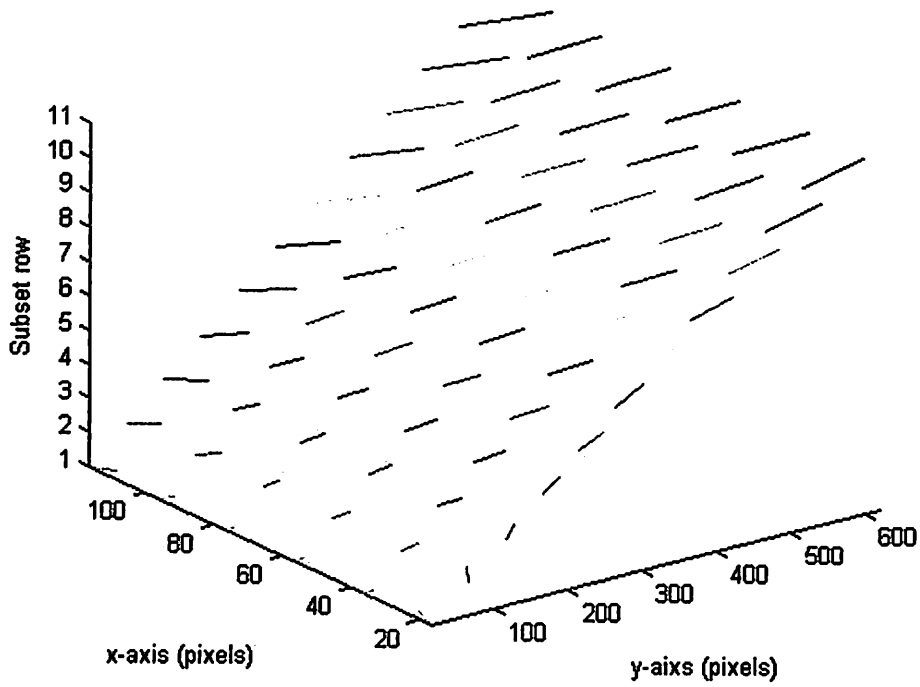


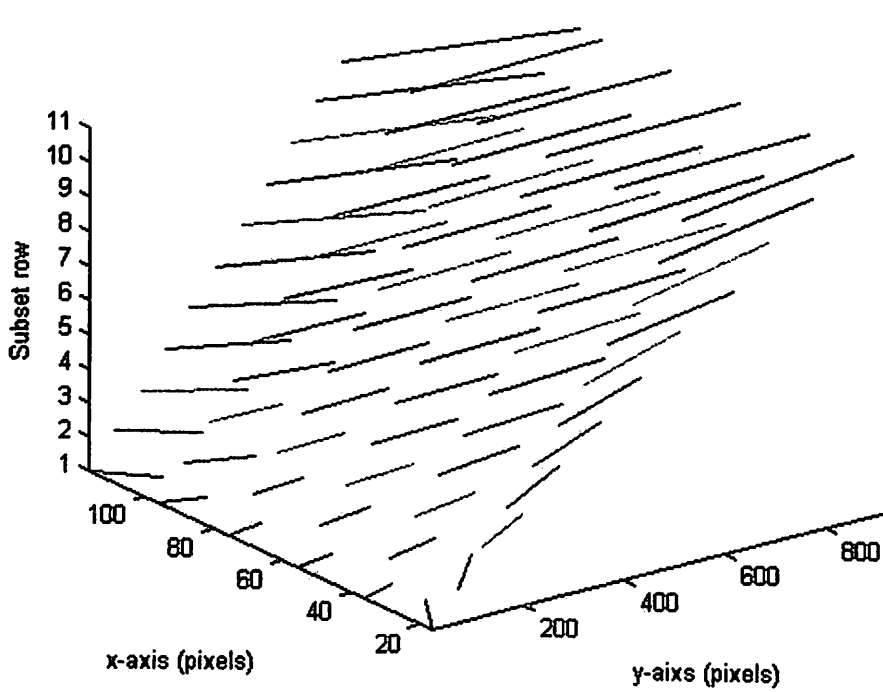
Figure 3.15 2-D displacement vector field at loads of (a) 0.19 MPa (b) 0.58 MPa (c) 1.14 MPa and (d) 1.82 MPa

Displacement field at stage 7 (0.19MPa)



(a)

Displacement field at stage 21 (0.58MPa)



(b)

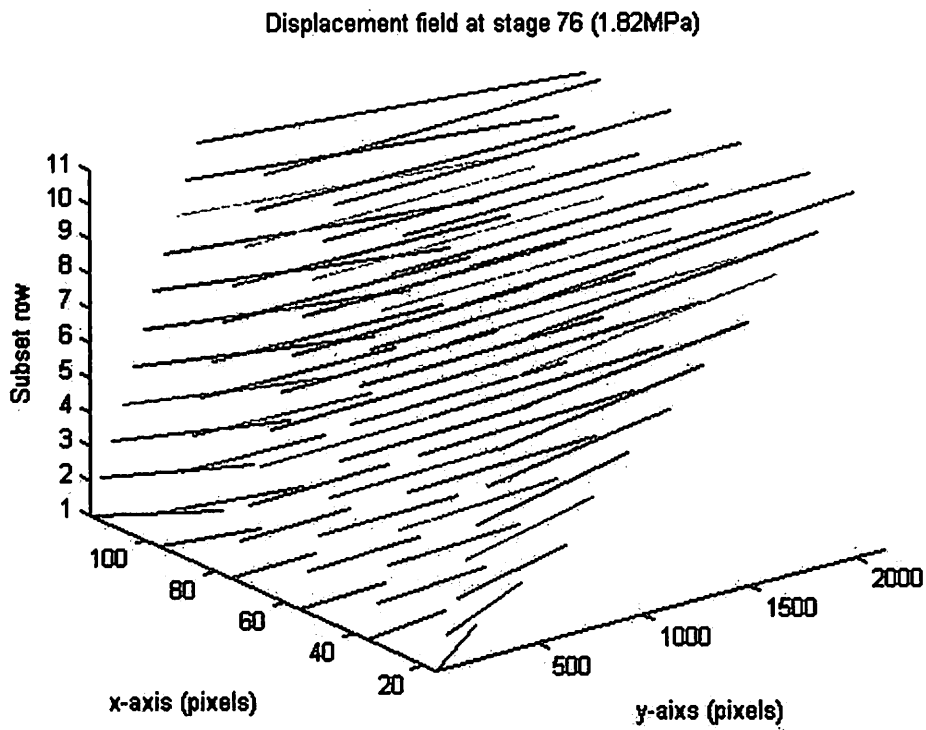
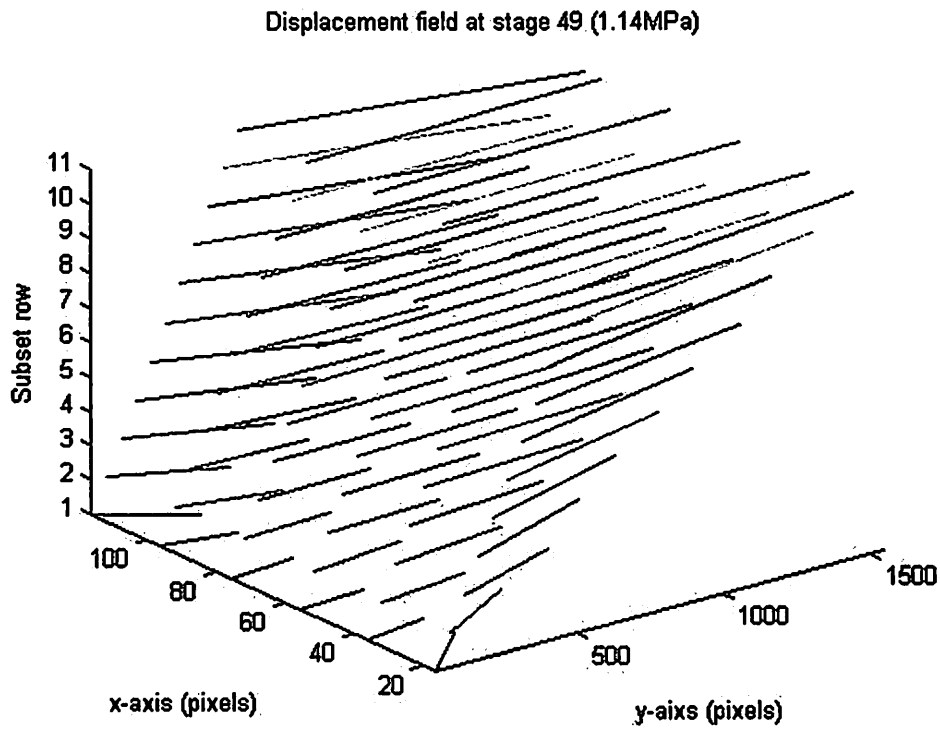


Figure 3.16 3-D representatives of in-plane displacement vector field at (a) 0.19 MPa (b) 0.58 MPa (c) 1.14 MPa and (d) 1.82 MPa

3.2.3 Comparison of stress-axial strain curve and Young's modulus between the incremental 2-D SB-DIC method and standard tensile test machine

The stress-axial strain data for the incremental 2-D SB-DIC method for each rubber specimen was plotted in terms of the global axial strain and compared with the Instron tensile test results. The range of axial strain values from 0 to 350% from the Instron tensile test results were taken to compare with the results obtain from the incremental 2-D SB-DIC method. This is because the maximum axial strain obtained by using incremental 2-D SB-DIC method was up to 350%. Figure 4.17 shows the stress versus axial strain graphs from five repeated experiments for the Instron and incremental 2-D SB-DIC methods. Comparison of the stress-axial strain behaviour of the five specimens using both methods shows a very similar trend.

The stress-axial strain data for each specimen in Figure 4.17 were fitted using third degree polynomial function. Then the third order polynomial equations for each of the rubber specimen were obtained. The selected axial strain values (range from 0 to 350% with each increment of 2.5% axial strain) were substituted into the third order polynomial equations in order to obtain the stresses value. The mean stress-axial strain data obtained from the five rubber specimens for each method were again plotted and fitted using a third degree polynomial as shown in Figure 4.18. As seen in Figure 4.18 the stress-axial strain curve from the incremental 2-D SB-DIC method is in good agreement with the fitted Instron curve.

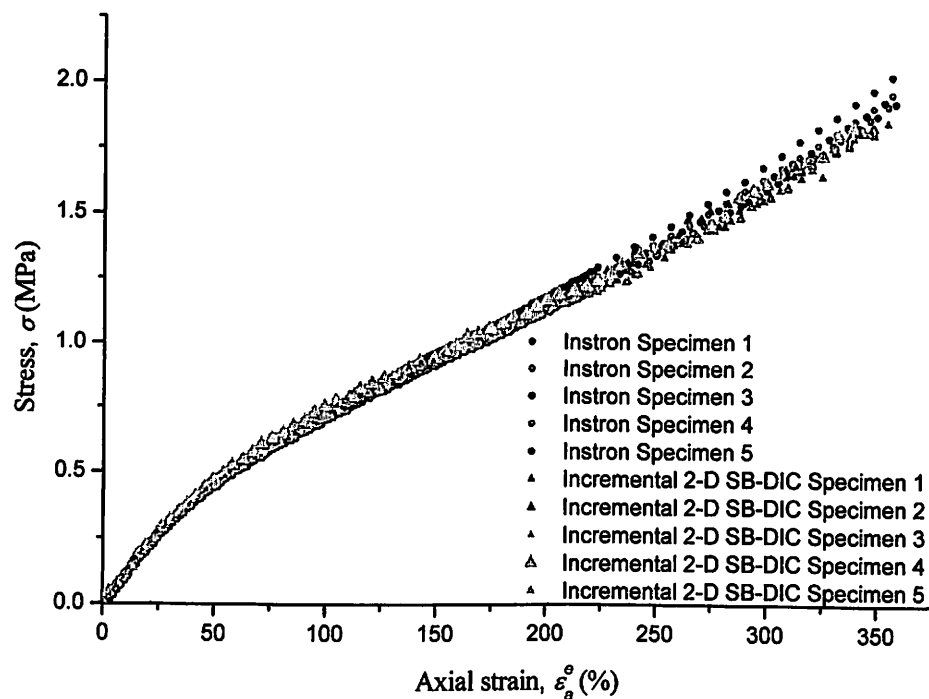


Figure 3.17 Stress-axial strain curves of incremental 2-D SB-DIC methods and Instron

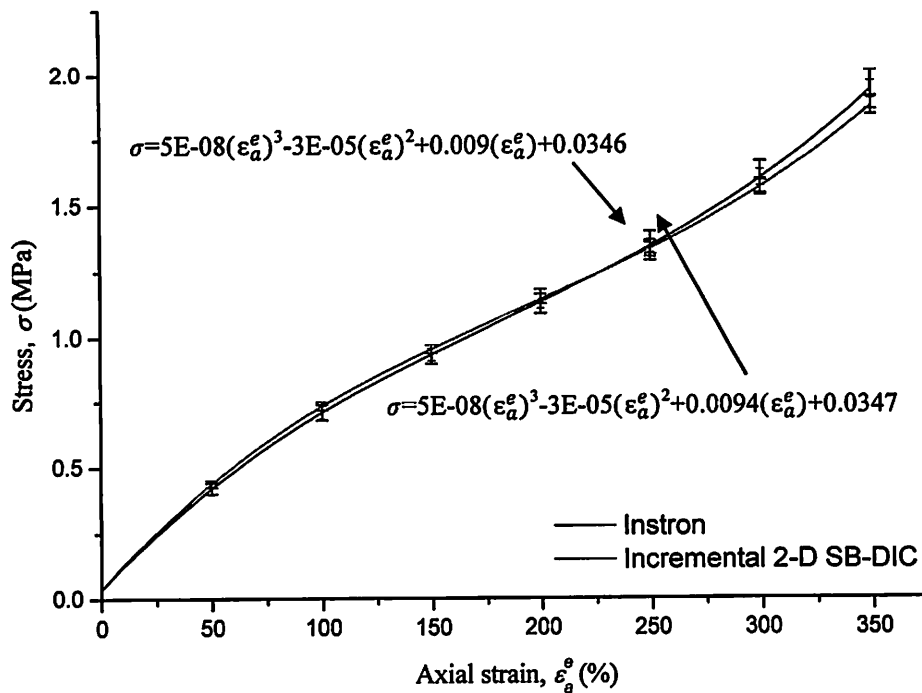


Figure 3.18 Comparison of fitted average stress-axial strain curve between incremental 2-D SB-DIC and Instron

Two types of moduli, namely the tangent modulus and secant modulus which are commonly used in measuring the stiffness of the material that exhibits non-linear stress-axial strain behaviour, were used to compare the results quantitatively up to 350% axial strain. The tangent modulus is the slope on a stress-axial strain curve at specific stress or axial strain value while the secant modulus is the ratio of stress to axial strain at any point in stress-axial strain curve. Table 4.3 shows the comparison of average tangent modulus between incremental 2-D SB-DIC and Instron methods at different axial strains values. The maximum and minimum errors of the tangent moduli are 9.49% and 0.60% at 250% and 100% axial strains, respectively. Although the comparison of tangent modulus between the incremental 2-D SB-DIC and the Instron methods is very close, the results however are affected by the types of curve fitting, i.e. a slight difference of slope at 250% and 300% causes big deviation in tangent modulus. Therefore, the secant modulus which can be obtained directly by taking the ratio of stress and axial strain at particular point (i.e. not affected by the types of curve fitting) was determined and the comparison is shown in Table 4.4. The maximum error in the secant modulus is 4.16% at 50% axial strain meanwhile the minimum error in the secant modulus is 0.70% at 200% axial strain. The deviation between the two methods is mainly due to the approach used in the computation of the axial strain data. In the proposed SB-DIC method the overall axial strain is determined by using the

individual axial strain values at various grid points on the specimen, whereas in the tensile test method the axial strain data is determined by using the overall extension of the specimen. Since the scanner-based method is sensitive to local variations in strains caused by material non-homogeneity the two methods will not yield the same results.

Table 3.3 Comparison of average tangent modulus between incremental 2-D SB-DIC and Instron methods

Average tangent modulus (MPa)			
Axial strains (%)	Instron	Incremental 2-D SB-DIC	Absolute error (%)
50	0.663	0.686	3.47
100	0.502	0.505	0.60
150	0.414	0.399	3.62
200	0.397	0.367	7.56
250	0.453	0.410	9.49
300	0.581	0.527	9.29
350	0.780	0.719	7.82

Table 3.4 Comparison of average secant modulus between incremental 2-D SB-DIC and Instron methods,

Average secant modulus (MPa)			
Axial strains (%)	Instron	Incremental 2-D SB-DIC	Absolute error (%)
50	0.842	0.877	4.16
100	0.710	0.733	3.24
150	0.624	0.638	2.24
200	0.568	0.572	0.70
250	0.538	0.534	0.74
300	0.533	0.522	2.06
350	0.554	0.536	3.25

The main advantage of the DIC method is that it is able to provide displacement vector and strain fields as a function of position on the specimen surface. Figure 4.19(a)-(i) shows the axial strain map for specimen 2 at different axial strain levels. The axial strain maps for all the other four rubber specimens were similar. During a small loading the

specimen is strained homogeneously and uniform distribution of axial strain was obtained as shown in Figure 3.19(a)-(c). But, beyond 100% axial strain the rubber specimens start to deform non-homogeneously as seen in Figure 3.19(d)-(i). A significant axial strain gradient can be seen as the deformation increases. Although the axial strain distribution is decreasing from the reference end at large deformation, the average local axial strain is almost equal to the axial strain obtain from the Instron method as shown in Figure 3.18. The non-uniform axial strain distribution at large deformation is caused by the microvoids present in the rubber specimens. Figure 3.20 shows the SEM micrographs at a small cross sectional area in the central region of rubber specimen in the undeformed state. The figures clearly show significant numbers of microvoids present in the rubber specimens causing non-uniform deformation at large strains. This statement is supported by the work done by Fang et al. (2006). Fang et al. (2006) studied the large deformation of PC/ABS alloy and found that the non-homogeneous deformation of PC/ABS alloy was due to the presence of microvoids in the specimens. The in-situ SEM observation showed that the crazing structure initiated from the original microvoids on the surface of the specimen as the deformation increased. Figure 3.18 shows that at above 200% axial strain the stress-axial strain curves of rubber specimens using SB-DIC method deviate from one another. This is because the number and the size of the voids are different in each rubber specimen although they were made from the same material.

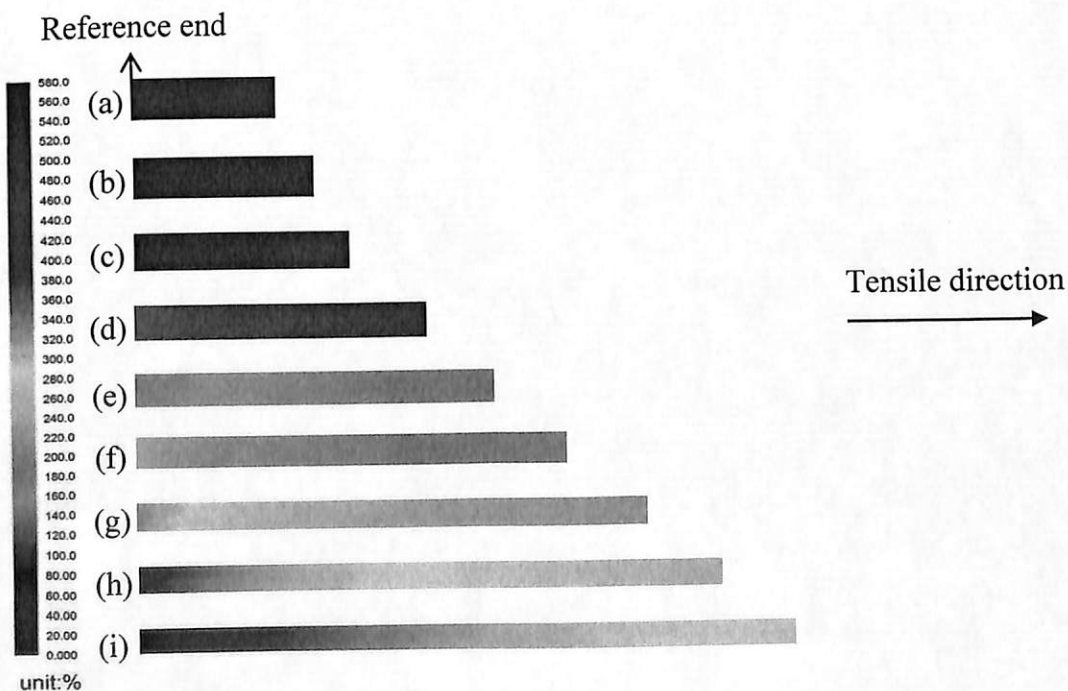
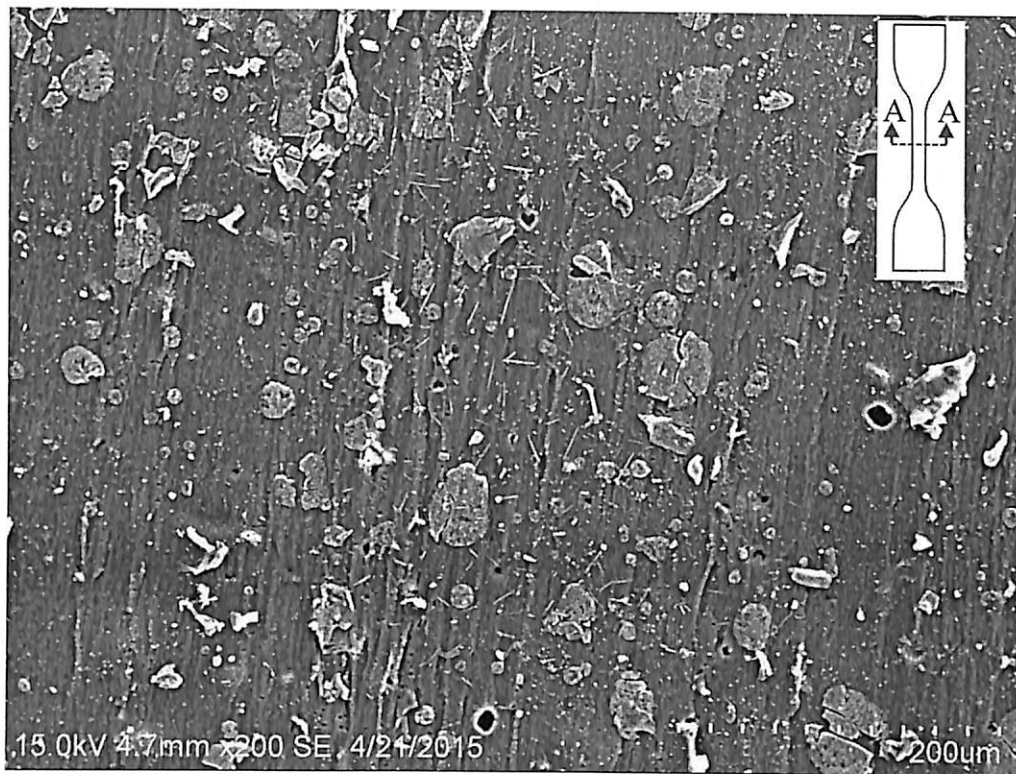


Figure 3.19 Axial strain map of the rubber specimen



(a)

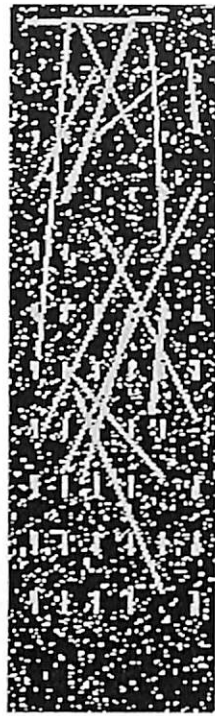


(b)

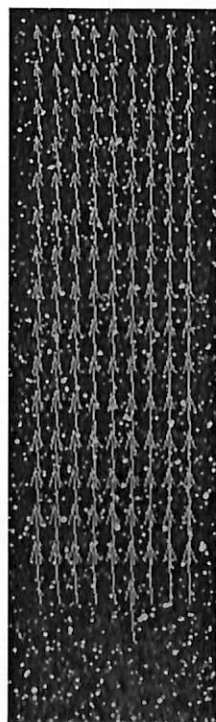
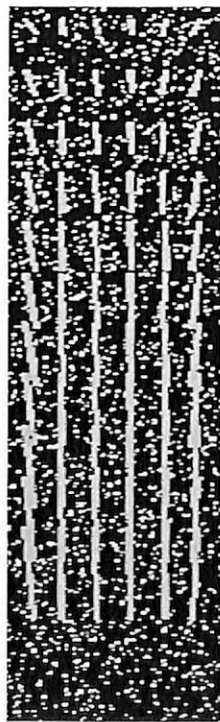
Figure 3.20 SEM micrograph taken in the cross section area at central part of (a) rubber specimens 1 and (b) rubber specimens 2

3.2.4 Comparison between incremental 2-D SB-DIC and LaVision DIC methods

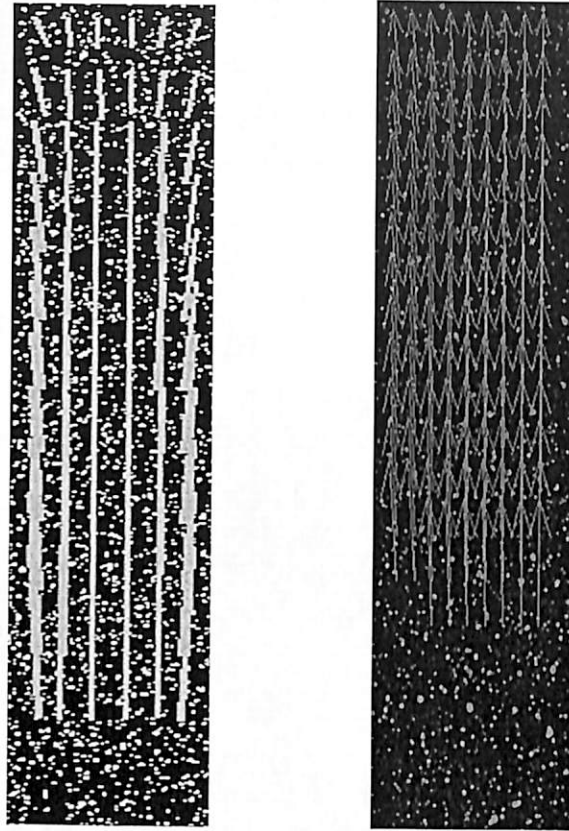
The reliability of the incremental 2-D SB-DIC method in obtaining the strain data was proven in the previous section. However, no comparison of the displacement vector field was made to verify the displacement vector field obtained from the incremental 2-D SB-DIC method since the Instron provides only the average strain data. Thus, a standard DIC method (LaVision) which is available in the market was used to obtain the displacement field and strain data. The results obtained from LaVision DIC method were used as a reference to compare with the results obtained from the incremental 2-D SB-DIC method. Figure 4.21 shows the comparison of the 2-D displacement vector fields between the incremental 2-D SB-DIC (yellow line) and LaVision DIC (red line) methods at three different loads. In contrast to the SB-DIC method, the relative displacement vector of the LaVision DIC method was plotted with respect to the un-deformed subset centroid location (i.e. the arrow was plotted from deformed centroid location to un-deformed centroid location). At low stress the displacement vector fields for the both methods are clearly seen as shown in Figure 4.21(a). However, the displacement vectors overlapped each other at higher loads (Figure 4.21(b)-(c)) because the final displacement locations of the reference subset were higher than the predefined center position of reference subset in the subsequent rows. The displacement vector field of the LaVision DIC method tend to the right hand side due to the non-parallel axis between the specimen axis and the clamping axis. Nevertheless, the strain result was not affected by the unsymmetrical displacement vector since the magnitude of each of the vector component was used in the strain calculation. Some of the displacement vectors for the LaVision DIC method were missing out from time to time (from Figure 4.21(a) to (b) and from (b) to (c)) because the reference subsets at the lower region were moving out of the field of view from the CCD camera but all the displacement vectors for the incremental 2-D SB-DIC method still remain on the specimen.



(a)



(b)



(c)

Figure 3.21 Comparison of 2-D displacement vector field between the incremental 2-D SB-DIC and the LaVision DIC methods at loads of (a) 0.08 MPa (b) 0.15 MPa and (c) 0.22 MPa

The stress-axial strain curve between the incremental 2-D SB-DIC and the LaVision DIC methods is compared as shown in Figure 3.22. Both incremental 2-D SB-DIC and the LaVision DIC methods show a similar trend up to 22% axial strain. The stress-axial strain data obtained from the LaVision DIC method was fitted using third order polynomial. Then the third order polynomial equation for the LaVision DIC methods was obtained from the fitted curve. The stress at a particular axial strain value was obtained by substituting the axial strain value into the third order polynomial equation. The result was plotted and compared with the result obtain from the incremental 2-D SB-DIC method (extracted from the Figure 3.18) up to 22% axial strain.

The stress values at different axial strain levels were compared as shown in Table 3.5. The highest and lowest absolute percentage errors of stress were 7.69% and 5.26% at 4% and 12% axial strains, respectively, while the mean error was 6.11%. The deviation between the two methods is mainly due to the non-synchronization determination of the stress and axial strain data from the LaVision DIC method. The stress of the LaVision DIC

method was obtained indirectly by using the fitted stress-axial strain curve (third order polynomial) from the Instron. The average axial strain value obtained from the LaVision DIC method was substituted into the third order polynomial equation to obtain the stress value. Thus, the stress value of the LaVision DIC method was biased from the actual stress value.

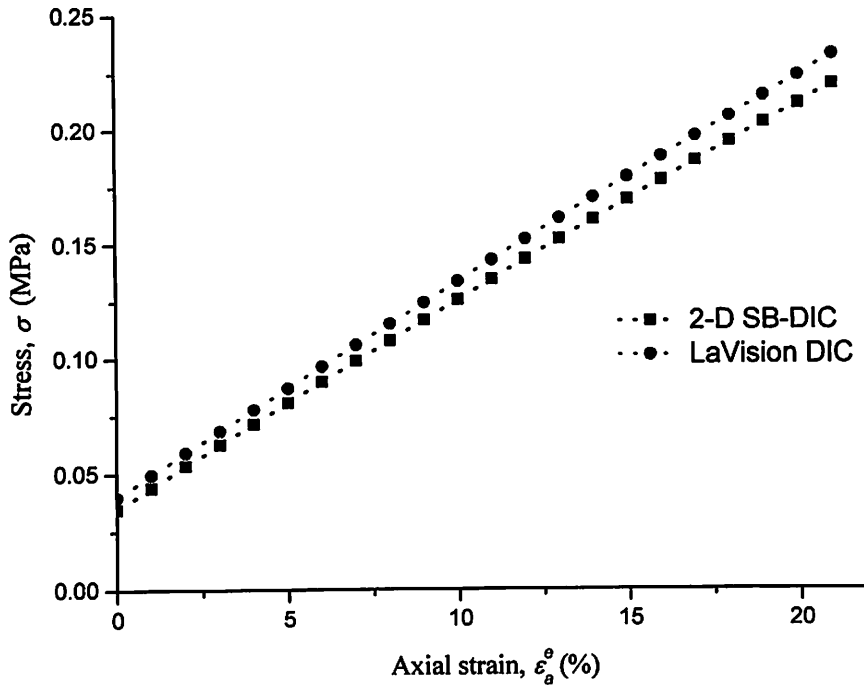


Figure 3.22 Comparison of stress-axial strain curve between the incremental 2D SB-DIC and the LaVision DIC methods

Table 3.5 Comparison of the stress value at different strain levels between the the incremental 2D SB-DIC and the LaVision DIC methods

Stress (MPa)			
Axial strains (%)	LaVision DIC	Incremental 2-D SB-DIC	Absolute error (%)
4	0.078	0.072	7.69
8	0.116	0.108	6.90
12	0.152	0.144	5.26
16	0.188	0.178	5.32
20	0.224	0.212	5.36

3.2.5 Comparison of Poisson's ratio between incremental 2-D SB-DIC method and theoretical function

The Poisson's ratios as a function of axial stretch ratio based on engineering and true strains are presented in Figure 4.23. The theoretical result of Poisson's ratio was plotted using Eq. (3.21). The data extracted from Eq. (3.21) and experimental results based on engineering strain were fitted using the following exponential decay function:

$$y = y_{off} + Be^{R_0x} \quad (3.2)$$

where y_{off} is offset from the x-axis, B is the initial value and R_0 is the decay rate. The fitted exponential graph from the experimental result agrees well with the fitted exponential graph obtained from theoretical result up to axial stretch ratio of 2.0. Table 4.5 shows the numerical comparison of the Poisson's ratio at different axial stretch ratios between the incremental 2-D SB-DIC method and theoretical result using the fitted curves shown in Figure 4.23. The maximum absolute deviation of Poisson's ratio up to the axial stretch ratio of 2.0 is 1.36% at axial stretch ratio of 2.0. Meanwhile, the maximum deviation of Poisson's ratio up to the range of experiment is 11.76% at axial stretch ratio of 3.5.

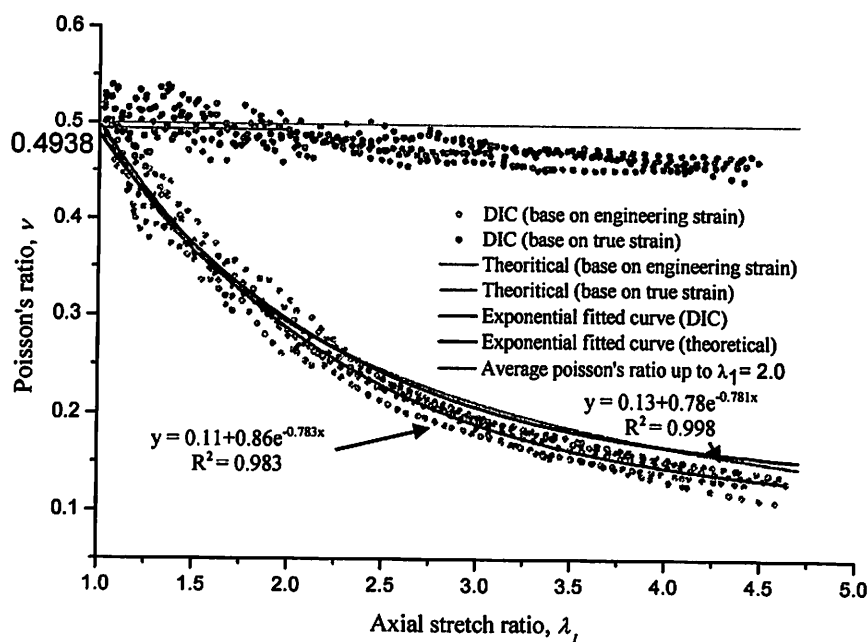


Figure 3.23 Poisson's ratio as a function of axial stretch ratio based on engineering and true strain

Table 3.6 Comparison of Poisson's ratio based on engineering strain in term of axial stretch ratio between incremental 2-D SB-DIC method and theoretical result

Axial stretch ratio	Theoretical	SB-DIC	Absolute deviation (%)
1.5	0.372	0.376	1.08
2.0	0.294	0.290	1.36
2.5	0.241	0.231	4.15
3.0	0.205	0.192	6.34
3.5	0.181	0.166	8.29
4.0	0.164	0.148	9.76
4.5	0.153	0.135	11.76

Nevertheless, the results were affected by the types of curve fitting used. Therefore, the Poisson's ratio based on true strain has been also studied since it is just a constant which can be obtained directly from the data and commonly adapted in the engineering field. The average value for Poisson's ratio up to axial stretch ratio of $\lambda_1 = 2.0$ is 0.4938, (1.24% deviates from the theoretical value) complying with the rule of incompressibility ($\nu^t=0.5$) shown in Figure 3.23. However, the Poisson's ratio starts to decrease beyond $\lambda_1=2.0$ due to the limit of incompressibility. The threshold value of the limit of incompressibility can be described with the graph plotted using Eq. (3.20) (page 67) as shown in Figure 3.24. Data from the incremental 2-D SB-DIC method agree well with the theoretical result up to axial stretch ratio of 2.0. But, at threshold of $\lambda_1 \geq 2.0$ significant deviation between the data obtained from the incremental 2-D SB-DIC method and theoretical result can be seen. The results show that the specimens start to deviate from the behaviour of an ideally incompressible material. The decrease in the Poisson's ratio after the threshold value is due to the large deformation-induced structural changes in rubber specimen caused by the microvoids present inside the rubber specimen (Figures 3.20(a)-(b)).

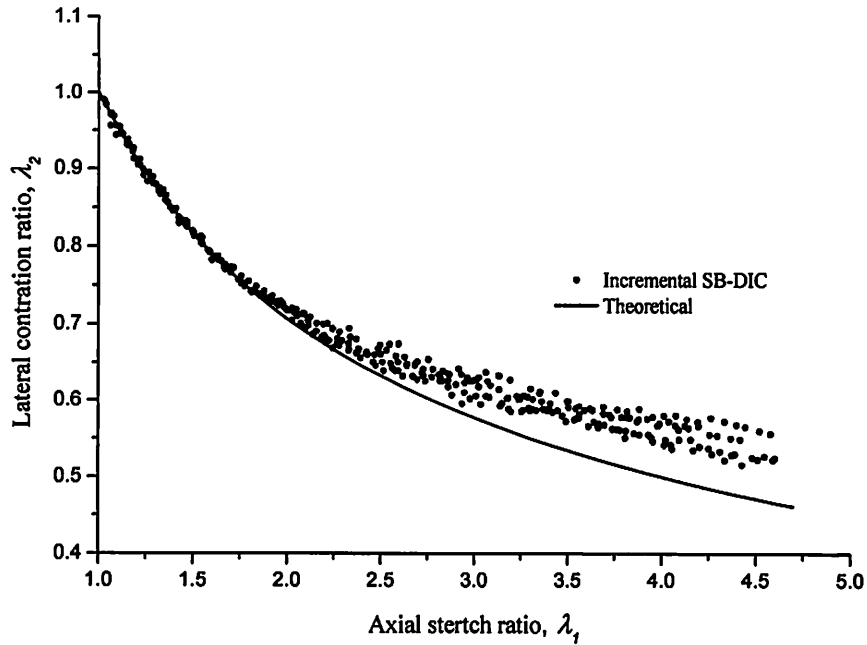


Figure 3.24 Lateral contraction as a function of axial stretch ratio used to describe the incompressible assumption

3.3 Single-step 2-D SB-DIC method

The 2-D displacement vector field superimposed onto the rubber specimen by using the single-step 2-D SB-DIC method is discussed in Section 4.3.1. The comparison of the axial strain-stress curve, normalized cross-correlation coefficient and time taken between the single-step 2-D SB-DIC and the incremental 2-D SB-DIC methods are discussed in Section 4.3.2 and Section 4.3.3. The comparison of the non-homogeneous resultant strain map between the single-step 2-D SB-DIC and the FEM methods is presented in the last part of this section.

3.3.1 Displacement vector field of the single-step 2-D SB-DIC method

The 2-D displacement vector fields at loading stages 7, 21, 49 and 76 in the tensile test on the dumbbell rubber specimens by using single-step 2-D SB-DIC method are shown in Figure 3.25. The displacement vector field is clearly seen in lower load (0.19 MPa) as shown in Figure 3.25(a). Most of the vectors overlapped one another at higher loads (0.66 MPa) as shown in Figure 3.25(b) and all of the displacement vectors overlapped one another at loads 1.21 to 1.91 MPa. This is because the displacement of the reference subset is higher than the predefined centre location of the adjacent row of the reference subset. The 3-D representation of the 2-D displacement vector fields are shown in Figure 4.26 to provide better view of the deformation at the eight stages. At more than 150% axial strain (\geq stage

35) some of the deformed reference subsets failed to track the corresponding location on the deformed images as shown in Figure 3.26(a). The mismatch displacement vectors were identified by using an outlier principle, whereby axial or lateral strains more than 1.5 of the interquartile range below the first quartile or above the third quartile were eliminated (Krzywinski and Altman, 2014) as shown in Figure 3.26(b). The displacement vectors which were eliminated were not be taken into strain calculation. The comparison of the strain data between the single-step 2-D SB-DIC and incremental 2-D SB-DIC is discussed in the following section.

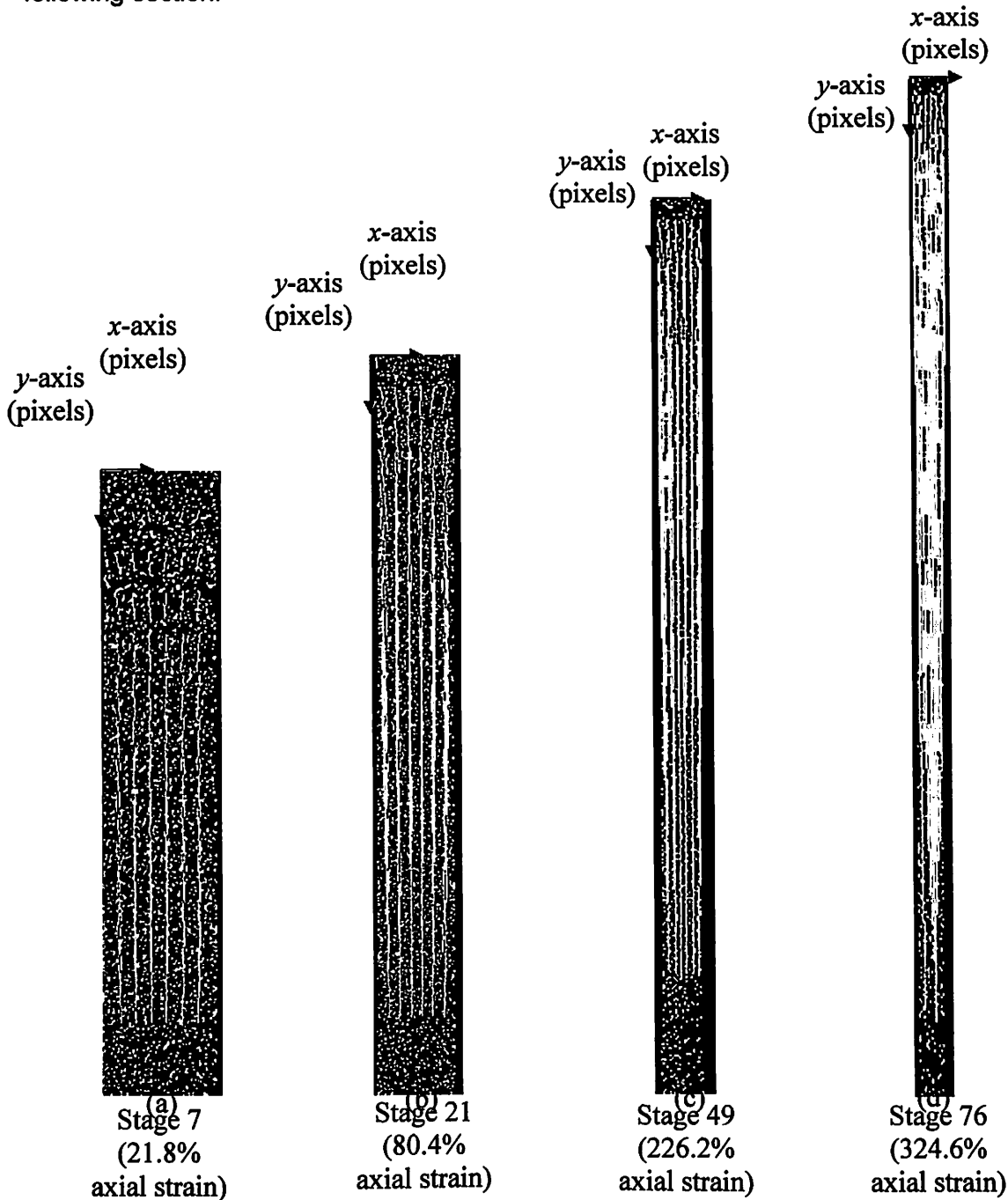
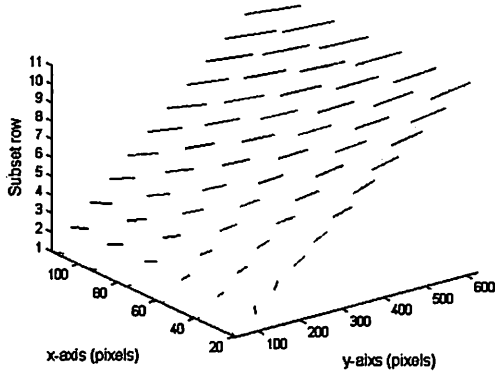
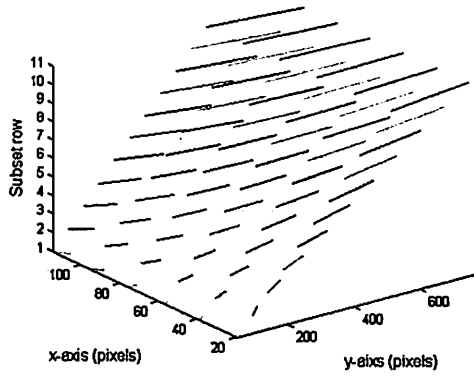


Figure 3.25 2-D displacement vector field at loads of (a) 0.23 MPa (b) 0.66 MPa (c) 1.21 MPa and (d) 1.91 MPa

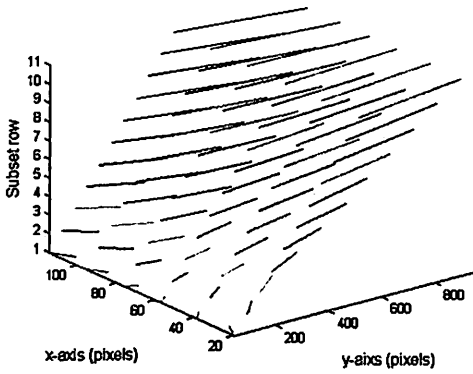
Displacement field at stage 7 (0.23MPa)



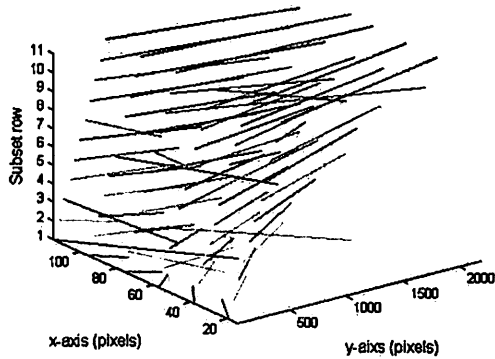
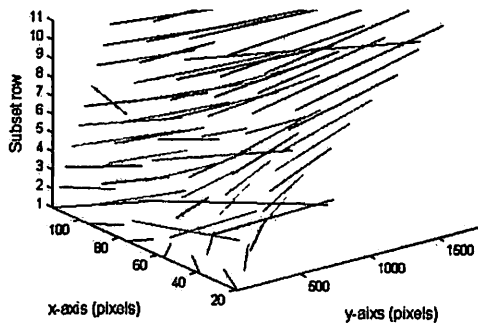
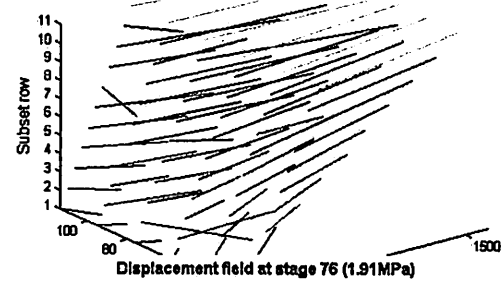
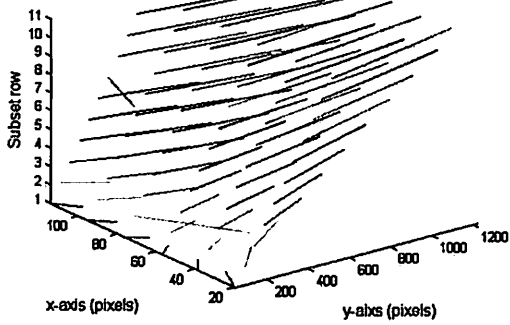
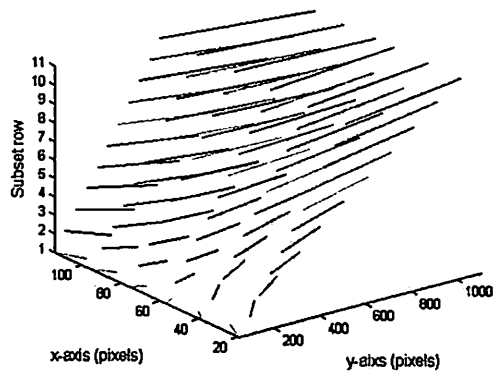
Displacement field at stage 14 (0.46MPa)



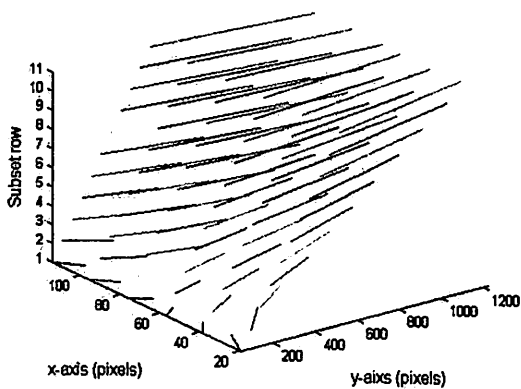
Displacement field at stage 21 (0.66MPa)



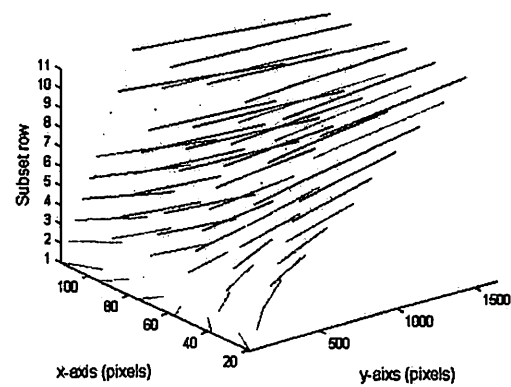
Displacement field at stage 28 (0.82MPa)



Displacement field at stage 36 (0.96MPa)



Displacement field at stage 49 (1.21MPa)



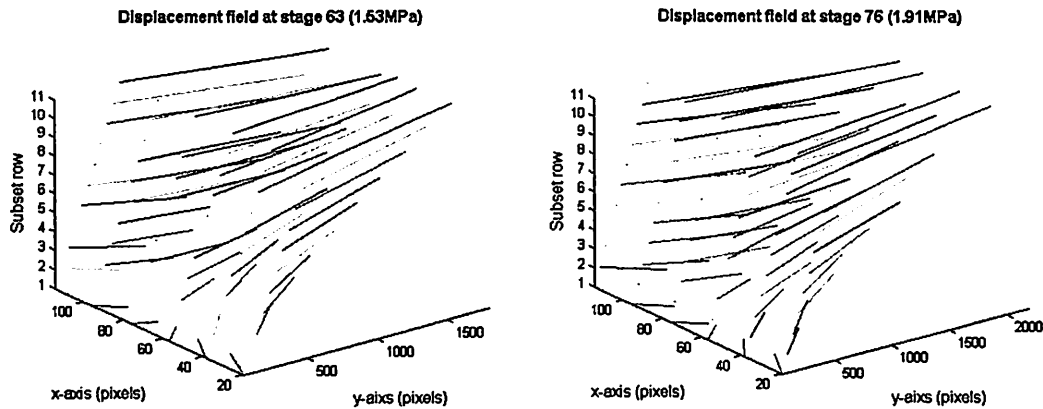


Figure 3.26 (a) 2-D displacement vector fields at stage 7, 21, 49 and 76 (b) 3-D representative of in-plane displacement vector field at stage 7, 21, 49 and 76

3.3.2 Comparison between single-step 2-D SB-DIC and incremental 2-D SB-DIC methods

The comparison of the axial strain between the single-step 2-D SB-DIC and the incremental 2-D SB-DIC methods and the normalized cross correlation coefficient for the single-step 2-D SB-DIC method is shown in Figure 3.27. Since the accuracy of the incremental 2-D SB-DIC method was verified previously (Section 3.2), this method was used as the reference to validate the results obtained from the newly developed single-step SB-DIC method. The range of the axial strains and normalized cross correlation coefficients in Figure 3.27 resulted from 66 reference subsets on the rubber specimen image (6 subsets in the x -direction and 11 subsets in the y -direction). At deformation below 100% axial strain, the axial strain range is small due to the homogeneous strain distribution. The deformed reference subsets were found to match accurately with their corresponding location on the deformed images.

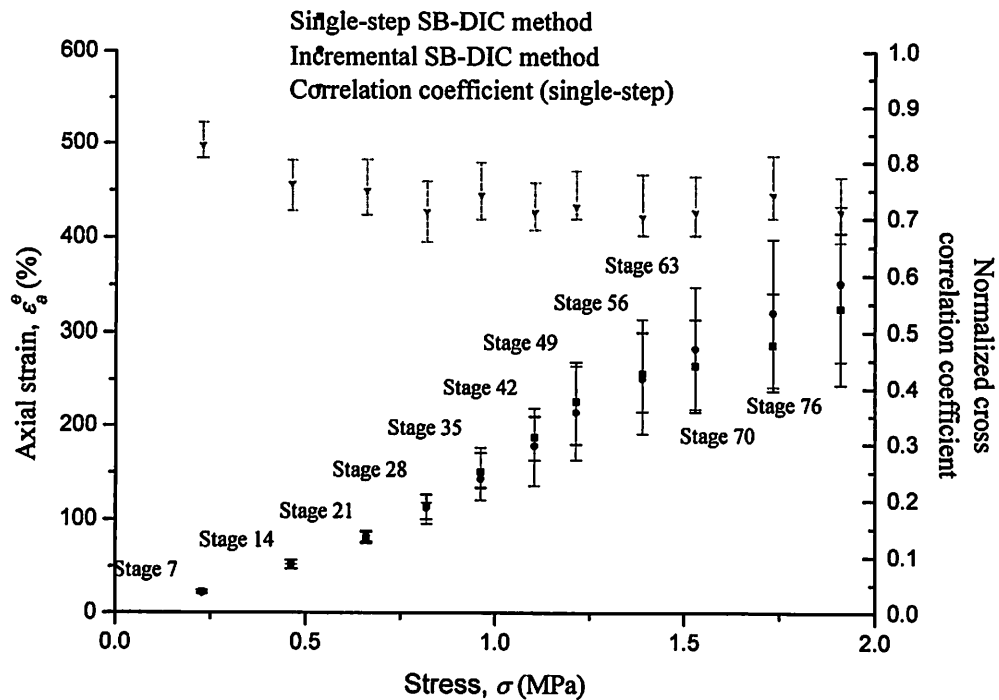


Figure 3.27 Comparison of axial strain between the single-step 2-D SB-DIC and the incremental 2-D SB-DIC methods and and normalized cross correlation coefficient of single-step SB-DIC method

The mean normalized cross correlation coefficient was between 0.75 (stage 21) and 0.83 (stage 7). The largest absolute deviation in the mean axial strain between the single-step 2-D SB-DIC and the incremental 2-D SB-DIC methods (deformation below 100% axial strain) is 3.32% at stage 7 as shown in Table 3.7. At stage above 28, the axial strain distribution had a larger range over the plane of the specimen. This is due to the non-uniform deformation in the specimen most probably caused by the presence of voids inside the rubber specimens as shown in Figure 3.20 (Section 3.2.3). At regions where the voids are present the speckle patterns were different from the reference image compared to those on the deformed reference image. However, due to the uniqueness of the speckle patterns in each subset the single-step SB-DIC method shows that the deformed reference subsets were able to track the inhomogeneous strain distribution from stage 28 to stage 76. The maximum absolute deviation of axial strain between the single-step 2-D SB-DIC and the incremental 2-D SB-DIC methods is 10.70% at stage 70 (1.73 MPa). The larger deviation between the single-step 2-D SB-DIC and the incremental 2-D SB-DIC methods at large deformation is due to the accumulated errors introduced in the incremental SB-DIC method. The normalized cross correlation coefficient of the single-step SB-DIC method shows decreasing trend (Figure 3.27) as the load increases due to the presence of voids in the rubber specimen. The displacement vector field and the axial strain result obtained from the

single-step SB-DIC method show that the proposed method is able to map the large deformations in a single-step.

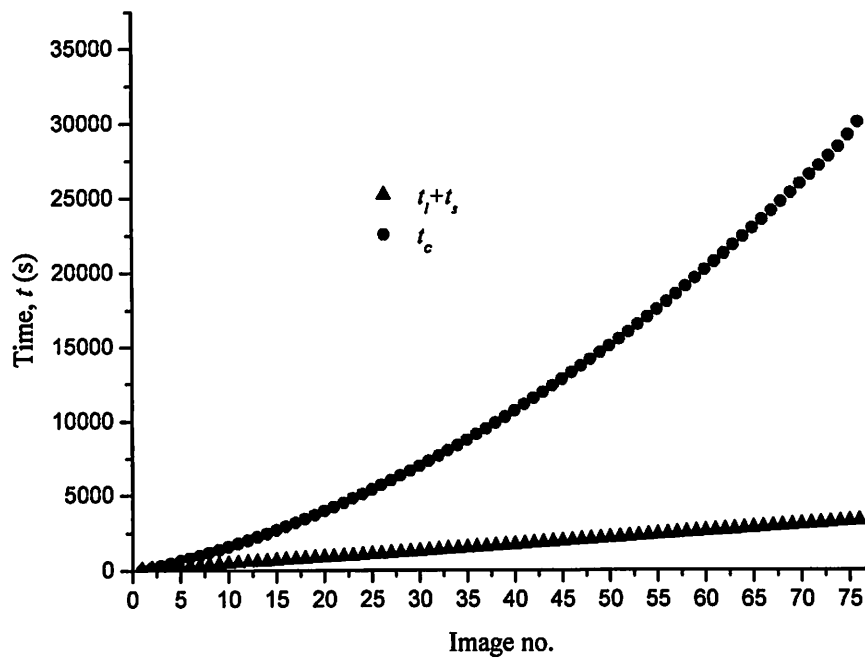
Table 3.7 Comparison of mean axial strain between single-step 2-D SB-DIC and incremental 2-D SB-DIC methods

Stage	Stress, σ (MPa)	Axial strain (%)		
		Incremental DIC method	Single step DIC method	Absolute deviation
7	0.23	21.1	21.8	3.32
14	0.46	50.3	51.1	1.59
21	0.66	82.6	80.4	2.66
28	0.82	112.1	114.3	1.96
35	0.96	143.2	150.5	5.10
42	1.10	178.4	187.5	5.10
49	1.21	214.3	226.2	5.55
56	1.39	251.2	256.4	2.07
63	1.53	282.5	264.7	6.30
70	1.73	320.6	286.3	10.70
76	1.91	351.4	324.6	7.63

3.3.3 Time comparison between the single-step 2-D SB-DIC and the incremental 2-D SB-DIC methods

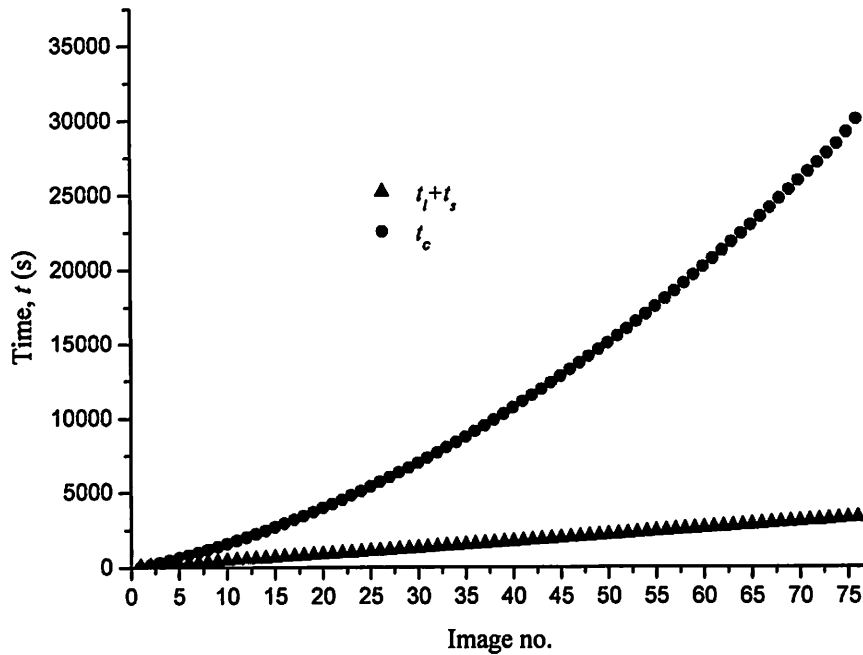
The loading time, scanning time and the DIC programme code running time of the incremental 2-D SB-DIC method is shown in Figure 3.28(a). The accumulated time taken for the loading-scanning process ($t_l + t_s$) and the programme code run, t_c for 76 images are 3264 seconds (54.4 minutes) and 30094 seconds (8.36 hours) respectively. The loading time and scanning time are combined together since the two processes run continuously. The DIC programme code running time is accumulated since the particular image used for processing is dependent on the series of images before the inspected image. Meanwhile, for the single step DIC method, the time taken for the loading-scanning process and the DIC programme code run are independent of the previous images. Thus, the time taken for the loading-scanning process and the DIC programme code run has been reduced tremendously as shown in Figure 3.28(b). Although the acquired images are independent of one other, the time taken for the loading-scanning process and DIC programme code run increased with the number of images. This is because each of the loading is equivalent to 4-5% axial strain.

In order to obtain large deformation image, higher load is required and thus, the time taken for the loading-scanning process increases. In addition, as the deformed reference subset size increases as the loading increases, the time taken for the tracking process is longer for large deformation image. The maximum time taken for loading-scanning process and programme run are 233 seconds (3.88 minutes) and 309 seconds (5.15 minutes) respectively at image 76. The comparison of the total processing time between the single step 2-D SB-DIC and incremental 2-D SB-DIC methods is shown in Figure 3.28(c). The total processing time for the incremental 2-D SB-DIC method to obtain strain up to 350% is 33358 seconds (9.27 hours) which is about 62 times more than the time taken for the single step 2-D SB-DIC method (0.15 hour).

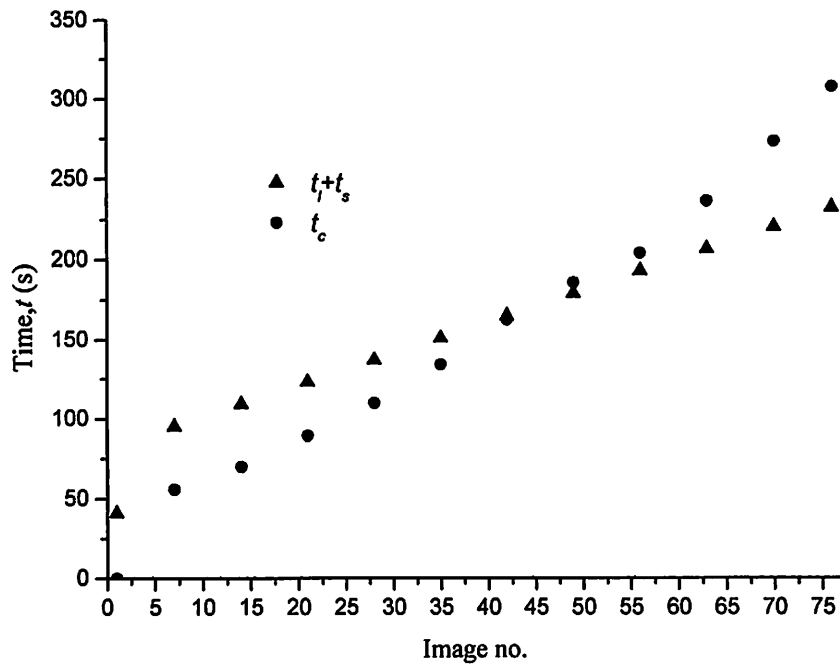


(a)

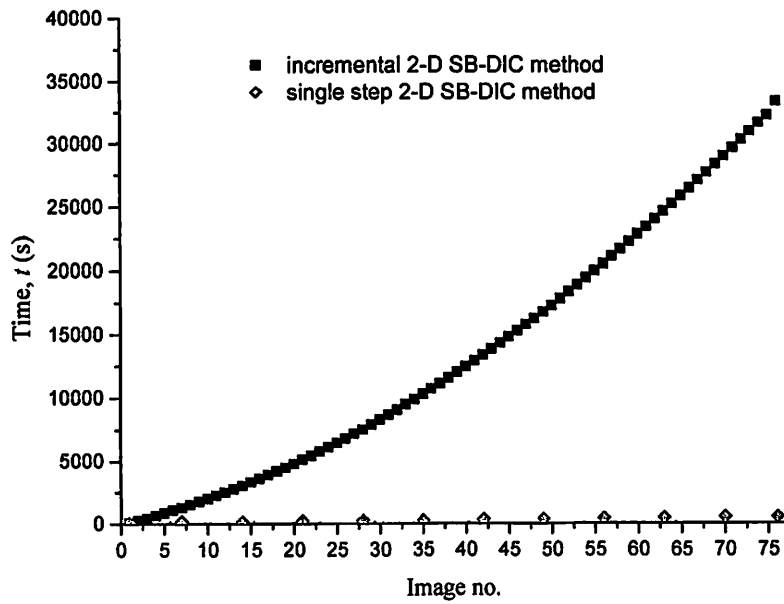
In order to obtain large deformation image, higher load is required and thus, the time taken for the loading-scanning process increases. In addition, as the deformed reference subset size increases as the loading increases, the time taken for the tracking process is longer for large deformation image. The maximum time taken for loading-scanning process and programme run are 233 seconds (3.88 minutes) and 309 seconds (5.15 minutes) respectively at image 76. The comparison of the total processing time between the single step 2-D SB-DIC and incremental 2-D SB-DIC methods is shown in Figure 3.28(c). The total processing time for the incremental 2-D SB-DIC method to obtain strain up to 350% is 33358 seconds (9.27 hours) which is about 62 times more than the time taken for the single step 2-D SB- DIC method (0.15 hour).



(a)



(b)



(c)

Figure 3.28 Loading time, scanning time and DIC programme code running time for (a) incremental DIC method and (b) single step DIC method, (c) comparison of total processing time between single-step 2-D SB-DIC and incremental 2-D SB-DIC methods

3.3.4 FEM analysis on non-homogeneous strain distribution

The comparison of the stress-axial strain graph between the prediction of the three models (Mooney-Rivlin two-parameter, Mooney-Rivlin five-parameter and Ogden three-parameter models) and the standard tensile test and is shown in Figure 3.29. A third order polynomial was used to fit the data for the standard tensile test and the FEM. At low deformation ($\leq 100\%$ axial strain), the Mooney-Rivlin two-parameter, Mooney-Rivlin five-parameter and Ogden three-parameter models show good prediction with the standard tensile test data. However, at deformations more than 100% axial strain, the stress-axial strain curves of the Mooney-Rivlin two-parameter and Mooney-Rivlin five-parameter models deviate from the standard tensile test data which do not take into account the stiffening effects of the materials (Meunier et al., 2008). Ogden three-parameter model has a good prediction for the whole range up to 350% axial strain of the standard tensile test data. Thus, the Ogden three-parameter model is the best hyperelastic model to depict the deformation of the rubber specimen and was chosen to characterize the hole-containing geometry rubber specimens.

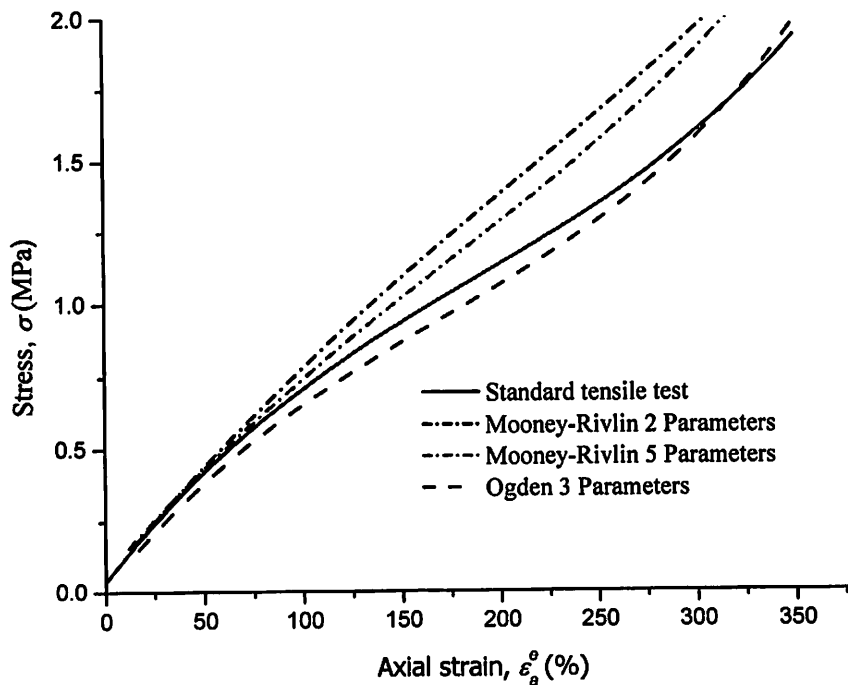


Figure 3.29 Comparison of the fitted stress-axial strain curve between the three hyperelastic models and the standard tensile test

Comparisons of the resultant strain maps of the rubber specimens containing circular and square holes between the single-step 2-D SB-DIC and the FEM methods are shown in Figure 3.30. The un-deformed image was subdivided into 1830 subsets (30 subsets in x-direction and 61 subsets in y-direction) with the reference subset size of 31×31 pixels. The

resultant strain maps in each case show significant inhomogeneity caused by the cut-outs. The discontinuity in the geometry causes the localized stress to increase above the average stress close to the geometry changes.

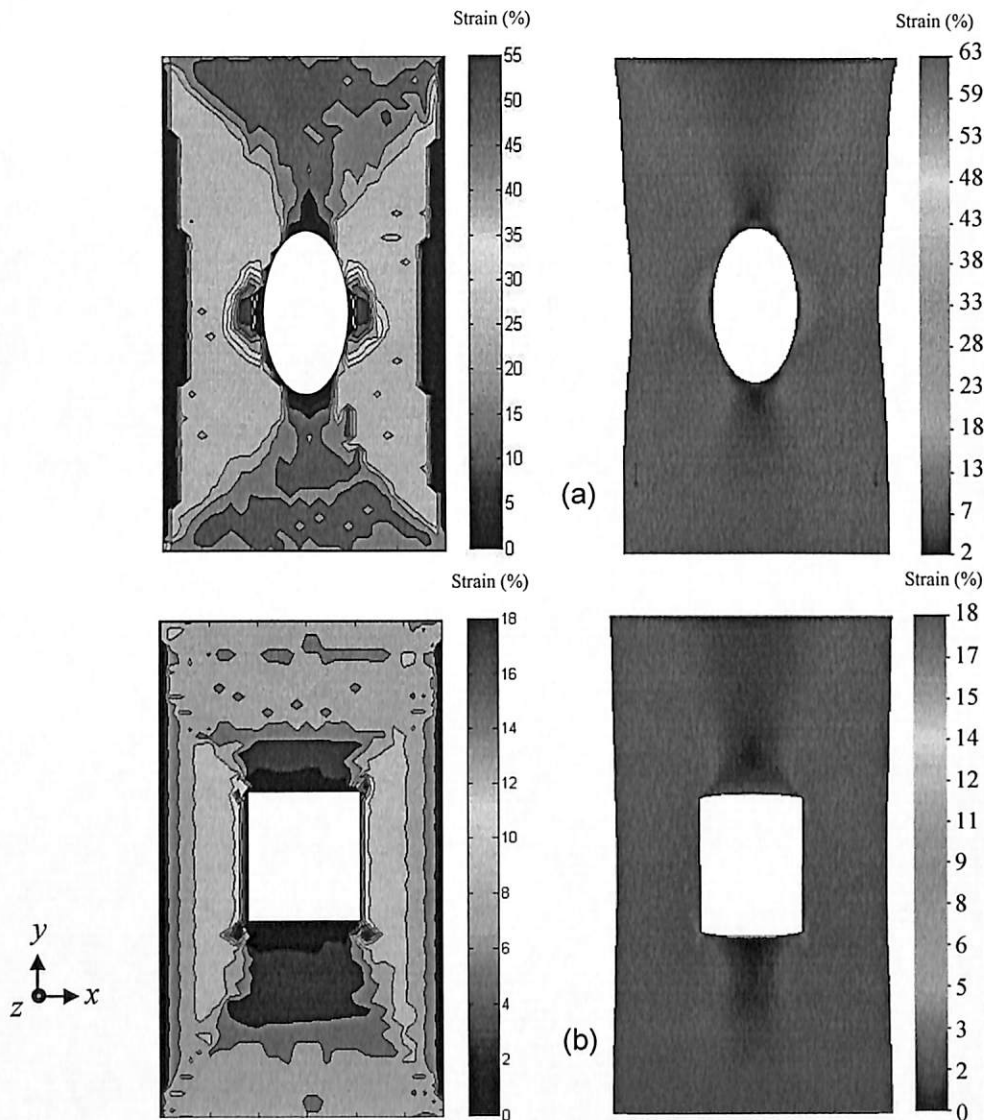


Figure 3.30 Comparison of resultant strain maps between single step 2-D SB-DIC method finite element modelling in (a) circular hole-containing rubber specimen and (b) square hole-containing rubber specimen

For the circular hole rubber specimen the stress concentration is dependent upon the polar coordinate references from the centroid of the circular hole relative to the direction of loading (Pilkey and Pilkey, 2008). The sideways exterior edges of the circular hole have the maximal strain values (53% and 63% strain for single-step SB-DIC and FEM methods, respectively) since the stress concentration is the highest at these areas. The upper and lower exterior edges of the circular hole have the minimum strain distribution (4% and 2%

strain for single-step SB-DIC and FEM methods, respectively) due to the lower stress concentration in these areas. For the square hole rubber specimen the stress concentrations focus on the sharp corners of the square due to the abrupt change in the surface area (Pilkey and Pilkey, 2008). Thus, the four sharp corners of the specimen have the maximum resultant strain (18% and 17% strain for single-step SB-DIC and FEM methods, respectively).

The resultant strain map of the circular hole containing model predicted by FEM method is slightly lower compared to the single-step 2-D SB-DIC method. This is because the gradient of the stress-axial strain curve of the rubber specimen is steeper than the stress-axial strain curve of the Ogden three-parameter model (Figure 4.28) at axial strain more than 25%. Moreover, the resultant strain equations for the 2-D SB-DIC and FEM methods are different. The resultant strain for the FEM method involves normal strains and shear strains in all three principal directions (x -, y - and z -directions) (refer to Section 3.6 page 83). Meanwhile, the resultant strain map for the square hole rubber specimen is similar to that of the FEM method since the stress-axial strain curve of the rubber specimen is well predicted by the FEM method at axial strain up to 25%. Nevertheless, the resultant strain maps show that the proposed single-step SB-DIC method can successfully measure large strain in inhomogeneous specimen.

CONCLUSION

In this research, the practicability to evaluate the scanned image using the commercial flatbed scanner for application in large in-plane displacement and strain measurement using 2-D DIC method is demonstrated. The simple low-cost document scanner is proven to be a useful image acquisition device for 2-D DIC application for elastomeric materials like rubber. Unlike in the conventional DIC setup the scanner-based DIC method does not use a CCD camera which needs to be moved due to the limited field-of-view. External lighting and a high-resolution camera or accurate specimen-imaging device positioning are not required. Using the scanner-based DIC method the full-field in-plane displacements in an elastomeric rubber specimen were measured at different loads. A loading fixture was specially designed for this purpose and functioned as specimen clamping system. The reference points on the fixture enable the specimen to be located and cropped out automatically using image processing. From the displacement of each subset the strain experienced by the rubber specimen at different points was measured. The mean deviations in the tangent and secant moduli between the incremental 2-D SB-DIC method and the standard tensile test method were only 6.0% and 2.3%, respectively. Meanwhile the mean deviations in the Poisson's ratio based on engineering and true strain were only 7.8% and 1.24%, respectively, thus confirming that the common document scanner is a potential tool for low-cost DIC application.

A direct large deformation mapping method, namely the single-step SB-DIC method, is proposed to measure large deformations without the use of a series of incremental deformation images. The factors used to reshape (deform) the reference subsets were determined from the experimental tensile test data for the rubber material and the theoretical Poisson function. The single-step SB-DIC method enables the target subsets on the deformed image to be tracked directly using the deformed reference subsets without the use of the intermediate images. Dumbbell-shaped rubber specimens were tested to verify the proposed single-step SB-DIC method. Displacement and strain fields up to 350% axial strain have been successfully measured using the proposed single-step SB-DIC method. The mean deviation in the axial strain between the incremental SB-DIC and the proposed single-step SB-DIC method was found to be only 4.7%. The resultant strain maps on rubber specimens containing circular and square holes obtained from FEM using the Ogden three-parameter hyperelastic model show good agreement with those from the single-step SB-DIC method. The proposed method eliminates cumulative errors that can be introduced when using the incremental SB-DIC method and significantly reduces the processing time in image acquisitions and coding implementation.

ACKNOWLEDGEMENT

The project leader and the co-researchers would like to thank Universiti Sains Malaysia for the RU(I) grant (Account number 1001/PMEKANIK/814182) that enabled this research work be carried out.

REFERENCES

- Coburn D., Slevin J. A. (1993) Development of a digital speckle correlation system for use in the non-destructive testing of advance engineering ceramics. *Key Engineering Materials* 86-87: 237-244.
- Dai Y. Z., Tay C. J., Chiang F. P. (1991) Determination of the plastic zone by laser-speckle correlation. *Experimental Mechanics* 31 (4): 348-352.
- De Crevoisier J., Besnard G., Merckel Y., Zhang H., Loisel F. V., Caillard J., Berghezan D., Creton C., Diani J., Brieu M., Hild F., Roux S. (2012) Volume changes in a filled elastomer studied via digital image correlation. *Polymer Testing* 31 (5): 663-670.
- Han Y., Rogalsky A. D., Zhao B., Hyock J. K. (2012) The application of digital image correlation techniques to determine the large stress-strain behaviors of soft materials. *Polymer Engineering and Science* 52 (4): 826-834.
- Kangasrääsio J., Hemming B. (2009) Calibration of a flatbed scanner for traceable paper area measurement. *Measurement Science and Technology* 20 (10): 107003.
- Kee C. W., Ratnam M. M. (2009) A simple approach to fine wire diameter measurement using a high-resolution flatbed scanner, *The International Journal of Advanced Manufacturing Technology* 40 (9): 940-947.
- Laraba-Abbes F., lenny P., Piques R. (2003a) A new 'tailor-made' methodology for the mechanical behaviour analysis of rubber-like materials: I. Kinematics measurements using a digital speckle extensometry. *Polymer* 44 (3): 807-820.
- Laraba-Abbes F, lenny P, Piques R. (2003b) A new 'tailor-made' methodology for the mechanical behaviour analysis of rubber-like materials: II. Application to the hyperelastic behaviour characterization of a carbon-black filled natural rubber vulcanizate. *Polymer* 44 (3): 821-840.
- Lim T. Y., Ratnam M. M. (2012) Edge detection and measurement of nose radii of cutting tool inserts from scanned 2-D images. *Optics and Lasers in Engineering* 50 (11): 1628-1642.
- Risbet M., Feissel P., Roland T., Brancherie D., Roelandt J.-M. (2010) Digital image correlation technique: application to early fatigue damage detection in stainless steel. *Procedia Engineering* 2 (1): 2219-2227.
- Tang Z., Liang J., Xiao Z., Guo C. (2012) Large deformation measurement scheme for 3D digital image correlation method. *Optics and Lasers in Engineering* 50 (2): 122-130.
- Wu D. J., Mao W. G., Zhou Y.C., Lu C. (2011a) Digital image correlation approach to cracking and decohesion in a brittle coating/ductile substrate system. *Applied Surface Science* 257 (14): 6040-6043.